INFLUENCE OF FILTERING ON LINEAR AND NONLINEAR SINGLE DEGREE OF FREEDOM DEFORMATION DEMANDS

A THESIS SUBMITTED TO
THE GRADUATE SCHOOL OF NATURAL AND APPLIED SCIENCES
OF
MIDDLE EAST TECHNICAL UNIVERSITY

BY

GARİP ÖNDER ÖZEN

IN PARTIAL FULFILLMENT OF THE REQUIREMENTS
FOR
THE DEGREE OF MASTER OF SCIENCE
IN
CIVIL ENGINEERING

NOVEMBER 2006

Approval of the Graduate School of Natural and Applied Sciences

Prof. Dr. Canan Özgen
Director

I certify that this thesis satisfies all the requirements as a thesis for the degree of Master of Science.

Prof. Dr. Güney Özcebe
Head of Department

This is to certify that we have read this thesis and that in our opinion it is fully adequate, in scope and quality, as a thesis for the degree of Master of Science.

Assoc. Prof. Dr. Sinan Akkar
Supervisor

Examining Committee Members

Prof. Dr. Haluk Sucuoğlu (METU,CE)_____

Assoc. Prof. Dr. Sinan Akkar (METU,CE) _____

Assoc. Prof. Dr. Ahmet Yakut (METU,CE) _____

Assist. Prof.Dr. Altuğ Erberik (METU,CE) _____

Dr. Tolga Yılmaz (METU,ES) _____

I hereby declare that all information in this document has been obtained and presented in accordance with academic rules and ethical conduct. I also declare that, as required by these rules and conduct, I have fully cited and referenced all material and results that are not original to this work.

Name, Last name : Garip Önder, ÖZEN

Signature :

ABSTRACT

INFLUENCE OF FILTERING ON LINEAR AND NONLINEAR SINGLE DEGREE OF FREEDOM DEMANDS

ÖZEN, Garip Önder

M.S., Department of Civil Engineering

Supervisor: Assoc. Prof. Dr. Sinan Akkar

December 2006, 115 pages

Ground-motion data processing is a necessity for most earthquake engineering related studies. Important engineering parameters such as the peak values of ground motion and the ordinates of the response spectra are determined from the strong ground-motion data recorded by accelerometers. However, the raw data needs to be processed since the recorded data always contains high- and low-frequency noise from different sources.

Low-cut filters are the most popular ground-motion data processing scheme for removing long-period noise. Removing long-period noise from the raw accelogram is important since the displacement spectrum that

provides primary information about deformation demands on structural systems is highly sensitive to the long-period noise.

The objective of this study is to investigate the effect of low-cut filtering period on linear and nonlinear deformation demands. A large number of strong ground motions from Europe and the Middle East representing different site classes as well as different magnitude and distance ranges are used to conduct statistical analysis. The statistical results are used to investigate the influence of low-cut filter period on spectral displacements.

The results of the study are believed to be useful for future generation ground-motion prediction equations on deformation demands that are of great importance in performance-based earthquake engineering.

Keywords: SDOF deformation demands, low-cut-filtering, European strong ground-motion dataset, linear and nonlinear oscillator response.

ÖZ

TEK SERBESTLİK DERECELİ SİSTEMLERİN LİNEER VE LİNEER OLMAYAN DEFORMASYON TALEPLERİNDE FİLTRE YÖNTEMİNİN ETKİLERİ

ÖZEN, Garip Önder

Yüksek Lisans, İnşaat Mühendisliği Bölümü

Tez Yöneticisi: Doç. Dr. Sinan Akkar

Kasım 2006, 115 Sayfa

Kuvvetli yer hareketi verilerini işleme deprem mühendisliğiyle ilgili çalışmalar için bir gerekliliktir. Kuvvetli yer hareketinin maksimum değerleri, tepki spektrumu ordinat değerleri gibi önemli mühendislik parametreleri ivme ölçerler tarafından kaydedilen kuvvetli yer hareketi verilerinden elde edilmektedir. Fakat ham veriler her zaman değişik nedenlere bağlı olarak gürültü içerdiklerinden bu verilerin işlenmesi gerekmektedir.

Alçak geçirimli filtreler yer hareketi verisi işleme yöntemleri arasında en çok kullanılan araçtır. Yapısal sistemlerin deplasman talepleri hakkında önemli bilgiler içeren deformasyon tepki spektrumu uzun periyot

gürültülerine karşı hassas olması sebebiyle, bu tip kusurların uzun periyot ham yer hareketi ivmesinden olabildiğince arındırılması alçak geçirimli filtreler aracılığıyla yapılabilir.

Bu çalışmanın amacı alçak geçirimli filtre periyodunun lineer ve lineer olmayan deplasman talepleri üzerindeki etkisini irdelemektir. Değişik zemin cinsi, uzaklık ve deprem aletsel büyüklülerinden oluşan Avrupa ve Orta Doğu bölgesinden derlenmiş kuvvetli yer hareketi veri tabanı işlenerek alçak geçirimli filtre periyodunun değişik zemin tipi ve deprem aletsel büyüklüğü de göz önüne alınarak deformasyon talepleri üzerindeki etkisi istatistik hesaplar kullanılarak araştırılmıştır.

Çalışma sonucu elde edilen bilgilerin, ileriki çalışmalara konu olabilecek ve performansa dayalı deprem mühendisliği için önemli olan kuvvetli yer hareketi deformasyon talebi tahmin ilişkilerinin çıkartılmasına katkı sağlayabileceği düşünülmektedir.

Anahtar Kelimeler: Tek serbestlik dereceli sistemlerin deformasyon talepleri, düşük geçirimli filtreleme, Avrupa kuvvetli yer hareketi veri tabanı, lineer ve lineer olmayan osilatör davranımı.

ACKNOWLEDGMENTS

"Hence to fight and conquer in all your battles is not supreme excellence;
supreme excellence consists in breaking the enemy's resistance without fighting"
Sun-Tzu

I wish to express my deepest gratitude to my supervisor Assoc. Prof. Dr. Sinan Akkar for his guidance, spending on his valuable time, advice, criticism, and encouragements and insight throughout the research. His attitude towards me like a brother made a lot of things more tolerable through the study.

I would like to extend my thanks to Prof. Dr. Polat Gülkan and Prof. Dr. Haluk Sucuoğlu for their courses on earthquake that motivated me positively for working on the challenging topics of earthquake engineering.

I also want to thank to Prof. J. Bommer who provided the raw European ground motion database.

Another thanks goes to Dr. Ünal İlker for his support during my career in professional engineering.

Lastly, I would like to express my appreciation to my family for their endless love and their support during all my life.

TABLE OF CONTENTS

APPENDICES

LIST OF FIGURES

FIGURE

LIST OF TABLES

TABLE

CHAPTER-1

INTRODUCTION

1.1. Argument

Strong ground-motion data recorded by accelerometers always contain noise from different sources, meaning that no strong ground-motion data is noise free. The raw data recorded by the accelerometers need to be processed before any engineering application such that an optimized trade-off is achieved between the processed signal and the particular engineering parameter under consideration. Removing the long-period noise from the raw accelogram is important for calculating displacement spectrum that reveals primary information about the deformation demands on structural systems. Reliable deformation demands are one of the most important quantitative measures for the performance-based seismic design of new or existing structures.

The most popular procedure for removing (in fact reducing) the long-period noise from raw accelogram is the application of low-cut (high-pass) filters to the raw data. The selection of low-cut filter parameters such as the filter cut-off period, order of filtering and the causality of the filter can affect the processed time series that in turn influence the displacement response spectrum. Among the parameters that influence the displacement response spectra and peak ground deformation, the choice of long-period filter cut-off is the most ambiguous task. The uncertainty

and subjectivity in the determination of long-period filter cut-off period (T_c) becomes important for engineering studies because of the particular influence of this filter parameter on the usable period range of spectral displacements computed from the processed accelograms.

1.2. Objectives

The objective of the study is to present the effects of T_c on elastic and inelastic oscillator displacements for analogue records. Strong ground motions from the recently compiled European strong ground motion database (Ambraseys et al., 2005) are processed by using different T_c values derived from previously proposed noise models. Observations obtained from these preliminary studies are used to propose a new record processing scheme at the end of this study. This method determines the low-cut filter periods by considering the influence of important seismological parameters (magnitude and site class). The robust statistics presented at the end of this study can be used to derive empirical relations for defining usable period ranges of elastic spectral displacements in terms of low-cut filter period, site class and magnitude.

1.3. Procedure

The study is conducted in three phases. In the first phase, a literature survey was carried out on the data processing methods, the emphasis being on the high-pass (low-cut) filter cut-off determination.

In the second phase, a total of 156 rock, 264 stiff and 108 soft site analogue records were selected from the recently compiled European ground-motion database (Ambraseys et al., 2005) and re-processed by

using the high-pass filter cut-off values determined by two noise spectra developed by Trifunac and Todorvska (2001) and Skarlatoudis et al. (2003). Mean statistics for the peak values of ground motion as well as the elastic and inelastic displacement spectra for different level of inelasticity were obtained by using the re-processed data from these alternative noise spectrum models.

The observations from the second phase were used to propose a consistent record processing scheme in the last phase. The proposed scheme determines the high-pass (low-cut) filter cut-offs by making use of important seismological features such as magnitude and site class. The new scheme was then employed by using the analogue records of the second phase to derive some useful statistics for observing the filter cut-off influence on the usable spectral range of peak elastic oscillator displacements. The observations are presented in terms of different site classes as well as magnitude ranges.

1.4. Disposition

The study consists of six chapters, this introduction section being the first one. The second chapter gives general information about the strong ground-motion accelograms, the sources of noise and its effects on spectra and strong ground-motion data processing methods; the emphasis being on high-pass filters and the determination of high-pass filter cut-off period.

The third chapter is about the basics and theory of filtering. In this chapter the basic parameters of digital filtering such as filter order, causality of the filter are discussed.

The fourth chapter investigates the influence of low-cut filter cut-off value determined for different noise-spectrum models. Analogue recordings from the recently compiled European ground-motion database by Ambraseys et al. (2005) are used for this purpose. Basic statistics for the peak values of ground motion (peak ground acceleration, peak ground velocity and peak ground deformation) are obtained. Elastic and inelastic displacement spectra are also obtained for these noise-spectrum models and comparisons are made to emphasize the low-cut filter effect on linear and nonlinear oscillator deformation demands.

The fifth chapter presents an alternative record processing scheme that is based on the observations presented in Chapter-4. This procedure defines the low-cut filter values by making use of the theoretical source spectra as well as the fixed trace information whenever available. The ground-motion database presented in Chapter-4 is re-processed by this alternative scheme and statistics are presented to describe the role of magnitude and site classes on the useful period range of elastic displacement spectrum.

The sixth chapter consists of summary, conclusions and recommendations for future studies.

CHAPTER-2

NECESSITY FOR STRONG GROUND-MOTION PROCESSING

2.1. Strong Ground-Motion Accelograms

The design of new structures, the evaluation of existing ones and estimation of earthquake induced losses depend on the relationship between earthquake ground motion (demand) and structural performance (capacity) (Bazzurro et al., 2004). The prime source of earthquake ground-motion is the strong ground-motion accelograms. The ordinates of the response spectra and the peak values of the ground motion used for engineering design are determined from the strong ground-motion data recorded by the accelerometers. Thus, reliable ground-motion record datasets are necessary for most research in earthquake engineering and engineering seismology.

The release of energy during an earthquake gives rise to seismic waves. Seismic waves loose their energy while traveling through different ground layers. These waves can be recorded by sensitive sensors that produce continuous recordings (accelograms). There are various types of accelerometers but the fundamental principle is the same: a free mass (pendulum) whose relative displacement is proportional to ground acceleration. Modern accelerometers record the ground motion in two horizontal and one perpendicular direction by using 3 separate channels.

The first free-field ground motion recorded by the accelerometers was on 10 March 1933, Long Beach, California earthquake. The first strong ground-motion accelogram in a building was recorded on 2 October 1933, in the Hollywood Storage Building, in Los Angeles, California. The strong ground-motion accelogram deployment increased rapidly since then. For example the number of accelograms in the U.S. has increased to 2000 from 61 between 1955 and 1990's (Trifunac and Todorovska, 2001; Trifunac, et al., 1999). Until now, thousands of accelerometers have been installed around the world and the databank of strong-motion records has been growing in an increasing rate.

Many strong-motion transducers (sensors) are similar to a pendulum that vibrate due to moving earth with respect to their supports. The motion in analogue instruments is recorded by a light beam projected on a paper or film by induction of voltage in a coil (Trifunac and Todorovska, 2001). Figures 2.1 and 2.2 show the transducer used in SMA-1, which is the most commonly used analogue accelerometer all around the world. Trifunac and Todorovska (2001) give information about the resolution and dynamic range of strong-motion accelograms. Between 1930 and 1980, the dynamic range of the accelograms was between 45-55 dB for analogue instruments. The rapid development of solid-state technology caused the digital accelerometers come into screen after 1980s that have dynamic range of 135 dB. (Note: decibel (dB) is a dimensionless measure used in electrical engineering and it is the ratio between two quantities. It is used in a wide variety of measurements in electrical engineering and it allows to represent very large or small ratios by using a conveniently small number such that $X_{dB} = 10\log(\frac{X}{X_0})$ where X and X_0 are the specified output and input for a given instrument).

Accelerometers can be either analogue or digital. Analogue accelerometers are the first generation instruments to be used for recording the strong ground motion. These devices are optical-mechanical devices which produce ground acceleration traces on 35mm film or paper. These instruments exhibit three important disadvantages: (1) they operate on stand-by not to waste recording medium, which causes the first arrivals of the seismic waves not to be recorded, (2) their dynamic range is limited to about 25Hz, (3) the traces of analogue accelograms need to be digitized, which is the primary source of noise. Digital accelograms provide solutions to the disadvantages of analogue accelograms. The first wave arrivals are captured by the device since they operate continuously. The dynamic range of digital accelograms is much higher when compared to analogue accelerometers. The digitization process is performed within the device, which causes higher resolution and lesser digitization noise (Boore and Bommer, 2005).

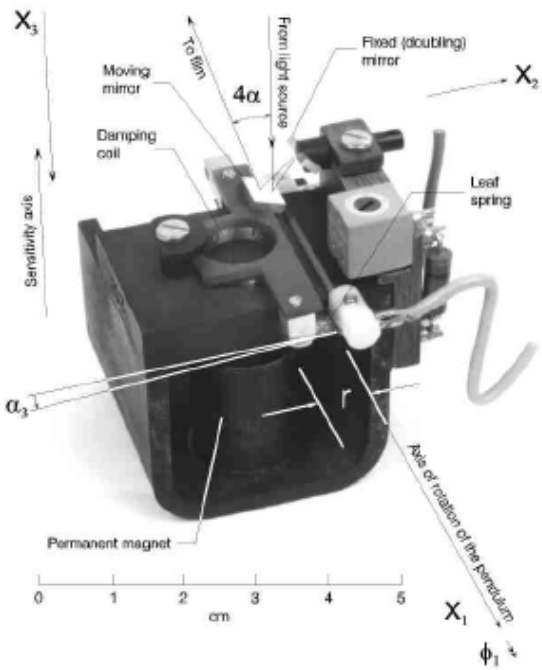

Figure 2.1 An SMA transducer removed from the box. Letter r indicates the arm of pendulum and α is the angle of deflection (Trifunac and Todorovska, 2001).

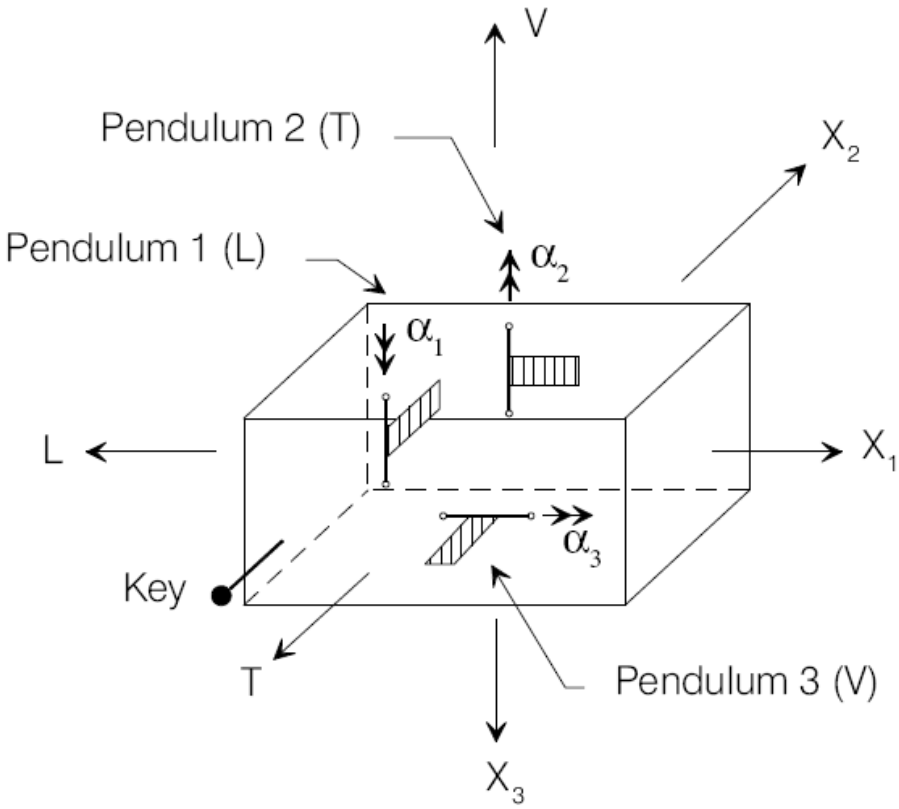

Figure 2.2 Schematic representation of three transducers a SMA-1. The coordinate axes X_1, X_2 and X_3 serve to describe the motion of the L, T and V transducers respectively, and are oriented in the opposite direction of the sensitivity axes of the transducers. Angles α_1, α_2 and α_3 describe the deflection of the transducer penduli (Trifunac and Todorovska, 2001).

The strong ground-motion data recorded by the accelerometers always contain noise from different sources. Therefore, the raw data recorded by the accelerometers need to be processed to obtain an optimized balance between the signal and the required engineering parameter for a particular application. The following sections of this chapter will focus on the sources of noise and the techniques applied to the strong-motion data to reduce the level of noise in the data recorded. Removing the long-period (low-frequency) noise from the raw accelogram is particularly important for calculating displacement spectrum that reveals primary information about the deformation demands on structural systems.

2.2. Noise Sources in Strong Ground-Motion Signals and Processing Methods

Analogue accelograms still dominantly contribute to strong ground-motion databases since most of the pre-1990 ground motions were recorded by analogue accelerometers. As discussed in the previous section, the long- and short-period noise are of great concern for analogue accelograms. Thus, it is important to understand the sources of noise, their effects on the engineering parameters and the methods applied for removing them to obtain reliable records for the calculation of unbiased engineering design parameters, such as response spectrum ordinates and peak values of ground motion.

The sources of noise in digital accelograms are not discussed in this study since the scope is limited to analogue records. However, it must be borne in mind that neither digital nor analogue accelerometers operate noiseless and whatever instrument is used, the signal captured due to ground shaking will always contain noise from different sources. The aim of applying filtering schemes to raw acceleration data is to reduce the level of noise, such that the ground-motion parameters can be obtained in a realistic manner. The principal objective of most filtering schemes is to determine part of the signal contaminated by noise and to reduce the level of noise for a selected interval of frequency or period.

Signals captured by analogue instruments have to be digitized before their implementation to engineering computation. The digitizing process results in non-standard and standard errors that are discussed in the following paragraphs.

Jerks, that can be defined as spurious spikes in the digitized signal, are an example for non-standard errors. The removal of spikes can be performed by replacing the acceleration ordinate of the spike with the mean acceleration ordinate of the data points either side (Boore and Bommer, 2005). Figure 2.3 shows an example of a jerk from one of the horizontal components of an aftershock (M_w=5.2) of the 1981, Lucano, Italy earthquake. The digitized acceleration waveform shows a jerk at about 10 seconds. Figure 2.4 shows the same acceleration trace with "jerk" removed case using the procedure described by Boore and Bommer (2005).

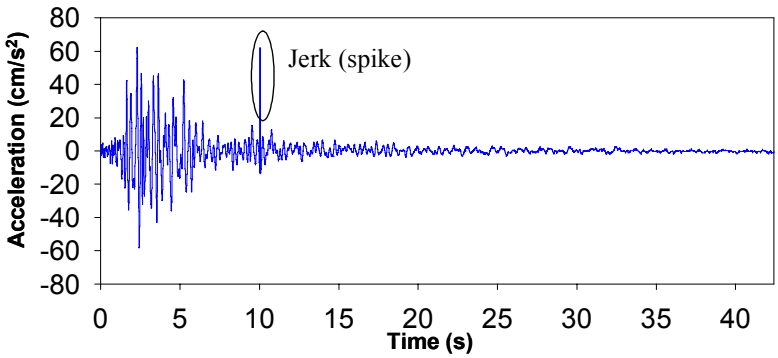

Figure 2.3 Acceleration trace for one horizontal component of an aftershock (M_w=5.2) from the 1981, Lucano Italy earthquake with a jerk at about 10 seconds.

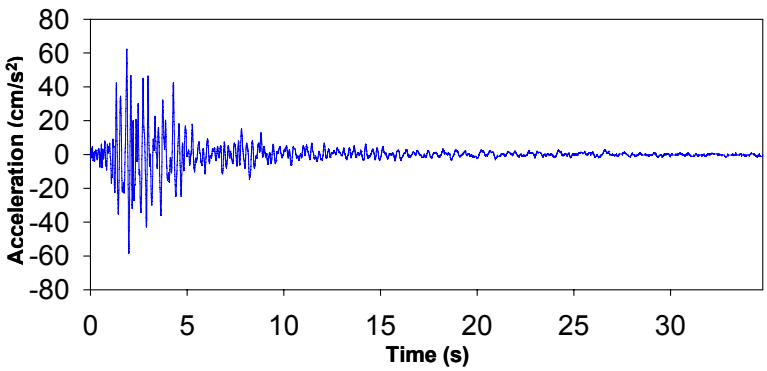

Figure 2.4 Acceleration trace for one horizontal component of an aftershock (M_w=5.2) from the 1981, Lucano Italy earthquake for jerk removed case.

Figure 2.5 shows the acceleration response spectra of the horizontal component of the Bajestan recording of the 1978 Tabas, Iran, earthquake with and without jerks. Removal of the jerk results in a significant change in the short-period range of the spectral acceleration.

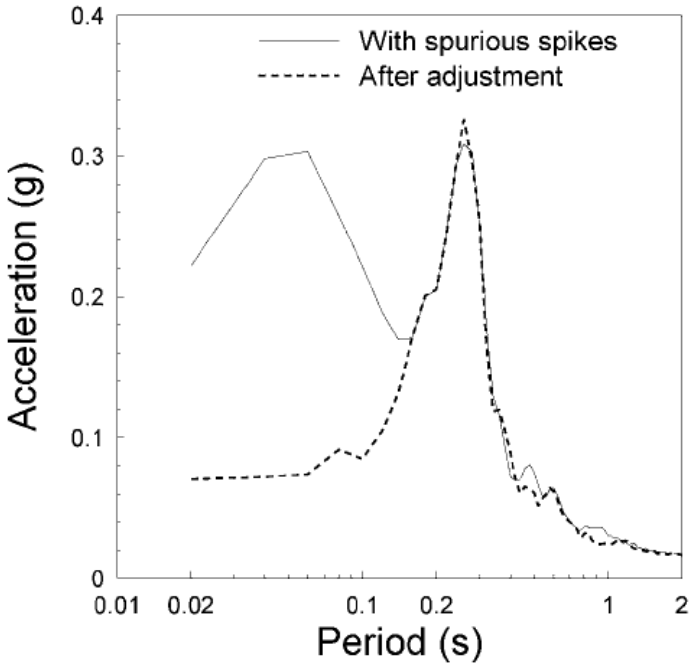

Figure 2.5 Acceleration response spectra (5% damped) for the Bajestan Station recording of the 1978 Tabas earthquake before and after the removal of spikes (Boore and Bommer, 2005).

Another source of non-standard error is the baseline shifts, which is a result of wrong splicing of the separately digitized sections. Baseline adjustment methods such as applying segmental straight lines or low order polynomials to the raw velocity trace and subtracting the derivatives from the acceleration trace can be an alternative for removing the baseline shifts. There are numerous methods for the baseline adjustments but such techniques are out of scope of this study. The reader is referred to Douglas (2001), Grazier (1979) and Iwan et al. (1985) for a detailed discussion about the baseline adjustment methods. Figure 2.6 illustrates

an example for the effect of baseline shifts in the ground-motion time series.

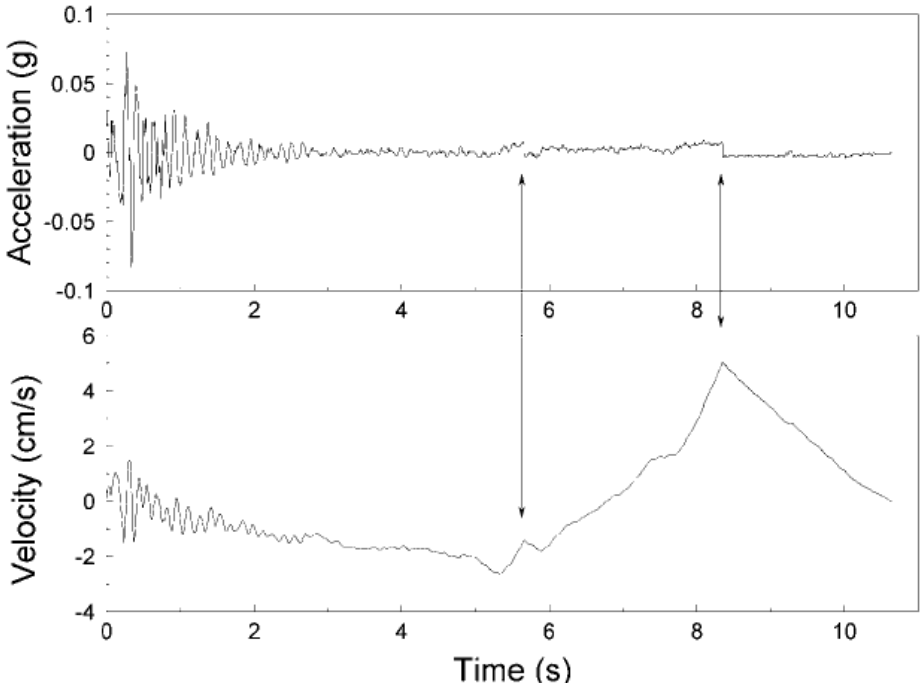

Figure 2.6 NS component of the 21 May 1979 Italian earthquake (12:36:41 UTC) recorded at Nocera Umbra, showing shifts in the baseline at 5.6 and 8.3 seconds. Note the unphysical velocity trace, which is a result of the baseline shifts (Boore and Bommer, 2005).

Long-period noise in analogue accelerograms mostly arise due to warping of the film or paper, and misalignment during the digitization process. This standard error type is the most important concern for analogue record processing as most of the ground-motion parameters of engineering interest are influenced by long-period errors depending on the level of noise contamination in the unprocessed data. Removal of long-period noise and its influence on important engineering parameters is the main scope of this study. Analogue recordings also contain short-period noise (the other standard error) that is related to the transducer imperfections and random error in the identification of the exact mid-point of the film

during digitizing process (Trifunac and Todorovska, 2001). High frequency noise is not a serious concern for most of the engineering studies since it dominates period intervals less than 0.04s. This type of noise can be reduced by applying low-pass (high-cut) filters to the analogue records (Boore and Bommer, 2005). Typically, frequencies higher than 25Hz. are removed from the analogue accelerogram in standard high-cut filtering process.

2.3. Methods for the Determination of Filter Corner Frequency

Among the various ground-motion processing schemes, application of low-cut (high-pass) filters is the most popular procedure for removing long-period noise. The function of low-cut filter is to remove the long-period noise from the raw accelogram. Removing the long-period noise from the raw accelogram is important since displacement spectrum that provides primary information about deformation demands on structural systems is highly sensitive to long-period noise. The selection of low-cut filter parameters such as filter corner period, order of filtering and causality of the filter can affect processed time series that in turn influence the displacement response spectrum. The basic theory of filters and important filter parameters are discussed in Chapter-3, except for the determination of filter corner period.

The choice of long-period filter cut-off period (T_c) or, as conventionally referred to as “low-cut filter cut-off frequency” ($f_c=1/T_c$) is the most important filter parameter for removing the long-period noise from the raw accelogram. The uncertainty and subjectivity in the determination of T_c becomes important for engineering studies because of the particular influence of this filter parameter on the usable period range of spectral

displacements computed from the processed accelograms (Boore and Bommer, 2005; Akkar and Bommer, 2006).

Figure 2.7 shows the time series of the 1978, Basso Tirreno, Italy earthquake (M_w=6) recorded at Naso station. The raw data was filtered for the low-cut periods of T_c = 20, 10, 6.67 and 5.0s (i.e. f_c=0.05, 0.10, 0.15 and 0.20Hz respectively). Prior to filtering, the mean of the raw acceleration trace was subtracted from the whole record in order to remove the possible constant trend that might cause linear shifts in the integrated velocity and displacement traces, respectively (designated as "Remove Mean" in the relevant plots of Figure 2.7). Leading and trailing zeros were added to the mean removed acceleration trace before filtering in order to accommodate filter transients. This subject will be described in detail in the next chapter. As can be seen from Figure 2.7, the influence of low-cut filtering on the acceleration traces are not visible by eye, whereas the displacement traces are very sensitive to the filter frequency. As the level of low-cut filter frequency value increases, the values of displacement traces become smaller. The level of decrease in peak ground displacement from T_c=20s. to T_c=5s. is approximately an order of magnitude. This issue is treated in detail in Chapter 3.

The particular effect of low-cut filter period can be understood better when the ratios of peak ground-motion values and spectral displacements are investigated for different filter cut-off values. Figure 2.8 shows the normalized peak ground-motion values of acceleration, velocity and displacement of the record given in Figure 2.7 that is low-cut filtered with different T_c values. The normalization is done by using the peak ground-motion values of T_c=20s. The absisca of the figure is plotted in terms of low-cut filter frequency (reciprocal of filter cut-off period). The ordinates show the variations in the ratio of peak ground motion parameter (PGMP)

normalized by the corresponding value computed when the record is low-cut filtered with T_c=20s ($PGMP_{fc=0.05Hz}$). The figure indicates that the peak ground acceleration and velocity are much more stable for different low-cut filter values when compared to the peak ground displacement. Figure 2.9 shows a similar comparison for 5% damped elastic displacement spectrum. Note that the spectral ordinates are virtually the same for periods less than 2 seconds. The discrepancy for spectral ordinates is notable for spectral periods longer than 2 seconds showing the sensitivity of filter cut-off values in the long periods. As the first glance, vibration periods longer than 2 seconds might be considered as of little importance for conventional engineering applications. This consideration is indecisive because representing nonlinear oscillator demands via equivalent linear methods (e.g. Gülkan and Sözen, 1971; Iwan, 1981) require reliable elastic spectral displacements at very long periods. A realistic representation of design spectrum that is compatible with displacement demands also requires trustworthy response spectrum information at long periods.

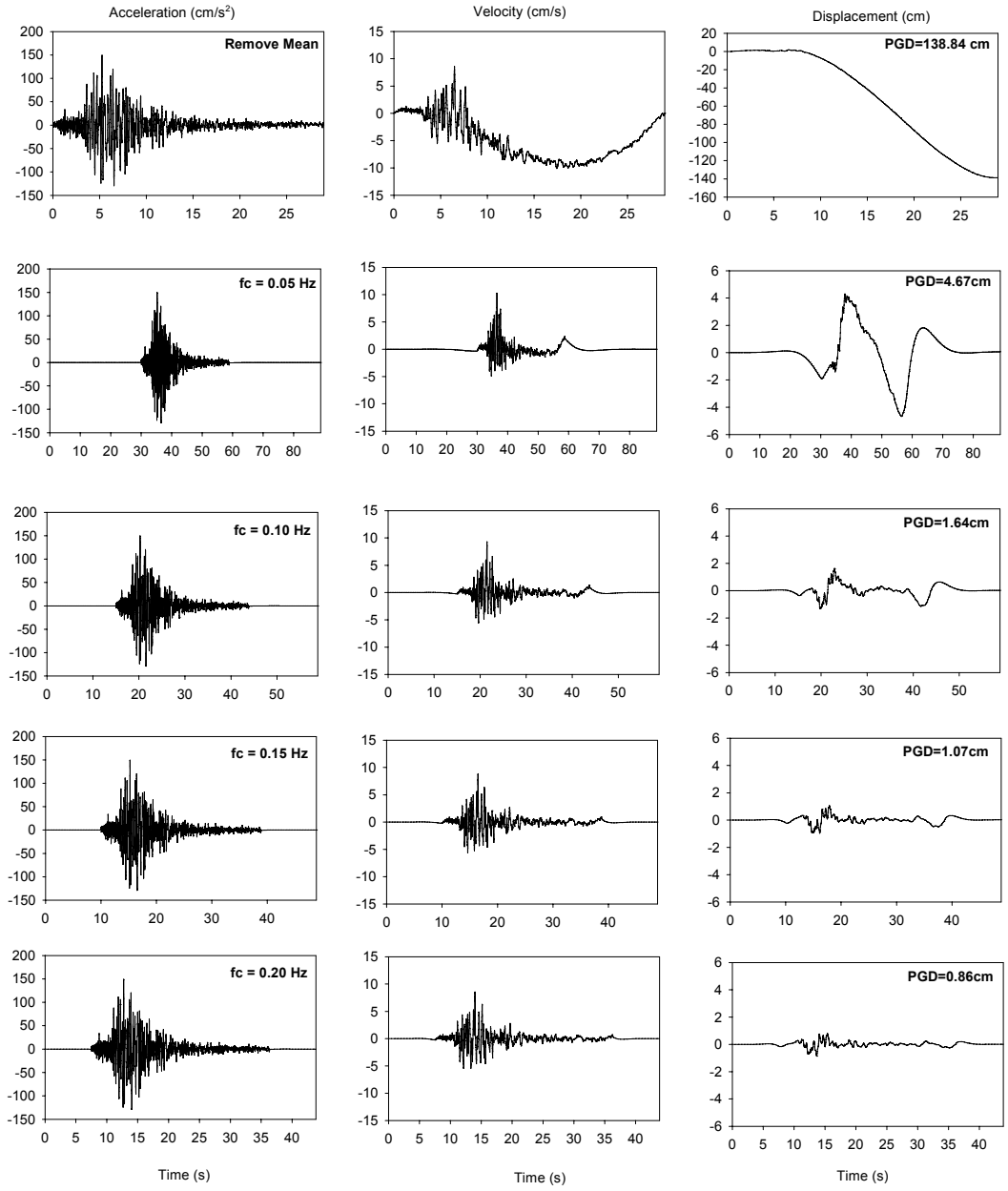

Figure 2.7 Traces of the 1978, Basso Tirreno, Italy earthquake (M_w=6) recorded at Naso station. The raw data is mean removed and filtered for low cut-off frequencies of 0.05, 0.10, 0.15 and 0.20Hz. (i.e. T_c=20, 10, 6.67 and 5s).

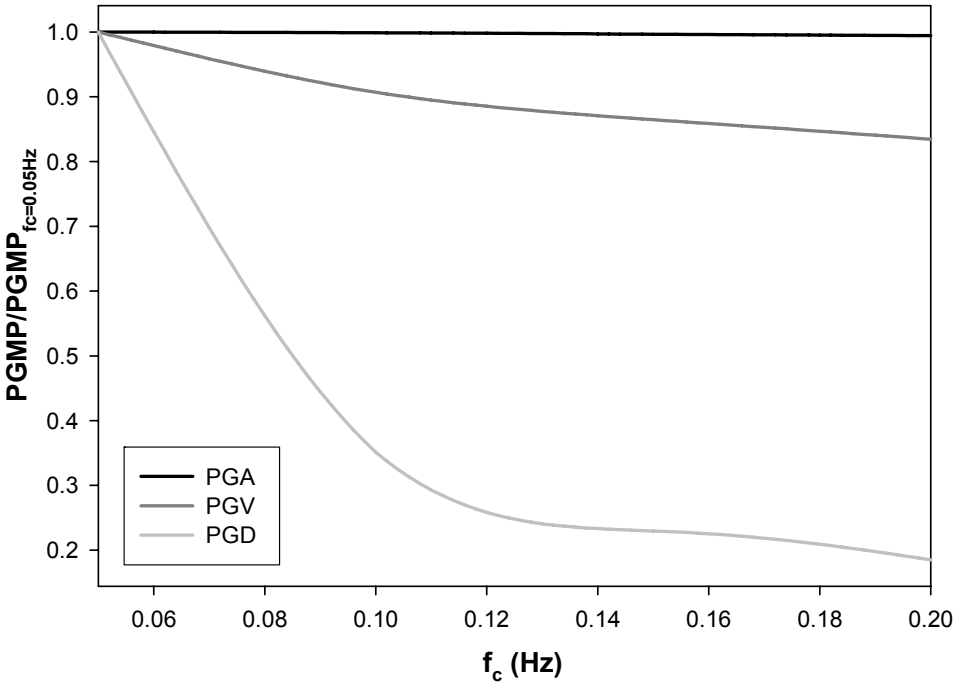

Figure 2.8 The peak values of acceleration, velocity and displacement of the 1978, Basso Tirreno, Italy earthquake (M_w=6) recorded at Naso station for different filter cut-off values normalized by the peak values of f_c=0.05Hz.

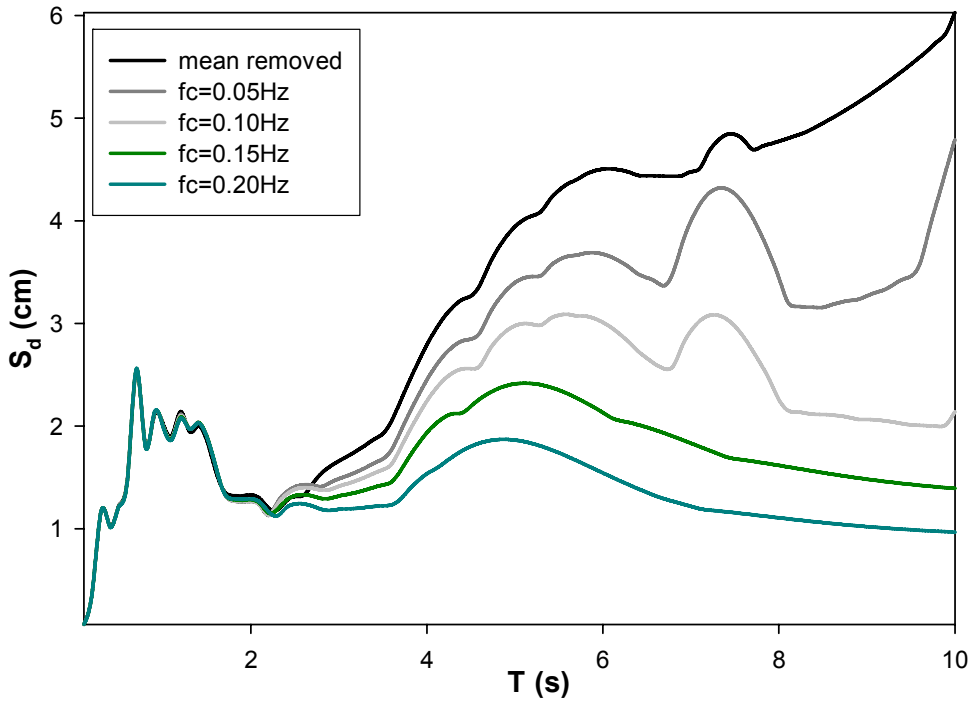

Figure 2.9 The spectral displacement spectrum of the 1978, Basso Tirreno, Italy earthquake (M_w=6) recorded at Naso station for different filter cut-off values.

The studies for the determination of a suitable T_c dates back to early 1970's. Trifunac and his co-workers offered a low-cut filter value of 0.06Hz to remove long-period noise from analogue accelograms (Trifunac, 1971; Trifunac et al., 1973). However, later studies indicated that low-cut filter value depends on the signal-to-noise ratio, so noise spectra models were proposed using fixed trace information on the original record (Lee and Trifunac, 1984; Lee and Trifunac, 1990; Trifunac and Todorovska, 2001; Skarlatoudis et al., 2003). Joyner and Boore (1988) used the theoretical corner frequency with a single-corner source spectrum model indicating that low-cut filter frequencies greater than the theoretical corner frequency of source spectrum may remove the actual frequency content of the signal. The corner frequency (f_c) defined by Joyner and Boore as a function of magnitude (M_w) is given in Eq. (2.1). The reciprocal of this therotical corner frequency is defined as the beginning of the constant displacement plateau by HAZUS (1997).

$$\log f_c = -0.5 \times (\mathrm{M_w} - 5) \qquad 2.1$$

Skarlatoudis et al. (2003) defined the low-cut filter frequency in a more complicated manner depending on the moment magnitude (M_w) and the hypocentral distance (D). The relationship between the filter cut-off corner frequency, moment magnitude and hypocentral distance (D) is given in Eq. (2.2). One particular difficulty in the application of Eq. (2.2) is the difficulty in obtaining the hypocentral distance for most events. In general, the ground motion catalogs do not display the full information for hypocentral distance because its precise calculation requires complete crustal information.

$$\log f_c = 0.1411 \log D - 0.32316\mathrm{M_w} + 1.36245 \qquad 2.2$$

The equations proposed by Trifunac and Todorovska (2001) for the determination of low-cut filter frequency is a function of shear-wave propagation velocity (V_s) in m/s and the moment magnitude. The relationship is given in Eq. (2.3). Similar to Eq. (2.2), the application of this expression can be difficult for sites that do not contain the shear wave velocity information.

$$\log f_c = \log(V_s) + 2.44 - 0.59\mathrm{M_w} \qquad 1.3$$

Boore and Bommer (2005) described the following possible methods for the determination of low-cut filter frequency for analogue records. The first one is the comparison of the Fourier Amplitude Spectrum (FAS) of the record with the FAS of the fixed trace. The decision on f_c is done by comparing the (signal+noise) to noise ratio. Figure 2.10 gives an example to illustrate this method. The FAS of the record given in Figure 2.7 is normalized by the FAS of the fixed trace of the same record. The (signal+noise) to noise ratio is taken as 3 (red line) for determining the low-cut filter value. It is accepted that below this limiting value, the signal is highly contaminated by noise. Figure 2.10 also displays a regression line that shows a general trend for the frequency interval beyond which the actual signal+noise to noise variation is significantly above the limiting value of 3. The analyst can assure that frequencies larger than the frequency value obtained by the intersection of regression line and (signal+noise)/noise=3 are dominated by the signal. For this particular example, the frequency computed from the intersection of these two trend lines is 0.35Hz (i.e. T_c=2.85s) that can be used for low-cut filtering the data.

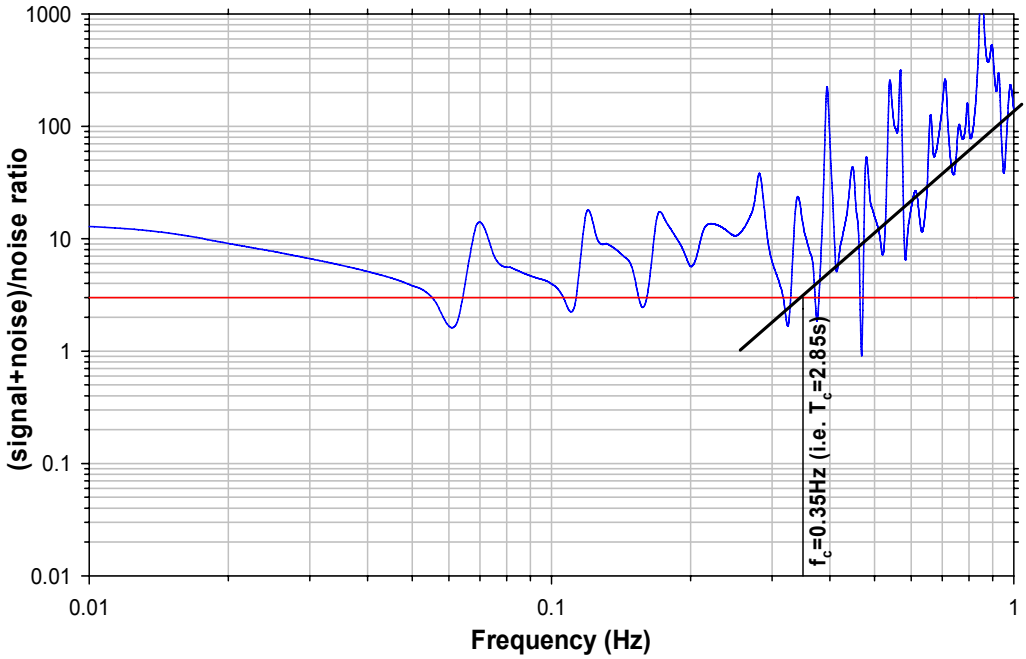

Figure 2.10 Direct comparison of (signal+noise) to noise ratio for the 1978, Basso Tirreno, Italy earthquake (M_w=6) recorded at Naso station for the determination of low-cut filter frequency.

The second method described by Boore and Bommer (2005) is the judgment of approximate low-cut filter frequency from the inspection of low frequency (i.e. long-period) behavior of FAS data. At low frequencies the FAS of the acceleration should decay proportional to the gradient of f^2 as dictated by the theoretical source spectrum (e.g., Brune 1970). Figure 2.11 shows the application of this method for the same record presented in Figure 2.10. The dashed red line approximately shows the decaying trend of f^2 gradient at low frequencies (long periods) that is fitted approximately by using the general behavior of FAS of the raw data. The general picture depicted suggests that frequencies approximately below 0.3Hz are contaminated by noise that results in an unexpected take-off with respect to the f^2 gradient of theoretical source spectrum. Therefore, the low-cut filter value should remove this undesired feature in order to yield a FAS trend compatible to theoretical behavior. This is achieved by applying a

low-cut filter value of 0.2Hz (i.e. T_c=5s) and the corresponding FAS is shown in Figure 2.11.

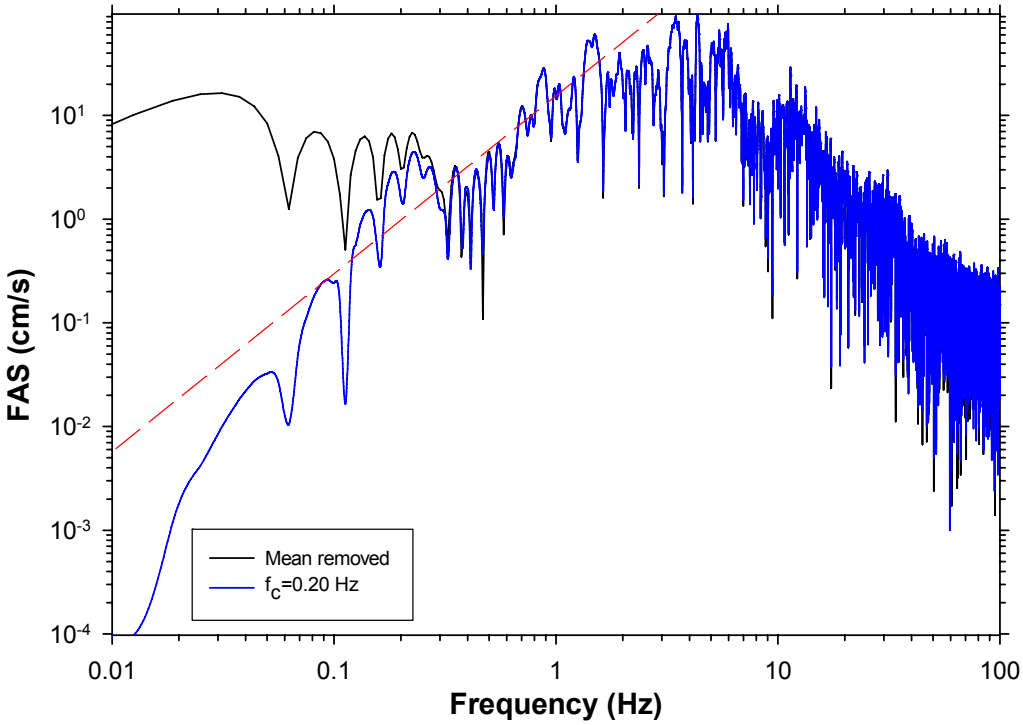

Figure 2.11 Comparison of FAS of the 1978, Basso Tirreno, Italy earthquake (M_w=6) recorded at Naso station with the FAS of the noise for the determination of filter corner frequency.

The resulting processed acceleration, velocity and displacement time series for the Naso station record are presented in Figure 2.12. The first column presents the low-cut filtered time series for a filter cut-off of T_c=2.85s determined from (signal+noise) to noise ratio (first alternative) and the second column displays the same information for a filter cut-off of T_c=5s computed from the second alternative that makes use of the low-frequency trend in theoretical source spectrum. The resulting velocity and displacement time series are reasonable by visual inspection which is another criterion that should be satisfied at the end of filtering process (

Boore and Bommer, 2005). The resulting velocity and displacement amplitudes of second procedure are larger than those obtained from the (signal+noise)/noise procedure that emphasizes the subjectivity in the determination of low-cut filter values during record processing. As the main objective of low cut filtering is the least distortion to the frequency content of the accelogram, one should prefer using the processed time series of second method for this particular example. This method results in a smaller T_c value with respect to the first method indicating lesser inference to the actual frequency content of ground motion.

The application of various methods for the determination of low-cut filter periods gives different results as illustrated by the examples presented. The subjectivity on this issue suggests that the analyst should consider various alternatives and decide on the best result that can be justified on a physical basis. Moreover, the analyst should be aware of the limitations of the filtered data for a given filter cut-off value. These issues will be treated in detail in the next chapters, particularly while presenting the proposed procedure.

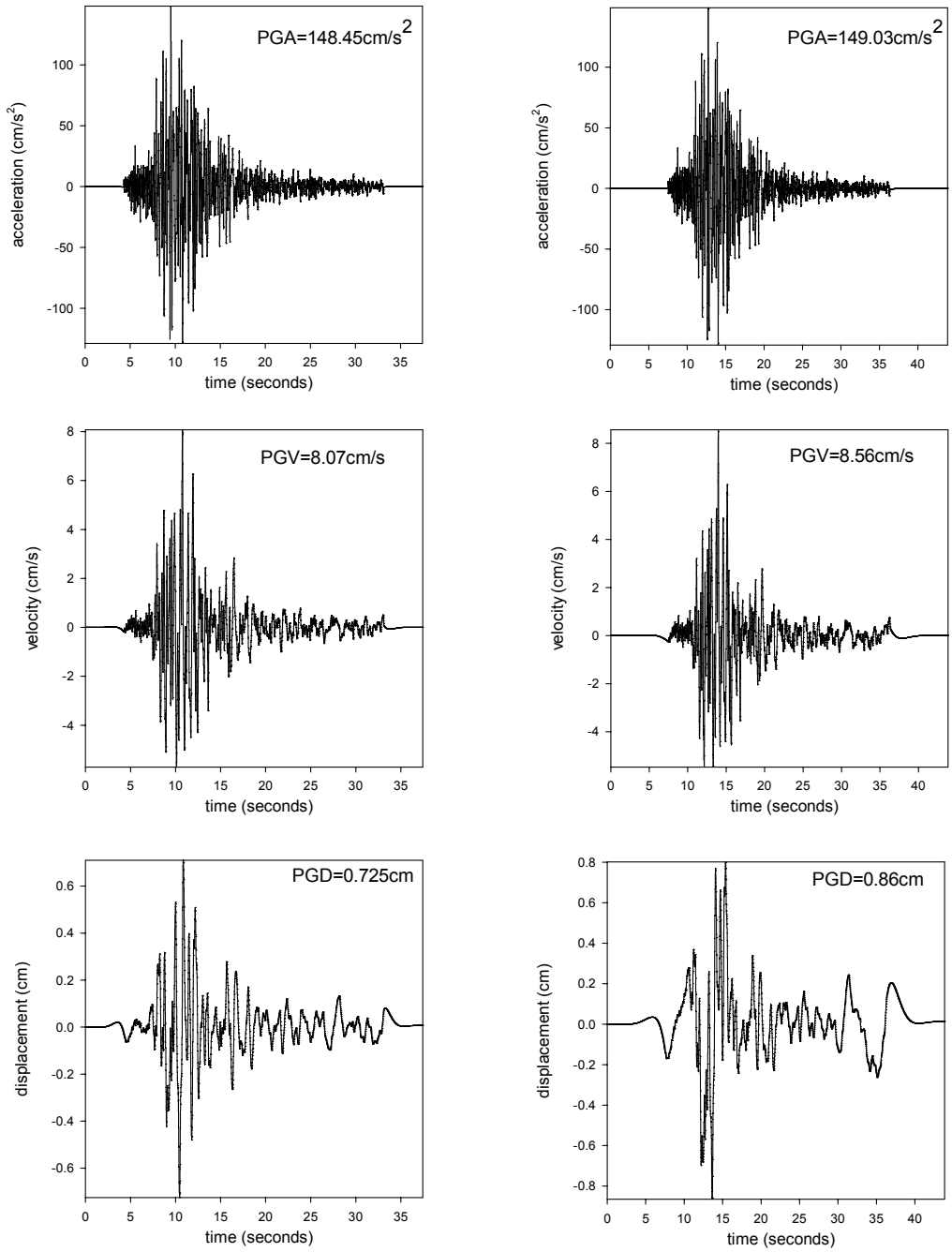

Figure 2.12 The resulting processed acceleration, velocity and displacement time series for the Naso Station.

CHAPTER-3

BASICS OF FILTERING

3.1. Introduction

In Chapter-2, it was stated that strong-motion accelograms provide detailed insight about ground shaking. They are the prime tools for earthquake engineering related research as well as professional work. The data obtained from accelograms is never noise-free; thus contaminated by noise from different sources. Therefore, the raw data from accelograms has to be processed to reduce the noise level as much as possible.

The subject of Chapter-3 is a brief description of digital filter theory since filters are the commonly used tools in ground-motion data processing. The purpose of filtering is to remove, in fact to reduce, the noise at long- and short-periods. Filters can be applied either in frequency or in time domain. A filter that removes high frequencies (short-periods) is called low-pass or high-cut filter, whereas a filter that removes the low-frequency content (long-periods) is called high-pass or low-cut filter. Although this chapter introduces the basics of filters, the main concern of the thesis is about high-pass (low-cut) filters that affect the spectral displacements significantly.

3.2. Basics of Filters

Basically, a filter response function has a value close to 1 in the range of frequencies that the analyst wishes to retain and close to 0 in the range of frequencies that the analyst wishes to eliminate. The filter can be applied in the time domain, by convolution of its transform function with the time series, or in the frequency domain by multiplying the filter transfer function with the Fourier Amplitude Spectrum (FAS) of the time series, resulting in the filtered time series after the inverse Fourier transform.

An ideal filter has a response of unity in the band-pass region and has a response of 0 outside the band-pass region. Figure 3.1 shows the response function of a low-pass, high-pass and a band-pass filter, respectively.

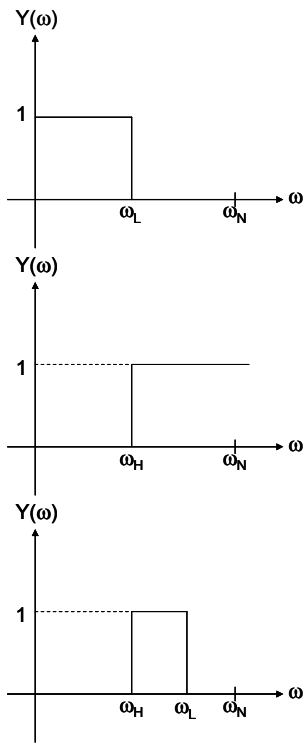

Figure 3.1 Transfer functions of ideal low-pass, high-pass and band-pass filters.

Depending on its functionality, structures like bridges or water tanks behave in the long-period range (low-frequency range). Moreover, even if the fundamental periods of some of the structures are initially in the short period range, when they behave beyond their elastic limits, their fundamental periods can shift towards longer periods due to the softening in their lateral stiffness properties. Thus, if the structural damage of such systems are correlated with the spectral displacement of ground motions, the influence of high-pass filtering becomes prominent. Reliable long-period info is also a necessity when equivalent linear methods are used in predicting nonlinear oscillator response or when one wants to have a spectral displacement compatible design spectrum. For this reason, the focus will be on high-pass filters. The detailed derivation of relevant equations about the filter theory is beyond the scope of the study. However, important equations that are useful in understanding the logic behind digital filtering are given in the following paragraphs.

The impulse response of an ideal high-pass filter is given as (Kanasewich, 1975):

$$W_n = -2\omega_H(\omega_N)^{-1} \times \frac{\left[\sin(\frac{n\pi\omega_H}{\omega_N})\right]}{\left[\frac{n\pi\omega_H}{\omega_N}\right]} \qquad n = \pm 1, \pm 2, ... \qquad 3.1$$

where; ω_N is the Nyquist frequency, that can be calculated by Eq. (3.2) The variable ω_H is the high-pass corner frequency given in Eq. 3.3.

$$\frac{\omega_N}{2\pi} = f_N = \frac{1}{2\Delta t} \qquad 3.2$$

$$\frac{\omega_H}{2\pi} = f_H \qquad 3.3$$

Figure 3.2 presents the impulse response of an ideal high-pass filter in time domain with a corner frequency of 100Hz for a digitizing time interval of Δt =0.002 seconds.

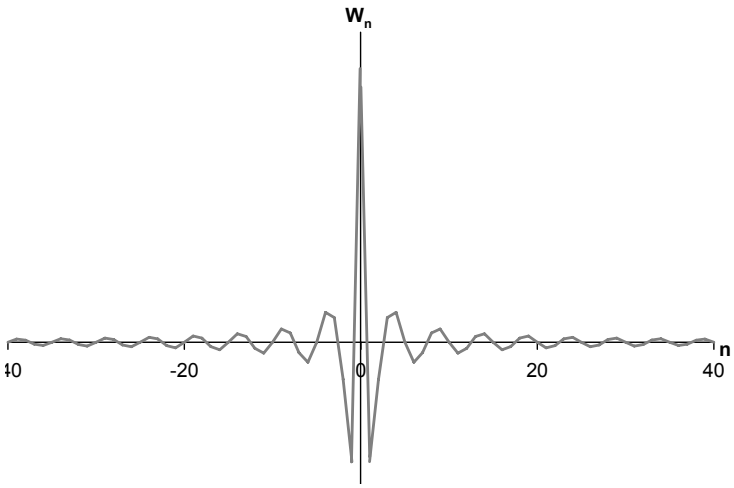

Figure 3.2 Impulse response of a high-pass filter with a cut-off frequency of 100Hz.

The impulse response is truncated after a certain number of terms. However, this truncation causes overshooting and ringing effects near points of discontinuity in the ideal high-pass filters. The overshooting and ringing is known as the Gibbs effect, which is a serious concern to obtain undistorted filtered data. This was explained by the mathematical physicist Josiah Gibbs in 1899 (Smith, 1999). Figure 3.3 shows the overshooting and ringing effect for 25 and 101 terms in impulse response for a truncated high-pass filter. Note that the increase in the number of terms causes the ringing effect to decrease, whereas the overshooting is slightly affected.

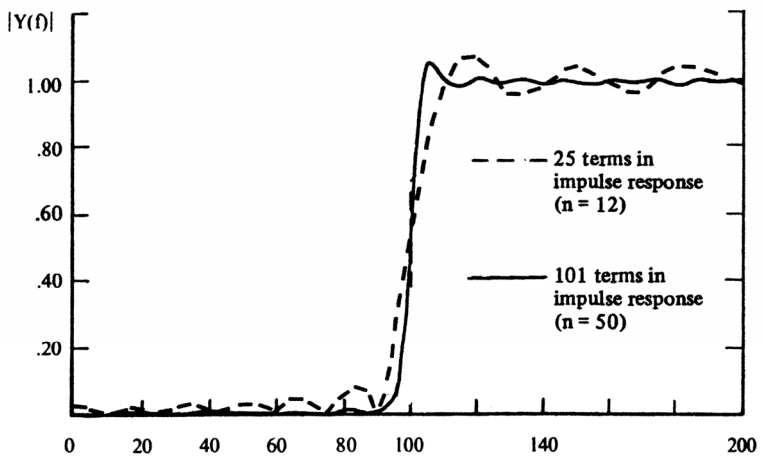

Figure 3.3 Overshoot and ringing effect for 25 and 101 terms in impulse response for a truncated high-pass filter (Kanasewich, 1975).

3.3. Butterworth Filters

Gibbs phenomenon is a restriction on the practical application of a truncated ideal filter. There are a wide range of filters such as Ormsby, elliptical, Butterworth, Chebychev and Bessel that minimize the Gibbs effect. Among these filters, Butterworth filter is the most widely used digital filter type in strong ground-motion data processing. The reason for its wide use is the maximally flat impulse response function inside and outside the band-pass. Moreover, the smooth transition of Butterworth filter between the roll-off frequency and the cut-off frequency does not experience the ringing effect that causes distortion in the processed data.

The square of the response of an ideal low-pass filter can be obtained in a more satisfactorily manner by a general function defined in Eq. (3.4) (Kanasewich, 1975):

$$\left|Y(\overline{\Omega})\right|^2 = \frac{1}{1 + A_n(\overline{\Omega})} \qquad 3.4$$

where; $\overline{\Omega}$ is the normalized frequency defined in Eq. 3.5.

$$\overline{\Omega} = \frac{\omega}{\omega_L} \qquad 3.5$$

The parameters ω and ω_L in Eq. (3.5) represent the circular frequency and the circular low-pass cut-off frequency, respectively. The function A_n takes values significantly greater than 1 when $\overline{\Omega} \rangle 1$. The values of A_n becomes significantly smaller than 1 when $\overline{\Omega}$ is in between 0 and 1.

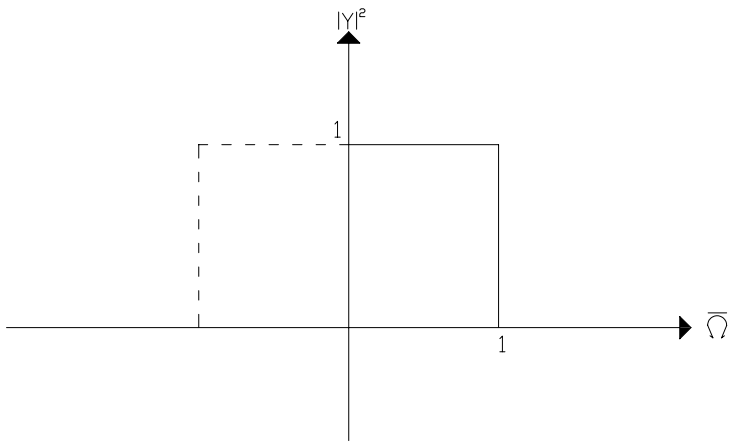

Figure 3.4 Response of an ideal low-pass filter given by equation (3.4).

The Butterworth filter lets;

$$A_n = \overline{\Omega}^{2n} \qquad n = 1,2,3,..... \qquad 3.6$$

to obtain a monotonic function as an approximation to the square response. The square of a low-pass Butterworth transfer function is expressed as follows (Kanasewich, 1975):

$$\left| Y_L(\overline{\Omega}) \right|^2 = \frac{1}{1 + \overline{\Omega}^{2n}} \qquad 3.7$$

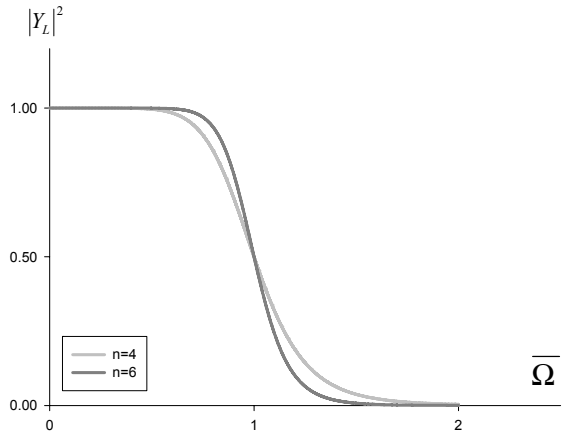

Figure 3.5 The square of the transfer functions of a low pass Butterworth filter for n=4 and n=6. The curve is maximally flat inside and outside the band pass. A larger value of order, n, yields a faster decay rate in filter response.

High-pass filters can be obtained by applying an appropriate complex-valued frequency transformation to the low-pass filter. Let the frequency for the low-pass functions be designated by (Kanasewich, 1975)

$$p = i\overline{\Omega} \qquad 3.8$$

The frequency in high-pass transfer function in complex frequency is given by

$$s = i\overline{\omega} \qquad 3.9$$

In Eqs. (3.8) and (3.9), $\overline{\Omega}$ and $\overline{\omega}$ are dimensionless frequencies. The index i denotes that parameters are complex valued. The relationship that converts one filter type to the other can be designated by

$$p = W(s) \qquad 3.10$$

For a high-pass filter, this relationship is

$$p = \frac{1}{s} \qquad 3.11$$

Substituting Eqs. (3.8) and (3.9) into Eq. (3.11) results in Eq. (3.12)

$$\overline{\Omega} = -\frac{1}{\overline{\omega}} \qquad 3.12$$

If the transformation given in Eq. (3.12) is applied to the low-pass Butterworth filter of order n (presented in Eq. (3.7)), the square of the transfer function for the high-pass Butterworth filter is obtained

$$\left|Y_H\right|^2 = \frac{1}{1+\left(-\frac{1}{\overline{\omega}}\right)^{2n}} = \frac{1}{1+\frac{1}{\overline{\omega}^{2n}}} = \frac{1}{\frac{\overline{\omega}^{2n}+1}{\overline{\omega}^{2n}}} = \frac{\overline{\omega}^{2n}}{1+\overline{\omega}^{2n}} \qquad 3.13$$

Note that the square of the transfer function of the high-pass filter is equal to subtracting the low-pass filter transfer function from 1.0 in the frequency domain. This is shown in Eq. (3.14). Note that the dimensionless frequency parameters $\overline{\Omega}$ and $\overline{\omega}$ are used interchangeably in Eqs. (3.13) and (3.14). This does not introduce any complexity because both parameters serve for the same purpose: definition of dimensionless frequency.

$$1-\left|Y_L(\overline{\Omega})\right|^2 = 1-\frac{1}{1+\overline{\Omega}^{2n}} = \frac{\overline{\Omega}^{2n}}{1+\overline{\Omega}^{2n}} \qquad 3.14$$

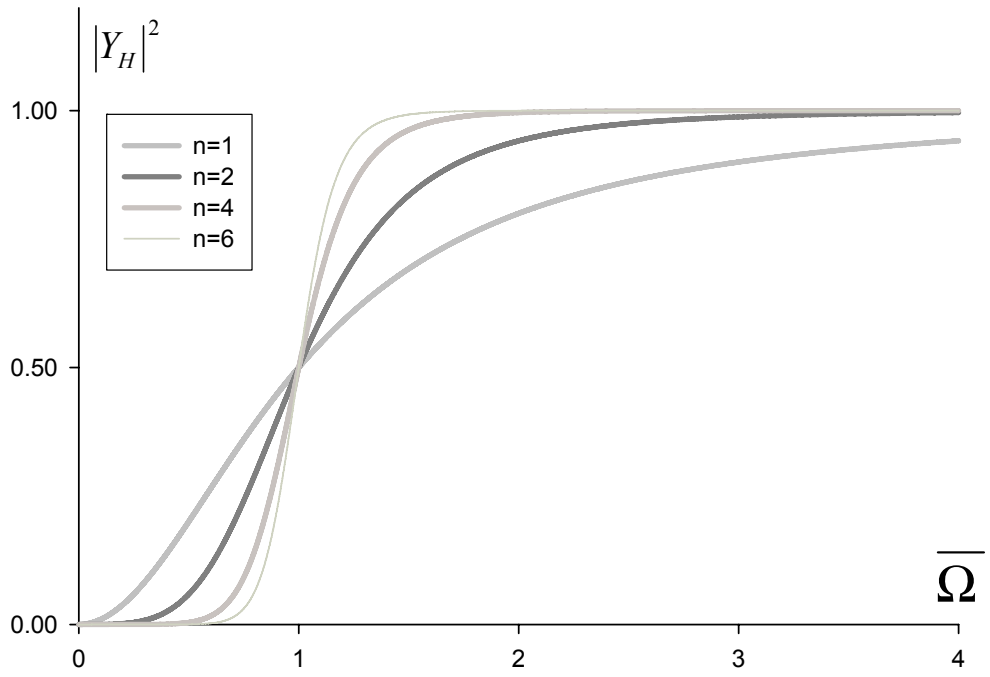

Figure 3.6 Square of the transfer functions for a high-pass Butterworth filter of different orders. Note that the decay rate of filter is related to the order of Butterworth filter.

3.4. Poles and Zeros of the Butterworth Filter

The values that make the transfer function zero are called zeros of the filter. When the transfer function of Butterworth filter is investigated, one can see that this digital filter has no zeros except at $\omega \to \infty$.

The singularities of a filter transfer function are called poles of the filter. The poles of a high-pass Butterworth filter and a low-pass Butterworth filter are equal since the denominator of low-pass and high-pass Butterworth filter transfer functions are the same. The poles of a Butterworth filter can be obtained easily by examining the Laplace transform of the transfer function. The Laplace transform is obtained from the Fourier transform by using $\rho = i\overline{\Omega}$ (Kanasewich, 1975). The parameter

ρ is designated as the Laplace transform variable. The Laplace transform of the denominator of Butterworth filter function is given in Eq. (3.15). The poles are located at places where this expression is zero.

$$1+(-1)^n \rho^{2n} = 0 \qquad 3.15$$

Multiplying both sides of Eq. (3.15) by $(-1)^n$ results

$$\rho^{2n} + (-1)^n = 0 \qquad 3.16$$

The location of the poles can be determined by using complex number theory. A complex number, ψ, can be written as (Kanasewich, 1975);

$$\psi = re^{i\theta} \qquad 3.17$$

The mth root of a complex number is found by Eq. 3.18.

$$\psi^{1/m} = r^{1/m} e^{(\theta+2\pi k)/m} \quad k = 0,1,2,...m-1 \qquad 3.18$$

The poles of a first order Butterworth filter (n=1) can be found by using Eq. (3.18) for $\theta = 0$. Setting n=1 in Eq. (3.16b);

$$\rho = 1^{1/2} = e^{1/2(2\pi k)} \quad k = 0,1$$
$$i\overline{\Omega} = e^0 = 1$$
$$i\overline{\Omega} = e^{\pi} = -1$$

The poles of a second order Butterworth filter is obtained by setting n=2 in Eq. (3.16).

$$\rho^4 + (-1)^2 = 0$$
$$(\rho^4 + 1) = 0$$

By using Eq. (3.18) for $\theta = \pi$

$$\rho = (-1)^{1/4} = e^{i(\pi+2\pi k)/4} \quad k = 0,1,2,3$$
$$\rho = e^{i\pi/4}, e^{i3\pi/4}, e^{i5\pi/4}, e^{i7\pi/4}$$

Therefore, the poles of a second order Butterworth filter are located at $-\sqrt{2} \pm i\sqrt{2}$ and $+\sqrt{2} \pm i\sqrt{2}$. The pole locations of the first and second order low-pass and high-pass Butterworth filters are shown in Figure 3.7. In the above examples the parameter θ takes different values. The only reason for the variation in θ is to satisfy the equality between Eqs. (3.16) and (3.19).

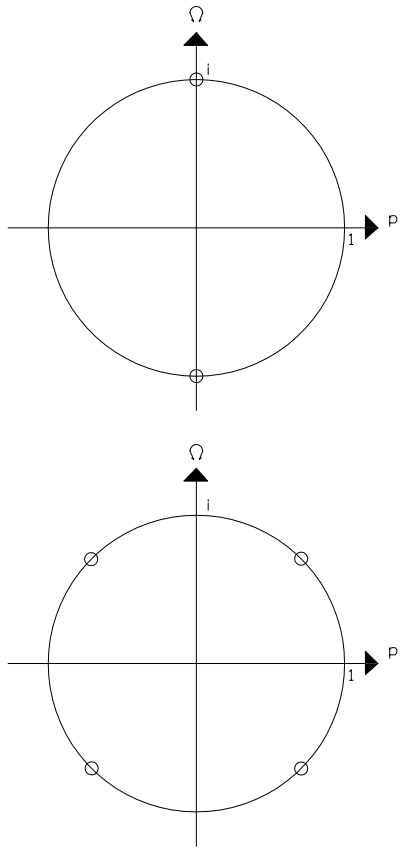

Figure 3.7 Pole locations of a first and a second order low-pass and high-pass Butterworth filters. Pole locations are displayed by open circles in the complex plane.

The decay rate of a filter is directly related with the number of poles. In general, a single pole in the transfer function changes the decay rate by 6 db (Kanasewich, 1975; Scherbaum, 2001). Figure 3.8 shows the square of

the transfer functions of high-pass Butterworth filters with different pole numbers.

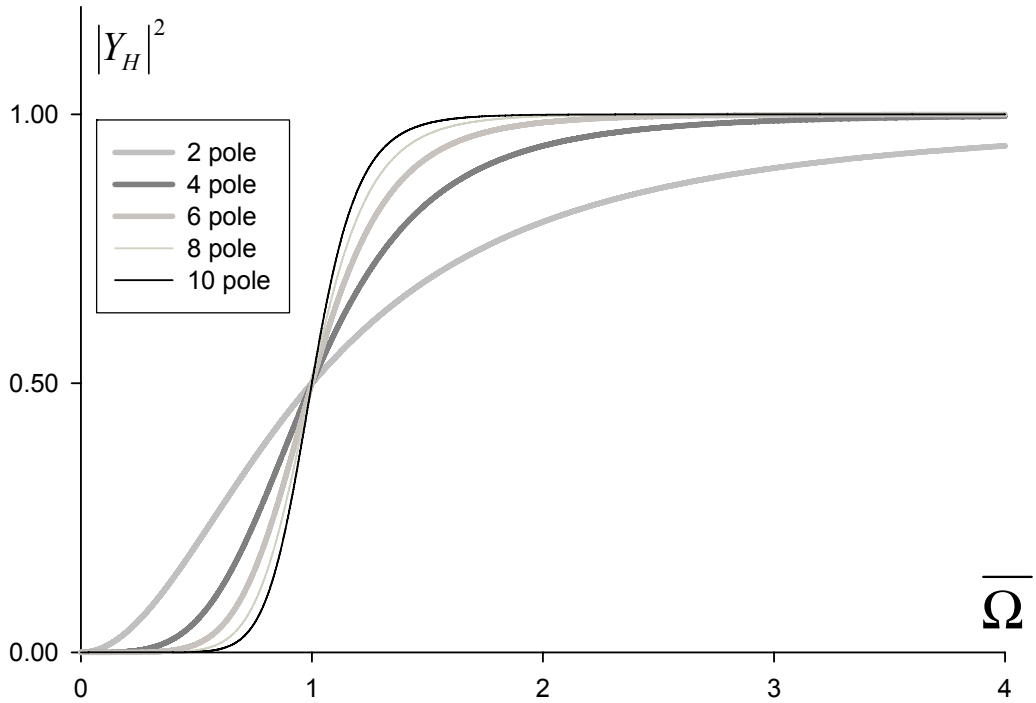

Figure 3.8 Square of the transfer function of a high-pass Butterworth filter for different number of poles.

3.5. Causal and Acausal Butterworth Filters

The fundamental choice between filters is the causality of the filter. Causal filters introduce phase shifts in the processed data since they are applied in one direction from the beginning to the end of the time series. The unidirectional application of a filter brings forward the phase differences that inherently exist in the complex fourier transform of the filter transfer function. Acausal filters do not produce any phase distortion (i.e. zero-phase shift). The zero phase shift at all frequencies can be obtained easily by implementing cascade form filtering (Kanasewich, 1975). The data can

be filtered using a convolution or a recursive technique in a normal manner (i.e. in one direction). The output from this process is reversed and passed through the same filter again. Reversing the once-filtered data and passing it from the same digital filter results in a zero-phase shift in the filtered data (acausally filtered data). In other words, the reverse filtering neutralizes the phase shifts introduced during the first-pass of the filter transfer function from the beginning to the end of the time series. The decay rate of the amplitude response at acausal filters is twice of the causal filters since the data is filtered twice. This can be visualized easily in the frequency space, because passing the same filter in the reverse direction is actually multiplying the original transfer function of the filter by itself again in the frequency domain. The schematic algorithm of cascade operation is shown in Figure 3.9.

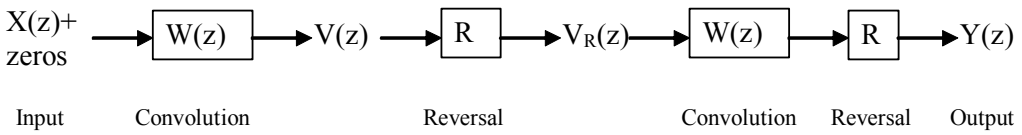

Figure 3.9 The cascade operation diagram

As indicated in the scheme presented in Figure 3.9, a sufficient number of zeros must be added to the data to allow the output from the initial stage of convolution to become significantly small (Kanasewich, 1975). In other words, the data should be padded with leading and trailing zeros in order to accommodate the filter transients due to forward-reverse direction filtering. The zero pad length can be determined by using Eq. (3.19) (Converse and Brady, 1992)

$$T_{zpad} = \frac{1.5n}{f_c} \qquad 3.19$$

where, T_{zpad} is the total length of zeros to be added to the record, n is the order of the Butterworth filter and f_c is the filter corner frequency. In the practical applications half of T_{zpad} is added at the beginning of the time series. The other half is added to the end of time series.

Figure 3.10 shows the total length of the time-domain zero pad lengths recommended by Converse and Brady (1992) for different filter corner frequencies and for different filter orders. As can be seen from the figure, the increase in filter order and decrease in the filter cut-off frequency (i.e. increase in the filter cut-off period) causes an increase in the zero pad length.

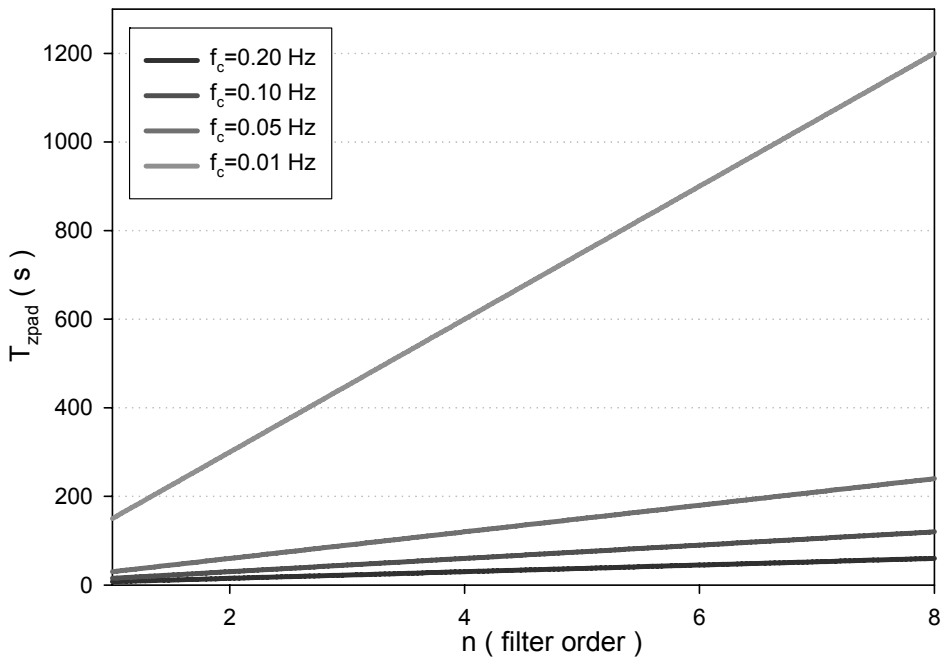

Figure 3.10 Total length of time-domain zero padding recommended by Converse and Brady (1992) for different filter orders and filter corner frequencies.

Removal of zero pads after the application of acausal filter results in incompatibility in the processed data. The consequence of this removal is

usually the offsets and the trends in the integrated velocity and displacement time series (Boore and Bommer, 2005). As a matter of fact, removal of zero-pads after acausal filtering causes the diminishing of genuine acausal filter effects. The zero pads should be kept as part of the originally filtered data after acausal filtering. Figure 3.11 shows the acceleration, velocity and displacement time series derived from the ground-motion record given in Figure 2.7 for padded and pad stripped-off data from the acausally filtered acceleration traces for a filter cut-off frequency of 0.1Hz (i.e. T_c=10s). As can be seen from the figure, the removal of pads after acausal filtering causes incompatibility in the displacement traces. This effect can also be observed in the integrated velocity traces.

The effects of causal and acausal filters come into the view especially when the concern is long spectral periods. By using two digital records of Hector Mine, California earthquake Boore and Akkar (2003) showed that the inelastic displacement spectrum is sensitive to the causality of the filter especially for long period ranges. Figure 3.12 shows the 5% damped response spectra of the analogue Tabas strong ground-motion record for different inelastic levels for causal and acausal filters. The level of inelasticity is presented by the constant strength factor (R) that is also called as the normalized lateral strength ratio. This ratio is defined as the elastic to yield strength of an oscillator. The plots in this figure indicate that, the sensitivity of spectral displacements to the filter cut-off increase as the level of inelasticity increases (i.e. R increases) especially for causally filtered data. It should be noted that the data is filtered for low-cut filter periods of 10 and 20 seconds (i.e. f_c=0.1 and 0.05Hz), respectively. The discrepancy between the causally filtered inelastic spectra for different filter cut-offs start at periods significantly earlier than the filter cut-off periods used. This is not the case for acausally filtered displacement

spectra. This observation marks once again how analogue records are sensitive to the changes in filter periods for causally filtered data.

Different organizations use different digital Butterworth filters in their data processing methods. Pacific Earthquake Engineering Research Center (PEER) uses a 4-pole causal Butterworth filter. U.S. Geological Survey (USGS) uses a cascade 2pole/2pole acausal Butterworth filter, whereas California Strong Motion Instrumentation Program (CSMIP) uses a 4-pole acausal Butterworth filter. CSMIP applies Butterworth filtering directly on the frequency domain (Skarlatoudis et al., 2003). Figure 3.13 shows gain vs. f/f_c graphs of different Butterworth filters.

In this study, a 2pole/2pole cascade acausal Butterworth filter is used for the calculation of spectral displacements that are discussed in the next chapters. Acausal Butterworth filter is used since it causes no phase shift and spectral values are less sensitive to the acaual filter particularly in the inelastic range. This is the recommendation of many authors such as Lee and Trifunac (1990), Boore and Akkar (2003) and Boore and Bommer (2005). The pads added to the acceleration traces for acausal filtering are not removed since their removal causes incompatible filtered time series as discussed in this chapter.

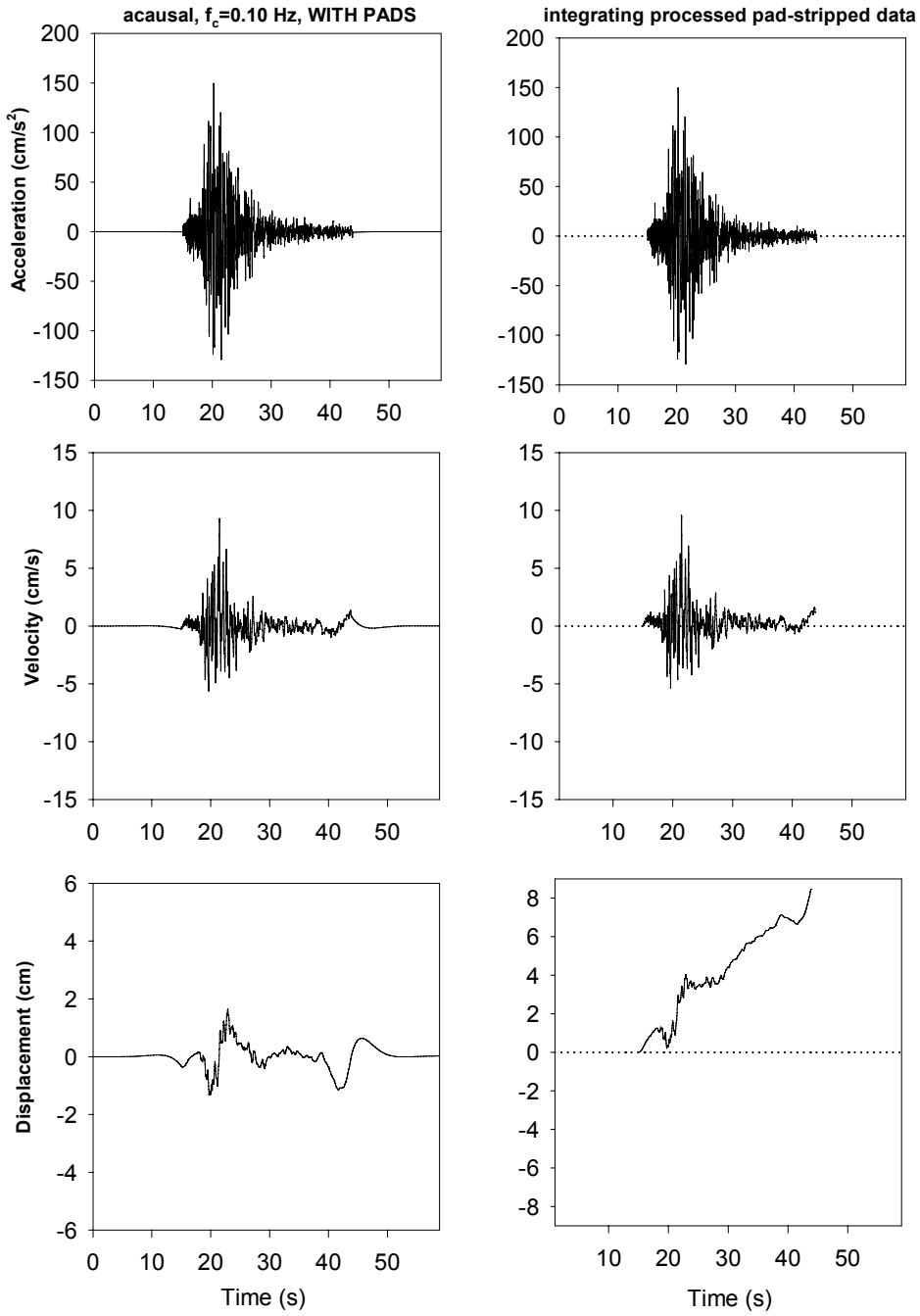

Figure 3.11 Acceleration, velocity and displacement traces derived from an acausally filtered data with zero pads and pads stripped-off. The ground motion used is from an aftershock (M_w=5.2) of the 1981, Lucano Italy earthquake.

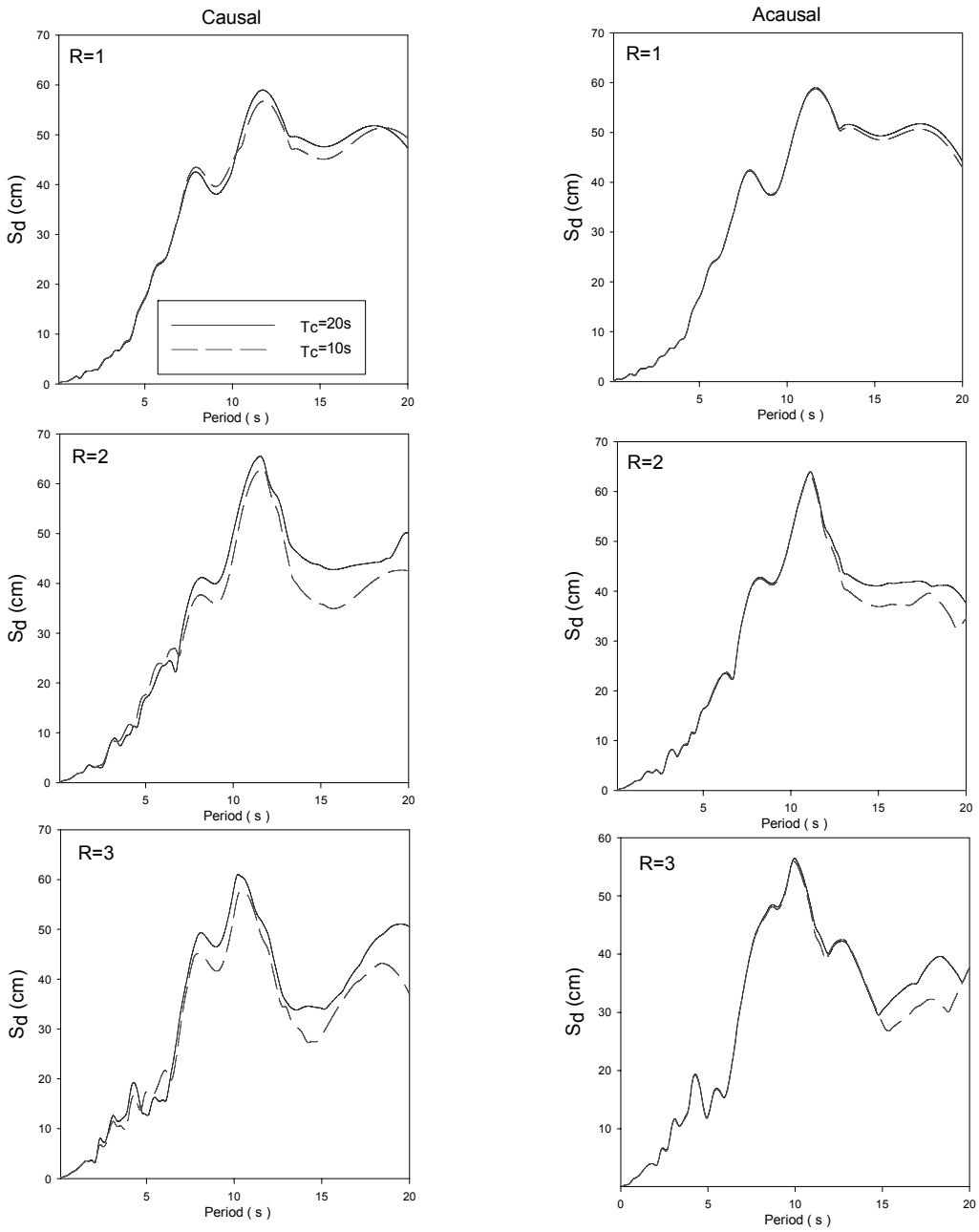

Figure 3.12 Displacement response spectra for 1990 Tabas, Iran earthquake (M_w=7.4) for R=1 (elastic),2 and 3 using causal and acausal filtering.

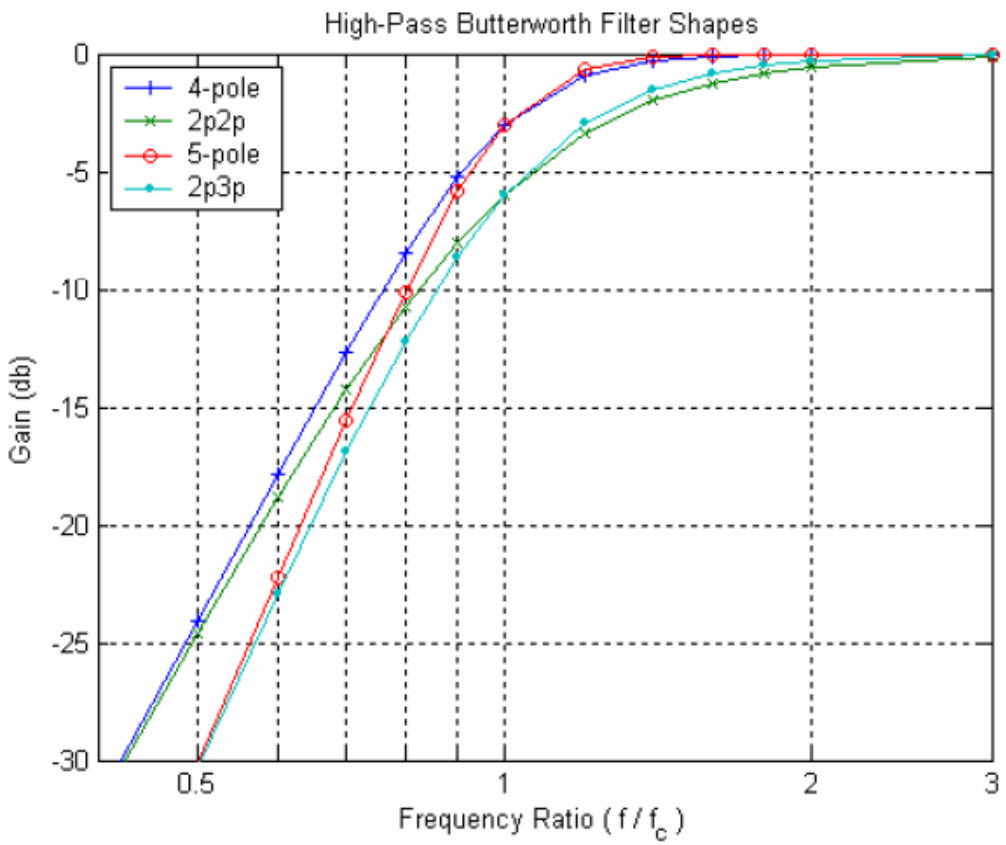

Figure 3.13 Frequency response of different Butterworth filters of different orders (Bazzurro et al., 2004).

CHAPTER-4

INFLUENCE OF LOW-CUT FILTER VALUES ON SDOF LINEAR AND NONLINEAR DEFORMATION DEMANDS

4.1. Introduction

The objective of this chapter is to evaluate the effect of low-cut filter period (T_c) on the elastic and inelastic single-degree-of-freedom (sdof) deformation demands for analogue records. The analogue records are selected from the recently compiled European ground-motion database (Ambraseys et al., 2005) and they consist of recordings from rock, stiff and soft sites for different magnitude ranges. Two distinct noise spectra are used to compute alternative T_c values for the subject ground-motion database in order to observe the particular effects of low-cut filter periods on sdof deformation demands. This chapter also discusses the influence of low-cut filter on peak ground motion values using the time series processed by the T_c values from the alternative noise spectra.

4.2. Ground-Motion Database and Noise Spectra Used

A total of 156 rock (V_s>750m/s), 264 stiff (360m/s<V_s<750m/s) and 108 soft site (V_s<360) records were selected from the recently compiled European ground-motion data-base (Ambraseys et al., 2005). The existence of pre- and post-event buffer was used as the criterion to decide

whether the record under consideration is analogue or digital. The records chosen do not exhibit pre- and post-event buffers. Each ground motion was pre-viewed to ensure that they do not contain any non-standard errors. The moment magnitude (M_w) values range between 5 and 7.6 and site-to-source distance (Joyner and Boore distance, R_{jb}, Joyner and Boore,1981) ranges between 0 to 50 km. Figure 4.1 presents the distance vs. magnitude scatter for the chosen ground motions. Tables given in Appendix-A list the ground motions used in this chapter.

The long-period noise was removed from the raw acceleration data by using two different noise spectrum models (Trifunac and Todorvska, 2001; Skarlatoudis et al., 2003). Prior to filtering, the mean acceleration value determined from the entire record length was subtracted from the accelogram as an initial baseline adjustment. The low-cut filtering was done as described in the last paragraph of Chapter-3. The noise models are based on detailed studies using the available fixed trace data featured on the original film record. The noise spectrum TT01 (Trifunac and Todorovska, 2001) represents typical digitization noise in analogue records digitized either manually or automatically. The noise spectrum SPM03 (Skarlatoudis et al., 2003) is derived by making use of the analogue ground motions recorded in Greece. These noise spectra are presented in Figure 4.2 with an extra model described in Lee and Trifunac (1990) for a record length of 22 seconds. The variability in the proposed noise levels is not surprising as each study focused on a particular sensor-digitizer combination of interest. The noise amplitude model used by Skarlatoudis et al. (2003) was discussed in Chapter-2. It considers the sensitivity of filter cut-off to moment magnitude and hypocentral distance.

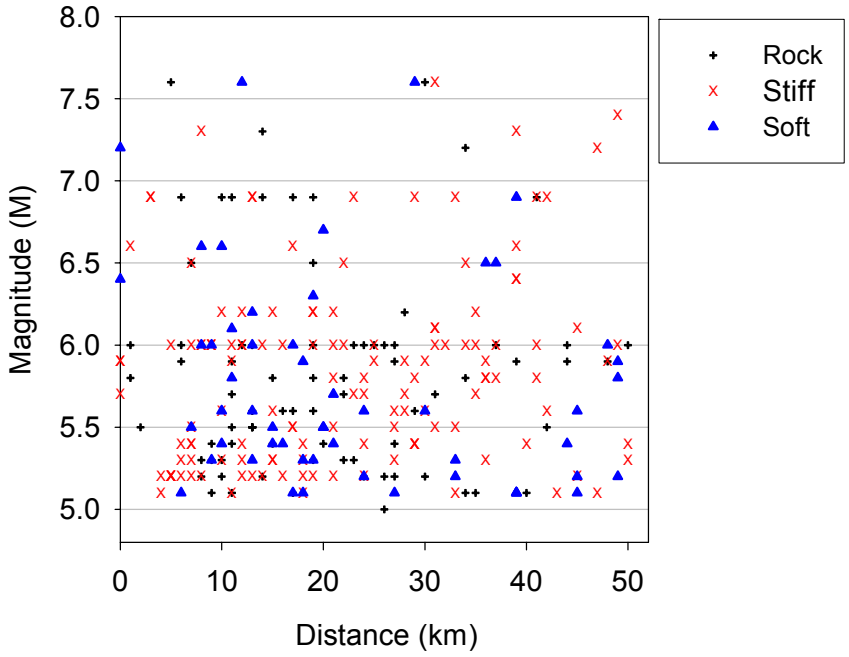

Figure 4.1 Distance vs. magnitude scatter for rock, stiff and soft site recordings used in Chapter-4.

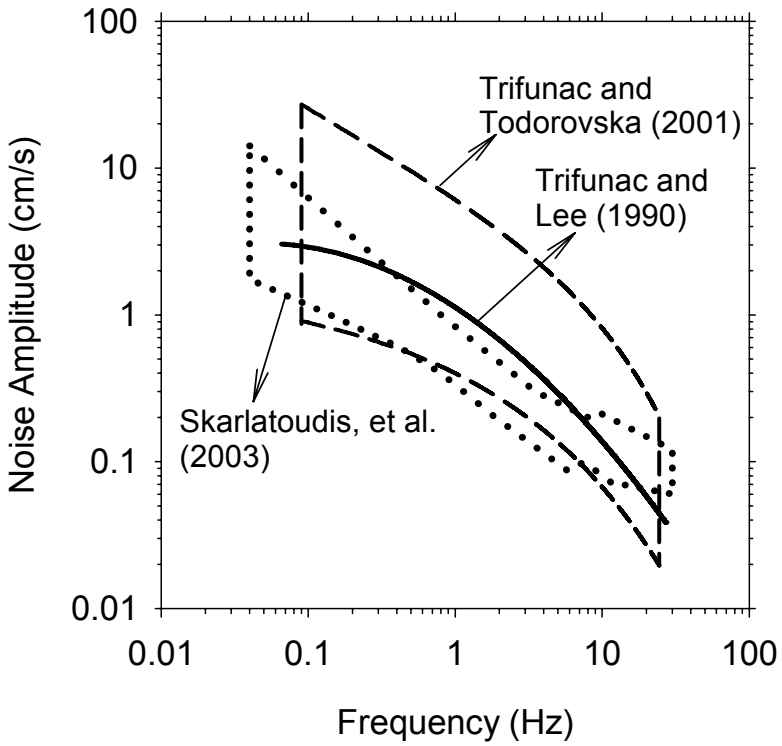

Figure 4.2 Some of the noise amplitude models for analogue records proposed in the literature.

Figure 4.3 shows the magnitude vs. f_c (f_c=1/T_c) scatter diagrams for TT01 and SPM03 for rock, stiff and soft site records. The low-cut filter values of SPM03 were computed by using Eq. (2.2) whereas f_c values of TT01 were computed using the lower and upper bounds illustrated in Figure 4.2. The smoothed Fourier amplitude spectrum (FAS) of the raw accelogram was compared with the upper and lower bounds of TT01. The smaller frequency value where signal-to-noise ratio is 2:1 at the intersection of the smoothed FAS and TT01 noise amplitude boundaries was determined as f_c. In some cases, when necessary, the lower and upper bounds of TT01 noise amplitude were prolonged towards lower frequency (i.e. longer periods) values in order to determine the f_c values. The decision on signal-to-noise ratio 2:1 is arguable but this criterion is compatible with Eq. (2.2) that is based on the same signal-to-noise ratio (Skarlatoudis et al., 2003). The plots in Figure 4.3 also show the general tendency of these two models with respect to magnitude by fitting simple regression curves. The low-cut filter frequency scatter and the corresponding regression curve for SPM03 show a clear dependence on magnitude as implied by Eq. (2.2). The low-cut filter values suggested by TT01 exhibit a dispersive picture but the pertaining regression curves also indicate a magnitude dependency for this relationship. The low-cut filter frequencies presented in these plots clearly show that the use of TT01 and SPM03 would result diverse f_c values for a particular record.

4.3. Effect of Low-Cut Filter Frequency on Peak Ground Motion Values

Figure 4.4 presents the mean statistics for peak ground acceleration (PGA), peak ground velocity (PGV) and peak ground displacement (PGD) for rock, stiff and soft soil sites, respectively. The peak ground-motion values of the processed data using TT01 low-cut filter values were

normalized by the processed PGA, PGV and PGD values computed by the f_c values of SPM03. The normalized peak ground-motion values are used for the derivation of the statistics. It is believed that the normalized mean statistics would allow making clear observations for the distinct effects of low-cut filter frequency on peak ground-motion values. A mean value less than 1 indicates that on average, peak ground-motion values computed from SPM03 model are higher than the peak ground values computed using the f_c values of TT01. Figure 4.4 also shows the standard deviations of normalized mean values that are displayed at the top of each vertical bar. As expected, the least affected peak ground-motion value from the low-cut filter frequencies is the peak ground acceleration. The normalized mean values are almost equal to 1 associated with very low standard deviations with respect to the standard deviations computed for PGV and PGD.

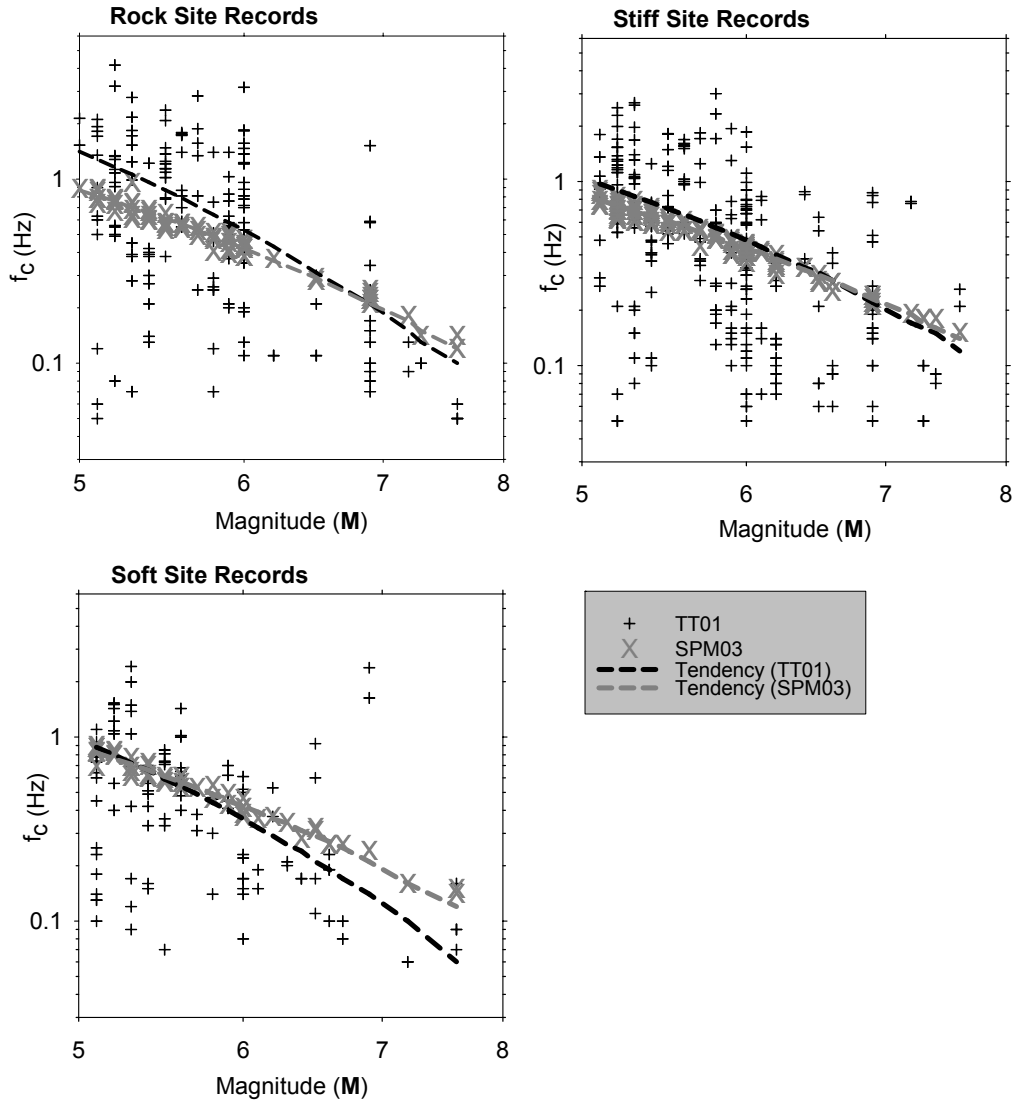

Figure 4.3 Scatter plots for f_c values suggested by TT01 and SPM03.

The normalized mean values for PGV do not show large variations with respect to PGD statistics. The corresponding standard deviations are also significantly lower than the ones computed for PGD. On average, the PGV values computed by using TT01 low-cut filter frequencies are 3 percent lower than the ones computed by SPM03 f_c values. This is expected as PGV is dominated by the mid-frequency components of ground motion where TT01 suggests higher low-cut filter values as presented in Figure 4.2. Figure 4.4 indicates that low-cut filter frequency has a considerable

influence on PGD. This ground-motion intensity measure does not portray a reliable picture for its use in seismic hazard or seismic damage-based studies. Peak ground displacements computed by using TT01 low-cut filter values are on average 20-,36- and 37-percent larger than the ones computed from the SPM03 low-cut frequency values for rock, stiff and soft site records, respectively. It is a well-known fact that low-frequency ground-motion components govern PGD. The lower bound noise amplitude of TT01 that yields smaller low-cut values at lower frequencies (i.e. at longer periods) with respect to SPM03 is the reason behind larger PGD values computed from the ground motions processed by TT01 low-cut filter values. The higher standard deviations for PGD fortify the above observations indicating that different low-cut filtering values impose significant uncertainty for this peak ground-motion parameter. It should be noted that the general procedure depicted from Figure 4.4 does not include the particular influence of magnitude and filter cut-off interaction on peak ground-motion values. A detailed discussion about the filter cut-off effects on peak ground-motion values considering the magnitude influence is presented in Akkar and Bommer (2007).

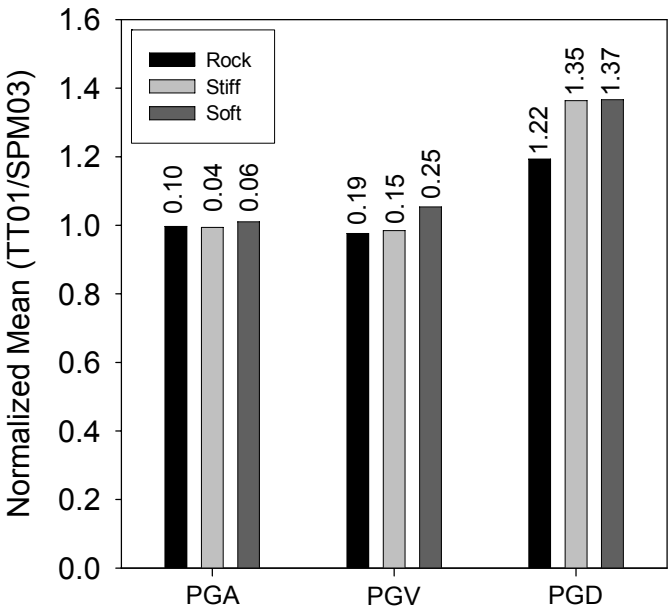

Figure 4.4 Normalized statistics for peak ground values.

4.4. Low-Cut Filter Period Effect on Elastic Spectral Displacements

Figures 4.5, 4.6 and 4.7 show the influence of low-cut filter periods on elastic spectral displacements for rock, stiff and soft site records, respectively. The ground motions for rock and soft sites are divided into 3 magnitude bins, whereas the number of bins for stiff sites are 4. The reason for the difference in the number of bins is due to the change in record numbers in different magnitude intervals. For rock and soft sites, the number of records for establishing meaningful statistics are only adequate when ground motions of M>6 are incorporated into one single bin. Using different magnitude intervals, the particular effect of magnitude for low-cut filter values on elastic displacement spectrum is investigated. The dashed lines in the figures show the mean low-cut filter values suggested by TT01 and SPM03 for each magnitude range. The dashed lines and spectral displacement curves in gray represent the pertaining values computed from the TT01 model whereas black color shows the spectral displacement and average low-cut filter values for SPM03. The displacement spectra were computed for a period range of 0.1 to 10 seconds.

Figures 4.5, 4.6 and 4.7 show that low-cut filtering has a significant effect on low-magnitude spectral displacements and the level of influence is more apparent for rock site records. This observation indicates that relatively large amount of long-period information can be retrieved from ground motions recorded on softer sites and for larger magnitude events after filtering. Another important observation that is highlighted in these figures is the sensitivity of spectral displacements to low-cut filtering at periods significantly shorter than the low-cut filter period. The spectral displacements of low-magnitude events and rock site records are more sensitive to the changes in low-cut filter values as the discrepancy in

spectral displacements computed from TT01 and SPM03 start at periods considerably shorter than the mean low-cut filter periods displayed by dashed lines. It should be noted that different noise amplitude models yield large variations in spectral displacements depending on the magnitude and site class. Previous studies suggested the use of spectral values up to $0.8T_c$ is insufficient to eliminate the filter cut-off effect on the spectral response (Spudich et al., 1999; Abrahamson and Silva, 1997). Based on the results presented here, magnitude and site class also play a role about the influence of low-cut filtering on spectral displacements and these seismological features should be considered for a proper choice of low-cut filter value during the record processing.

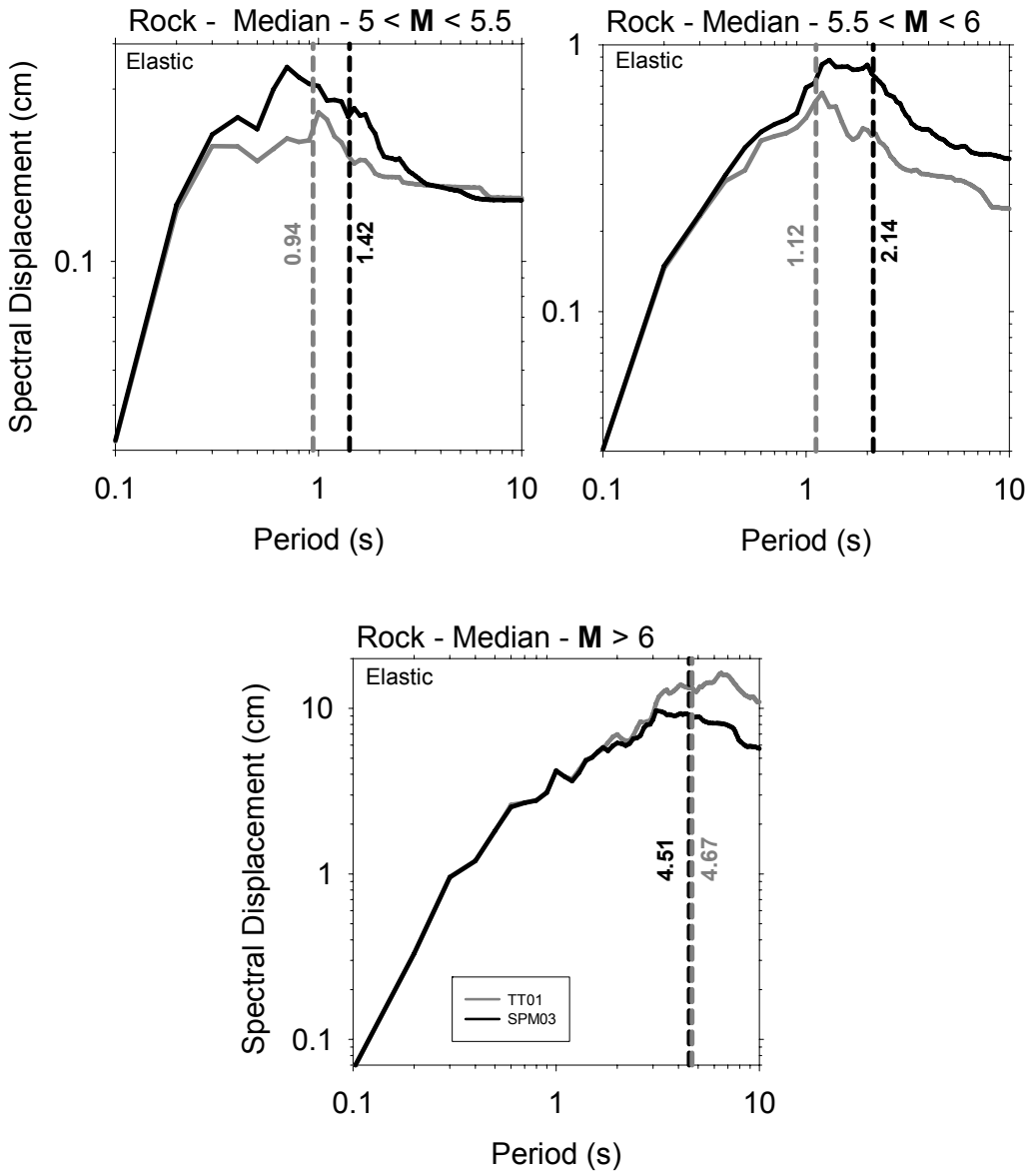

Figure 4.5 Elastic spectral displacements for rock site records.

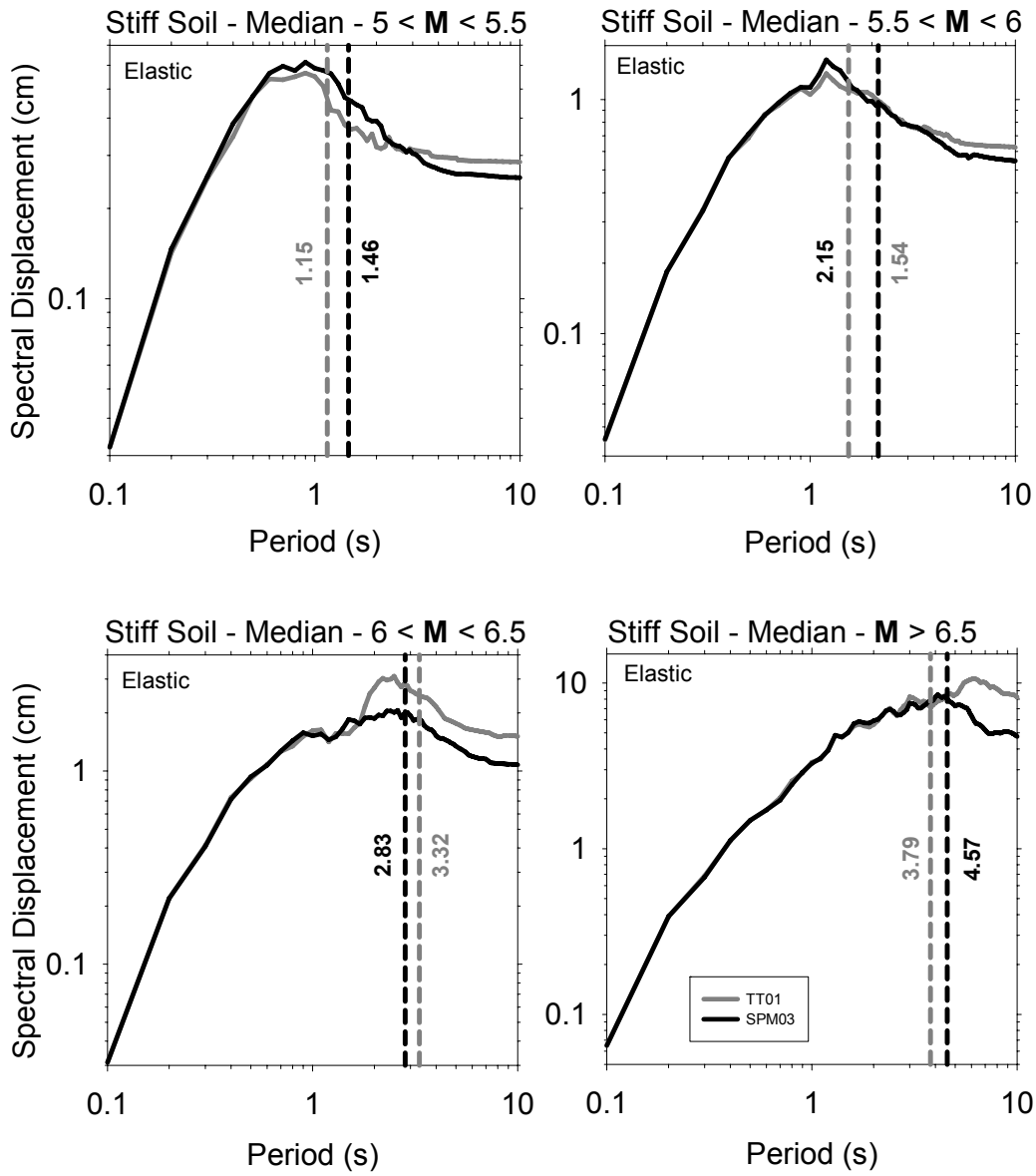

Figure 4.6 Elastic spectral displacements for stiff site records.

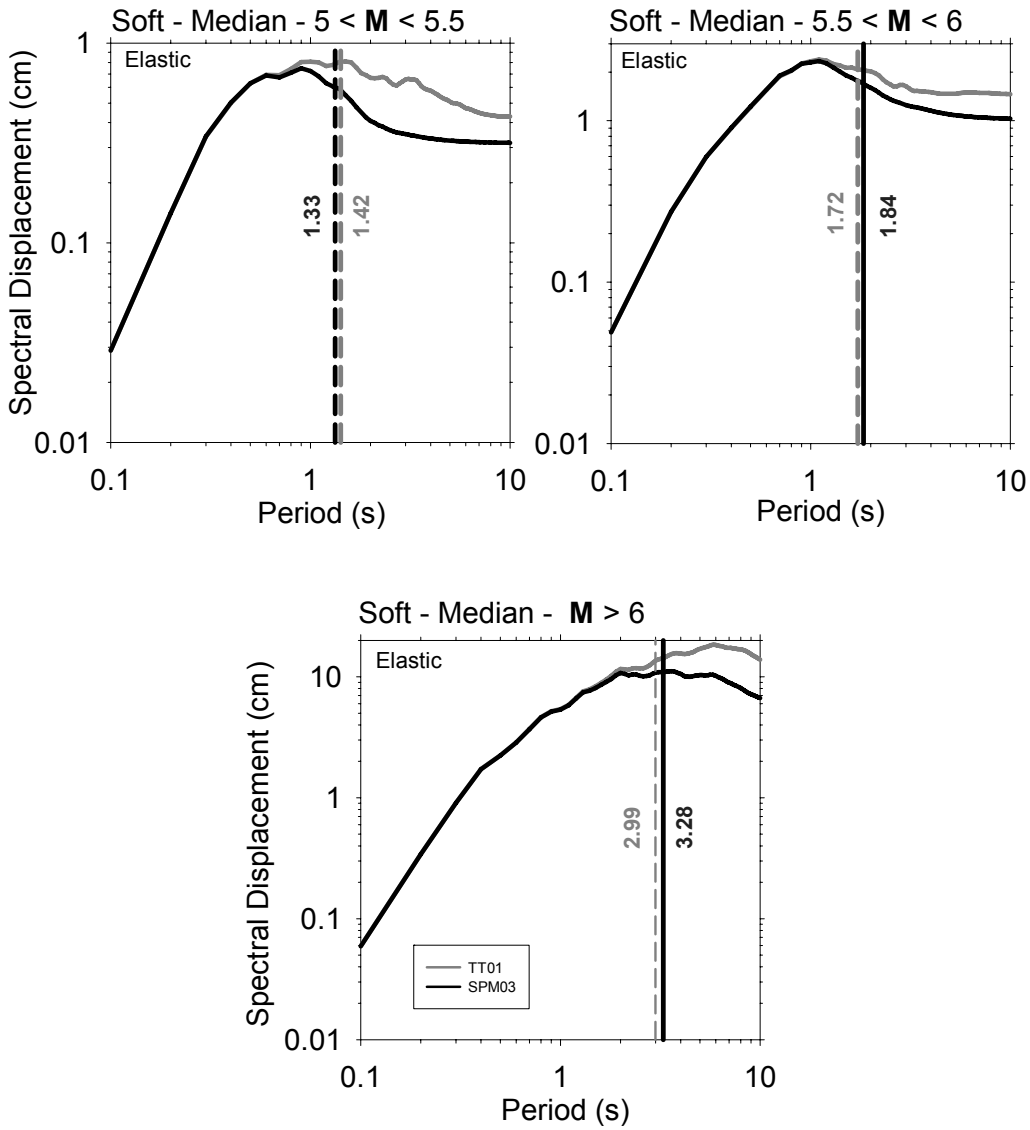

Figure 4.7 Elastic spectral displacements for soft site records.

4.5. Low-Cut Filter Period Effect on Inelastic Spectral Displacements

The influence of low-cut filtering on inelastic spectral displacements are shown in Figures 4.8 to 4.13. The format of these figures is similar to the ones presented in Figures 4.5 to 4.7. Figure 4.8 show the constant ductility (μ) spectral displacements for rock sites, whereas Figure 4.9 present the constant normalized strength (R) spectral displacements. Same information in the same order is given in Figures 4.10 to 4.11 and Figures 4.12 to 4.13 for stiff and soft site records, respectively. Constant ductility spectrum yields inelastic deformation demands on sdof systems for a predetermined maximum absolute displacement ratio. Constant normalized strength spectrum gives maximum absolute inelastic deformation demands on oscillators for a given elastic strength to yield strength ratio. The first columns in these figures represent a low level of inelasticity (μ=1.5 and R=1.5). The second columns in these figures mimic a higher level of inelasticity (μ=8 and R=8).

The inelastic displacement spectra presented in these figures suggest similar comments to the ones made for elastic oscillator behavior. Confined to the database used in this study, the contributions of magnitude and site class play a role for low-cut filter influence on inelastic spectral displacements. The influence of low-cut filtering is more prominent for lower magnitude events and ground motions recorded on rock sites. The increase in the level of inelasticity also contributes to the influence of low-cut filtering on inelastic spectral displacements. This is more apparent for constant strength spectra as this inelastic spectrum type does not impose limitations to the spectral displacements computed at each vibration period unlike the constant ductility spectrum.

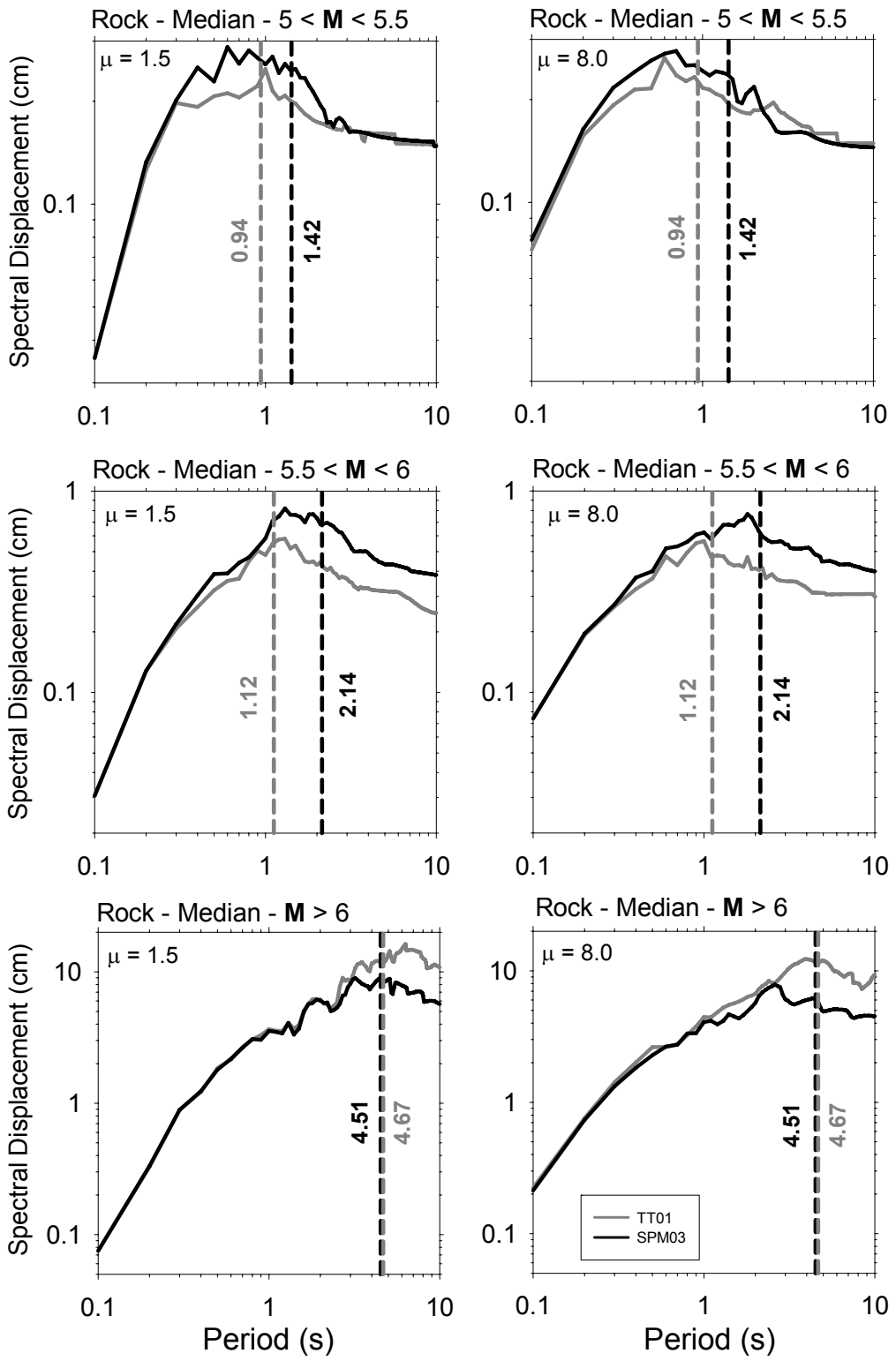

Figure 4.8 Constant ductility spectra for rock site records.

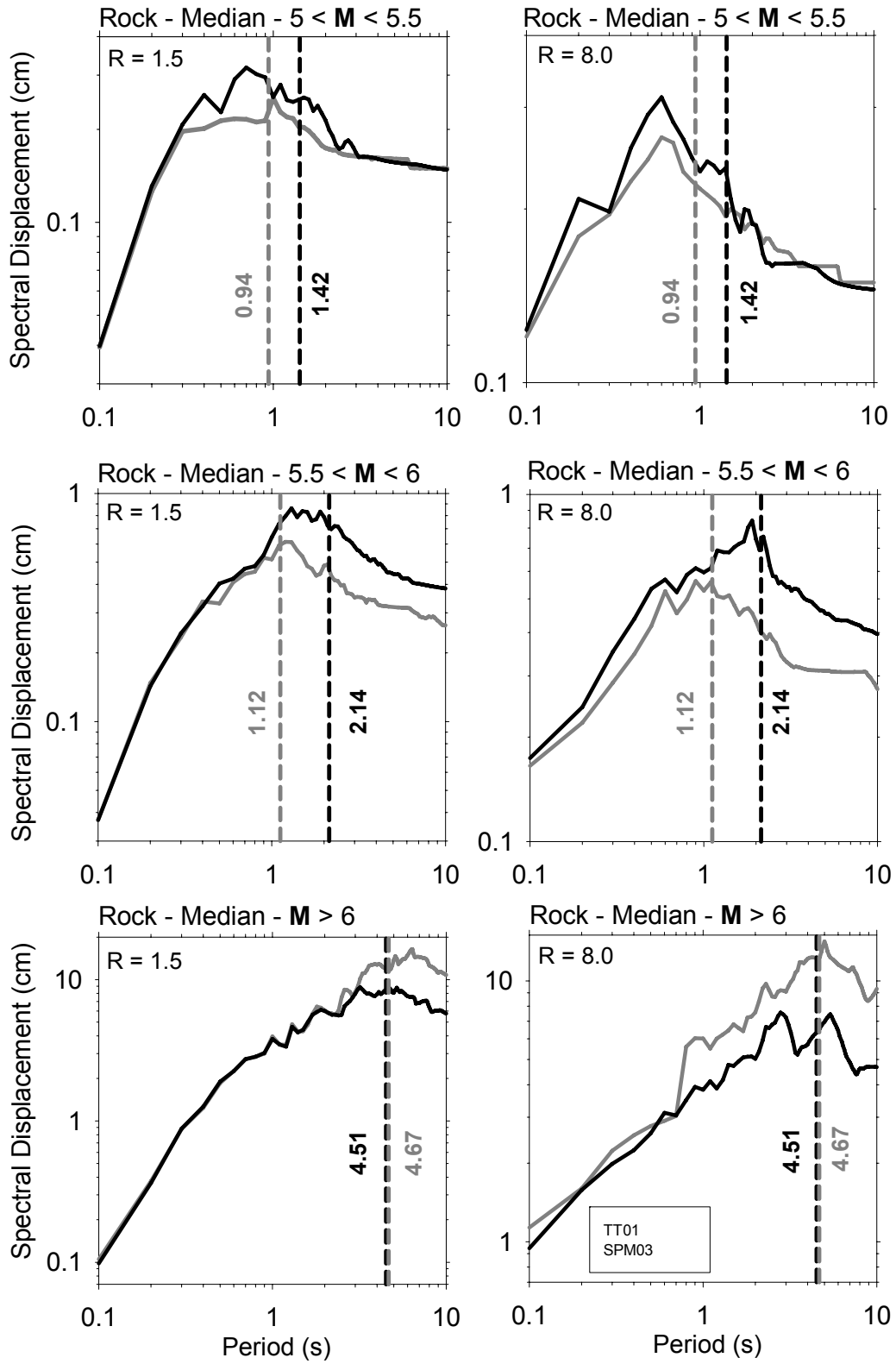

Figure 4.9 Constant normalized strength spectra for rock site records.

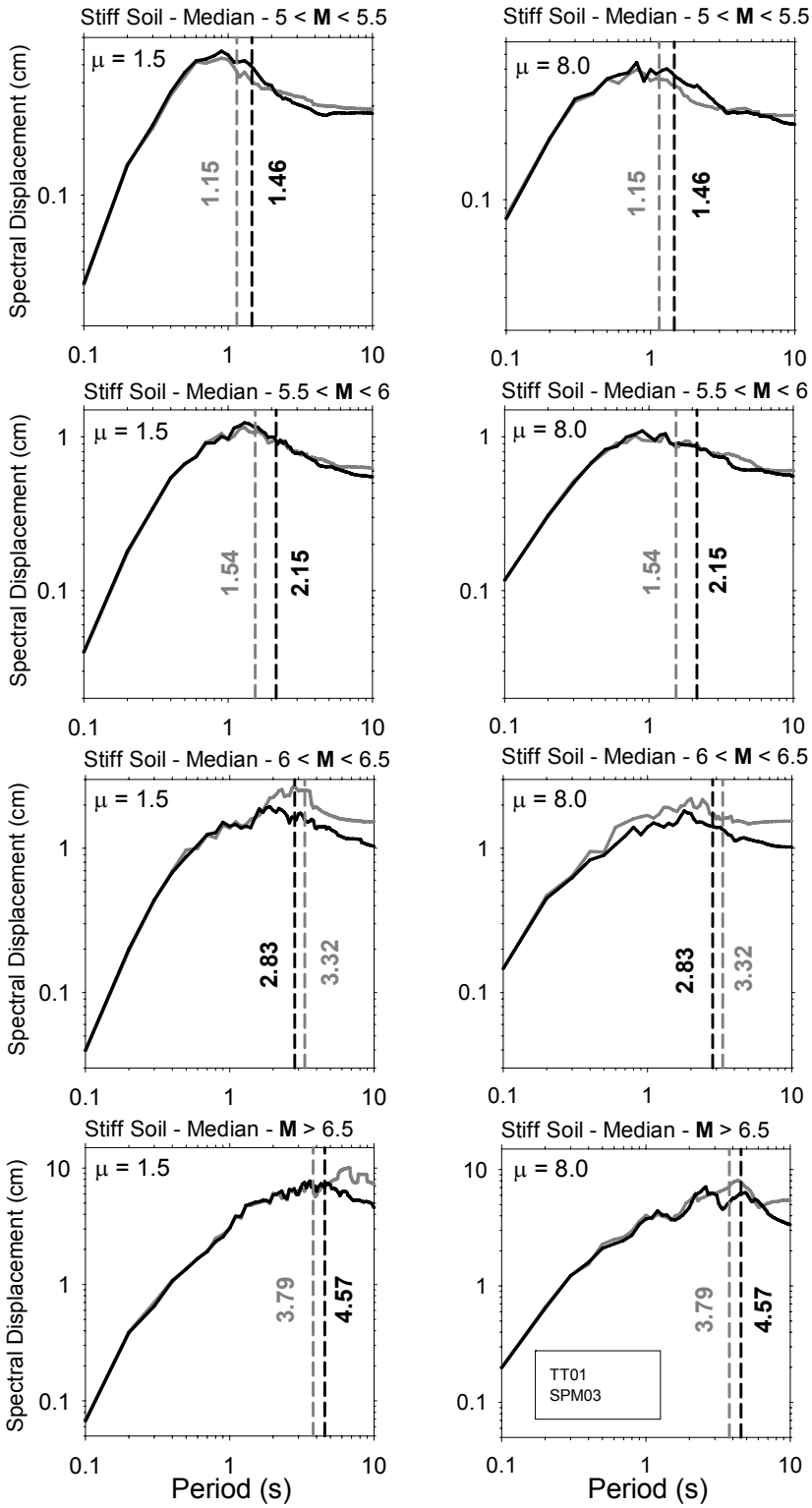

Figure 4.10 Constant ductility spectra for stiff site records.

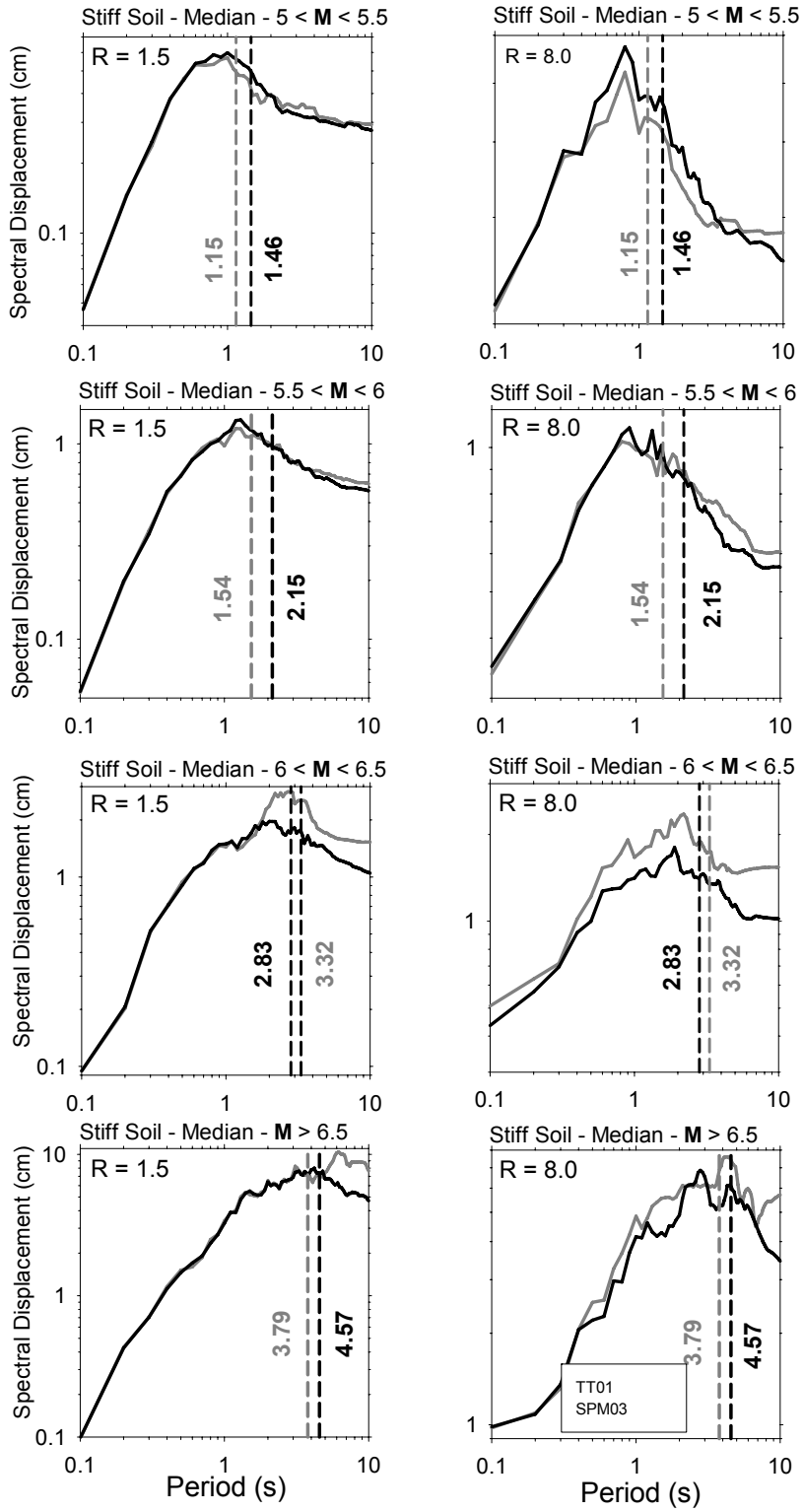

Figure 4.11 Constant normalized strength spectra for stiff site records.

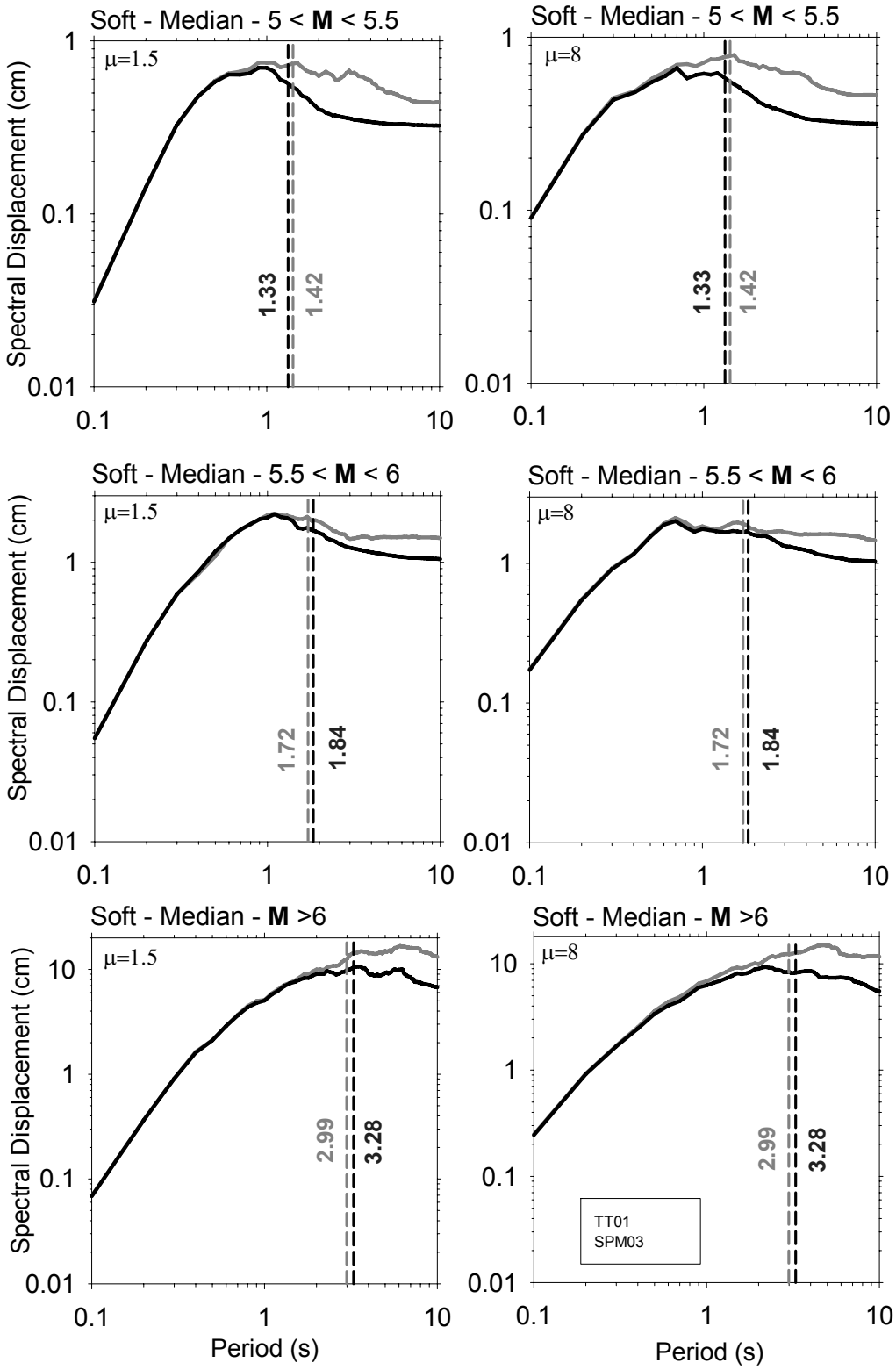

Figure 4.12 Constant ductility spectra for soft site records.

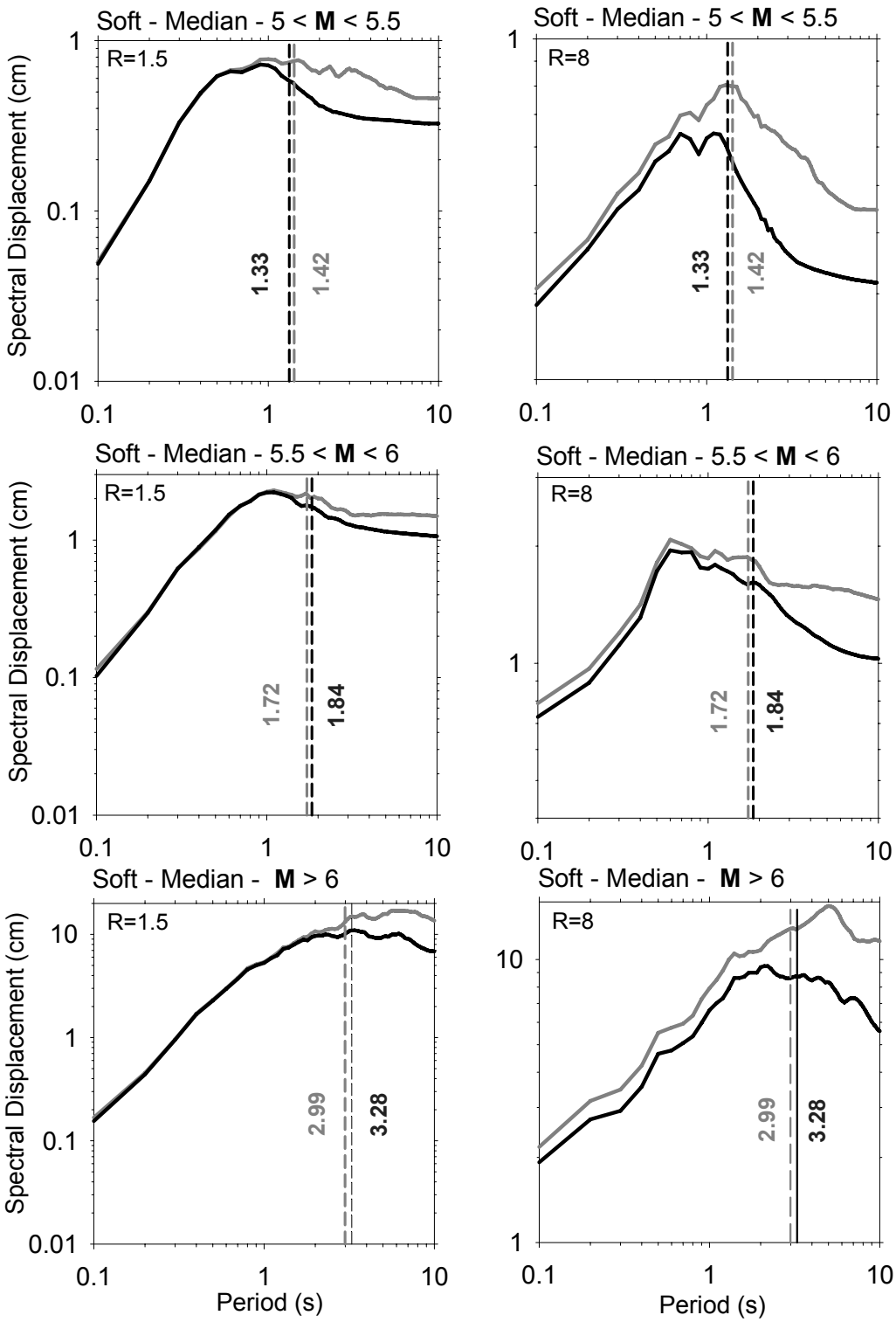

Figure 4.13 Constant normalized strength spectra for soft site records.

CHAPTER-5

A NEW PROCEDURE FOR DATA PROCESSING OF ANALOGUE RECORDS

5.1. Introduction

The observations presented in Chapter-4 showed that the displacement spectrum is highly sensitive to the long-period filter cut-off. The displacement spectra that were computed by using two different noise models were significantly different from each other after a certain period range. The dispersion between the spectra computed from these two models start increasing at periods that are significantly smaller than low-cut filter periods suggested by these alternative noise models. Magnitude and site class are also observed to be the fundamental seismological features that influence spectral displacements. These preliminary results strengthen the fact that the choice of long-period filter cut-off period (T_c) is the prime concern for the computation of displacement spectra, particularly for reliable long period information.

The studies for the determination of a suitable T_c using noise models are summarized in Chapter- 4. Most of the strong ground-motion prediction equations that are used to estimate the spectral ordinates define the useful period range as a fraction of long-period filter cut-off. The use of such a factor reduces the filter response effects (such as roll-off and filter order). There are different studies and organizations that propose using

different fractions of T_c to define the usable period range. For the derivation of recent European strong ground-motion prediction equations, Ambraseys et al. (2005) used $0.8T_c$ as the usable bandwidth. Similar to Ambraseys et al. (2005), PEER (Pacific Earthquake Engineering Research Center) recommended the use of $0.8T_c$ as the usable bandwidth for ground motions that are processed by using 4-pole Butterworth filter. Abrahamson and Silva (1997) and Spudich et al. (1999) offered this factor to be 0.8 for 5-pole acausal and causal Butterworth filter response, respectively. Different from these ratios, CSMIP (California Strong-Motion Instrumentation Program) suggested using the processed data up to the long-period filter cut-off for an acausal 4-pole Butterworth filter. The displacement based design spectrum that was derived by Bommer and Elnashai (1999) computed the displacement ordinates up to 0.1 seconds below the filter cut-off period.

This chapter presents a record processing scheme that determines the low-cut filter values considering the influence of magnitude on the frequency content of the ground motion. The proposed scheme is used to re-process the analogue ground motions presented in the previous chapter. Later, the spectral displacements computed from the re-processed database are used to derive statistics to describe the influence of magnitude and site conditions on the usable period range of filtered data as a function of low-cut filter values.

5.2. Ground-Motion Data Set and Data-Processing Scheme

The ground-motion database presented in Chapter-4 is also used in this chapter to describe the new data-processing scheme. It constitutes the analogue recordings of the recently compiled European ground-motion

data that is comprised of accelograms from Europe and the surrounding countries in the Middle East and North Africa (Ambraseys et al., 2005).

The first well-organized European data set record processing was performed by Ambraseys et al. (1996) to obtain strong ground-motion prediction equations for spectral acceleration by using a long-period filter cut-off period of 5 seconds for all records. Ambraseys et al. (2000) re-processed the data base in the same way, but with a long-period cut-off value of 4 seconds. However, the decision on the long-period filter cut-off values disregarded the frequency and noise content of the raw data. Bommer and Elnashai (1999) processed the European database by starting a T_c value of 10 seconds and reducing it until the physical appearance of the velocity and displacement traces were judged to be acceptable. The most recent processing of European ground-motion data base was performed by Ambraseys et al. (2004). The determination of T_c was based on the fixed trace information whenever it was available. The low-cut filter value value was determined by using the signal-to-noise ratio. Frequency content of the records retained for signal-to-noise ratio greater than 2. For analogue records with no fixed trace information, T_c value was determined by using the noise-spectra model of Trifunac and Todorovska (2001) or investigating the acceleration FAS in order to identify T_c as the period where FAS no longer tends towards zero at long periods. Note that none of the above procedures determine T_c considering the influence of magnitude that is observed to be important for the low-cut filter effects on spectral displacements (see Chapter-4).

The raw analog records of ground-motion data base were re-processed by the new record processing scheme presented in the following paragraphs. Similar to Chapter-4, 2pole/2pole acausal Butterworth filter was used during the low-cut filtering. The total length of leading and trailing zero

pads were computed as recommended by Converse and Brady (1992). The processing scheme developed for this study is summarized below:

Step-1: Compute the mean of the accelogram using the total record length and remove it from the entire record. The record obtained after this step is referred as “mean removed” in this study.

Step-2: If the digitized fixed trace information is available, compute (signal+noise)/noise ratio and decide on T_c at the period where (signal+noise)/noise ratio is greater than 3. If the (signal+noise)/noise ratio fluctuates about given limit, determine an approximate trend by fitting a straight line on this ratio. The low-cut filter period is approximately the intersection of regression line and (signal+noise)/noise=3. Apply low-cut filtering using the T_c computed from this criterion. If physically unjustifiable trends still exist in the velocity and displacement traces, decrease T_c value until the velocity and displacement traces are judged to be physically meaningful. Reject the record for use in spectral calculations, if T_c is significantly smaller than the one determined from (signal+noise)/noise ratio.

Step-3: In the absence of fixed trace information, use the guidance of acceleration FAS corner periods estimated from two theoretical source models (Joyner and Boore, 1988; Atkinson and Silva, 2000) to select T_c iteratively. Note that the use of source models would imply the contribution of magnitude as explained in the paragraphs below.

Step-3-1: Compute the theoretical FAS corner periods using the single-corner frequency model (JB88) proposed by Joyner and Boore (1988) and two-corner frequency model (AS00) proposed by Atkinson and Silva (2000) to have information on the theoretical long-period content of the records. The double corner source spectrum describes the influence of

finite fault size by the corner period (T_a) whereas theoretical corner period T_b accounts for the rupture process. The corner period T_a is larger than T_b. The single corner frequency model proposed by Joyner and Boore (1988) is the result of Brune's single source spectrum (1970) for a stress drop of 100 bars.

Step-3-2: Start with a T_c value that is not longer than the theoretical corner periods estimated from the above models and reduce it until the displacement traces do not contain long-period fluctuations or do not end with very large displacements. Note that the FAS of record processed with the chosen T_c should always decay proportional to f^2 gradient at long periods, which is the common point for all theoretical source spectra. Choosing a T_c value shorter than the theoretical FAS corner periods may imply the removal of actual long-period information after low-cut filtering. The records should be rejected for use in spectral displacements if extremely short cut-off periods are determined with respect to those suggested by the source spectrum models. Such records are severely distorted during the recording stage.

Although the choice of reference source spectra and the decision on the physically reasonable velocity and displacement traces are still subjective, the advantage of this procedure is that it provides information about the frequency content of the filtered data in the range of theoretical source models. No instrument response correction was applied to the data since the database does not contain adequate information about the sensor characteristics of the accelerometers. Note that instrument correction influences the short period contents of the accelograms that is of little importance for spectral displacements. The reader is referred to Boore and Bommer (2005) for a detailed discussion about the use and necessity of instrument correction for strong ground-motion data processing. Figure 5.1 shows the application scheme of the proposed method. It should also

be noted that whenever the fixed trace information is available, Steps 2 and 3 should be considered separately to define two distinct filter cut-off periods. The analyst should choose the one with larger T_c unless the computed velocity and displacement traces are physically unjustifiable. A recent study by Yenier et al. (2006) showed that the sole use of fixed trace information and disregarding Step 3 presented above may result in significantly conservative T_c values.

The application of Step-2 is illustrated in Figure 5.2 for one of the horizontal components of the Nasso station record recorded during the 1978, Basso Tirreno (M_w=6) earthquake. This case has been presented previously in Chapter-2 while discussing the alternative methods for determining T_c. The first plot shows the comparison of the (signal+noise)/noise ratio. The red dashed line indicates (signal+noise)/noise ratio=3. The blue dashed line shows the approximate location of the period where the (signal+noise)/noise ratio trend is greater than 3. Note that the (signal+noise)/noise ratio fluctuates about the red dashed line for a wide frequency range and a trend line is adjusted for this particular case in order to approximate the low-cut filter period. The computations resulted in a T_c estimate of 2.85 s (i.e. the trend line intersects the (signal+noise)/noise=3 at about 0.35Hz). The first raw following the (signal+noise)/noise ratio are velocity and displacement traces of the data low-cut filtered by T_c=2.85s. The last raw shows the velocity and displacement traces for low-cut filtered data by T_c=5s determined from the theoretical source spectra and actual FAS comparisons (Step 3) presented in Figure 2.11. As discussed previously, the comparisons between the time series filtered by these two low-cut off filter values yield reasonably well-behaved ground velocity and displacement. Thus, the analyst should prefer T_c=5s for this particular case.

Figure 5.3 shows the application for determining the low-cut filter period for records that no dot contain fixed trace information. The chosen example is a record from the 1980, Compano Lucano earthquake (M_w=6.9) that was recorded at the ICSMA station located on a rock site. The theoretical JB88 FAS corner period was determined as 8.91 seconds, whereas the upper and lower limits of the theoretical AS00 FAS corner values were 17.43 and 2.54 seconds, respectively. The filtering procedure was applied by choosing an initial low-cut filter period of 20 seconds, which is slightly longer than the upper period limit dictated by the AS00 model. The filter period value was decreased until the displacement traces were considered to be reasonable. The final filter cut-off value (10s) is in between the theoretical FAS corner periods computed by the chosen source spectrum models and it is accepted as reasonable since it falls in between the bands of the theoretical corner periods determined from the chosen source spectra. The first graph of Figure 5.3 shows the FAS comparisons between the processed and raw data. The low frequency of the processed data is compatible with the f^2 gradient indicating that the chosen T_c is consistent.

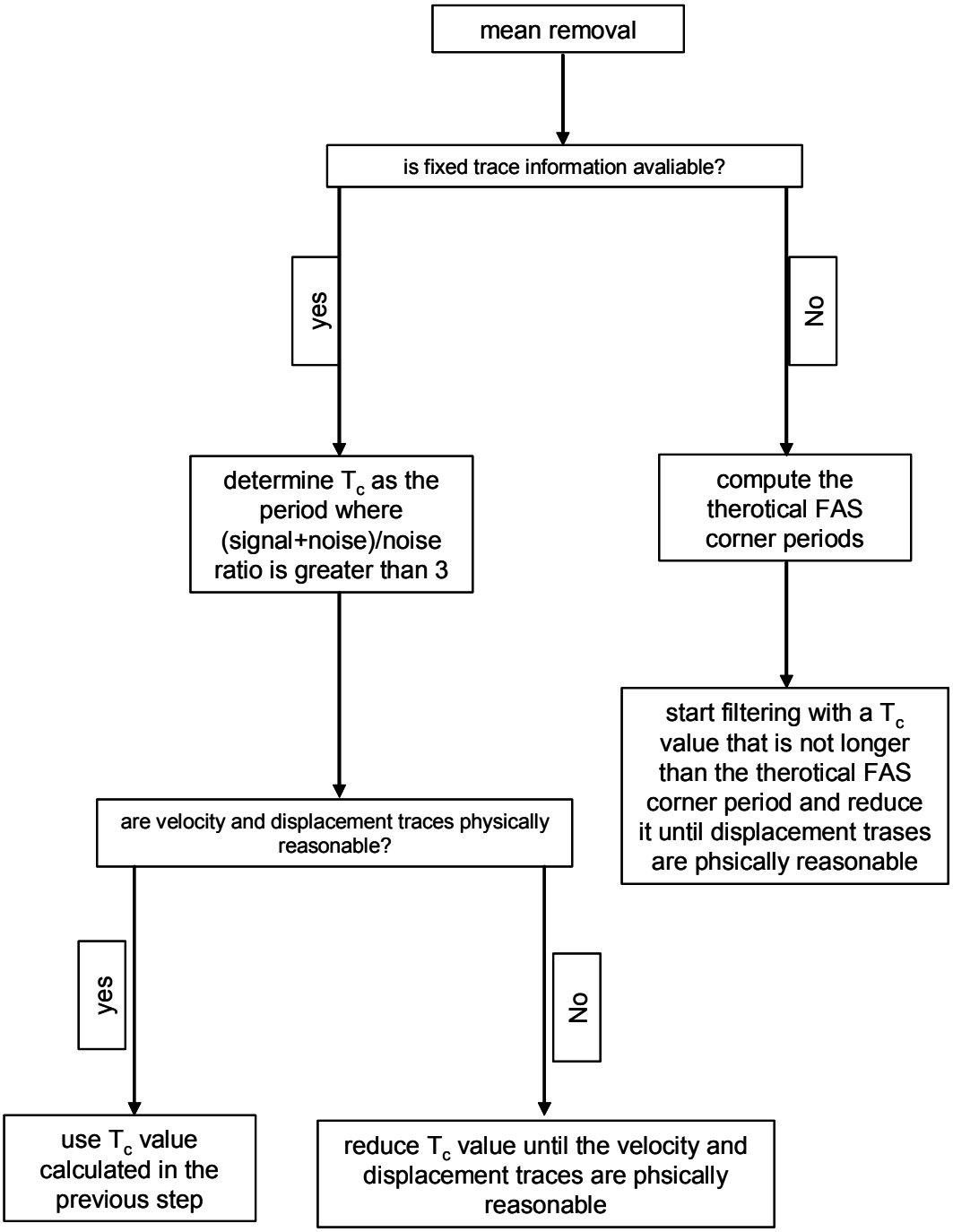

Figure 5.1 The scheme of the data processing scheme used in the study.

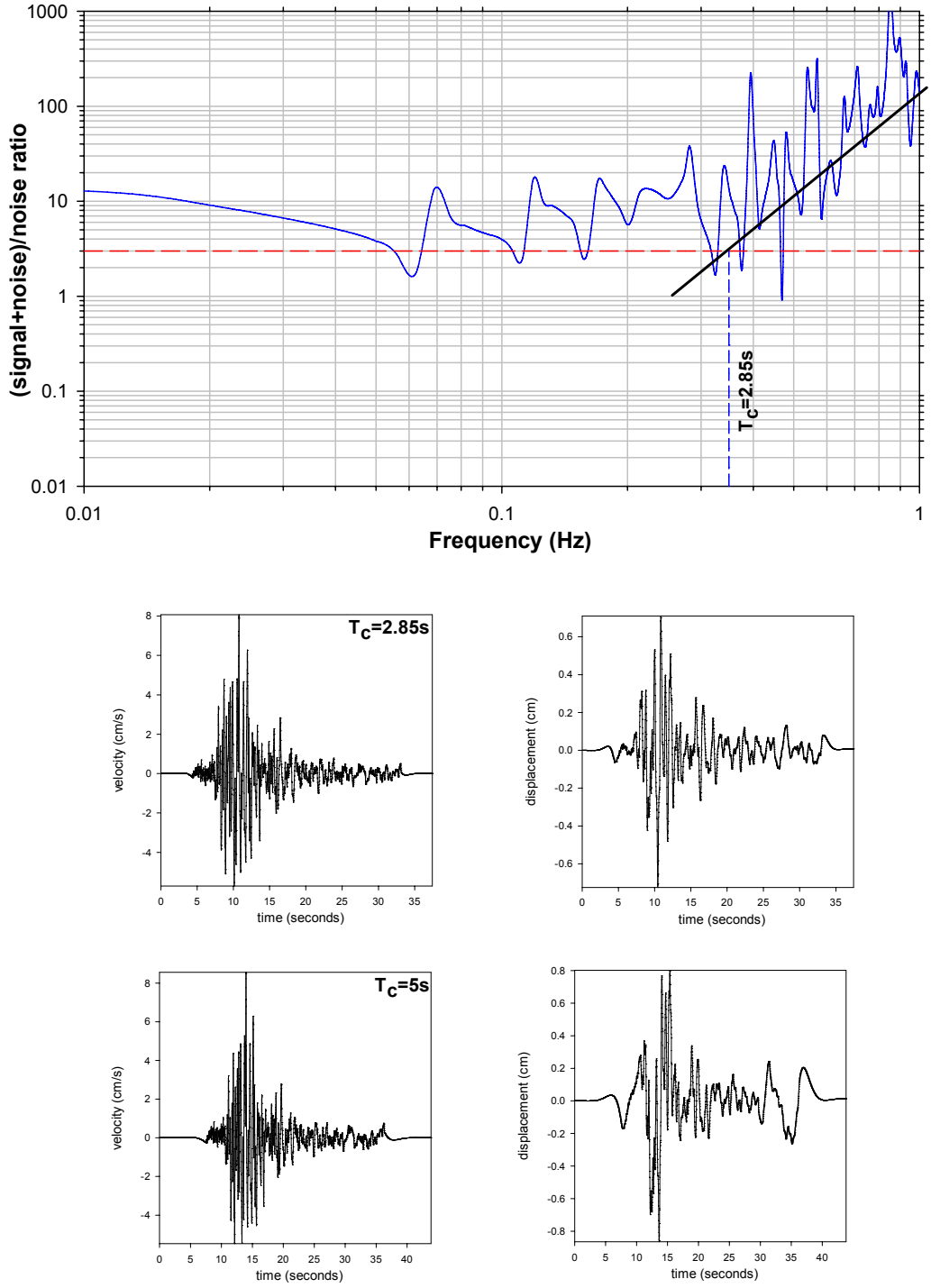

Figure 5.2 Determination of T_c by comparing the (signal+noise)/noise ratio

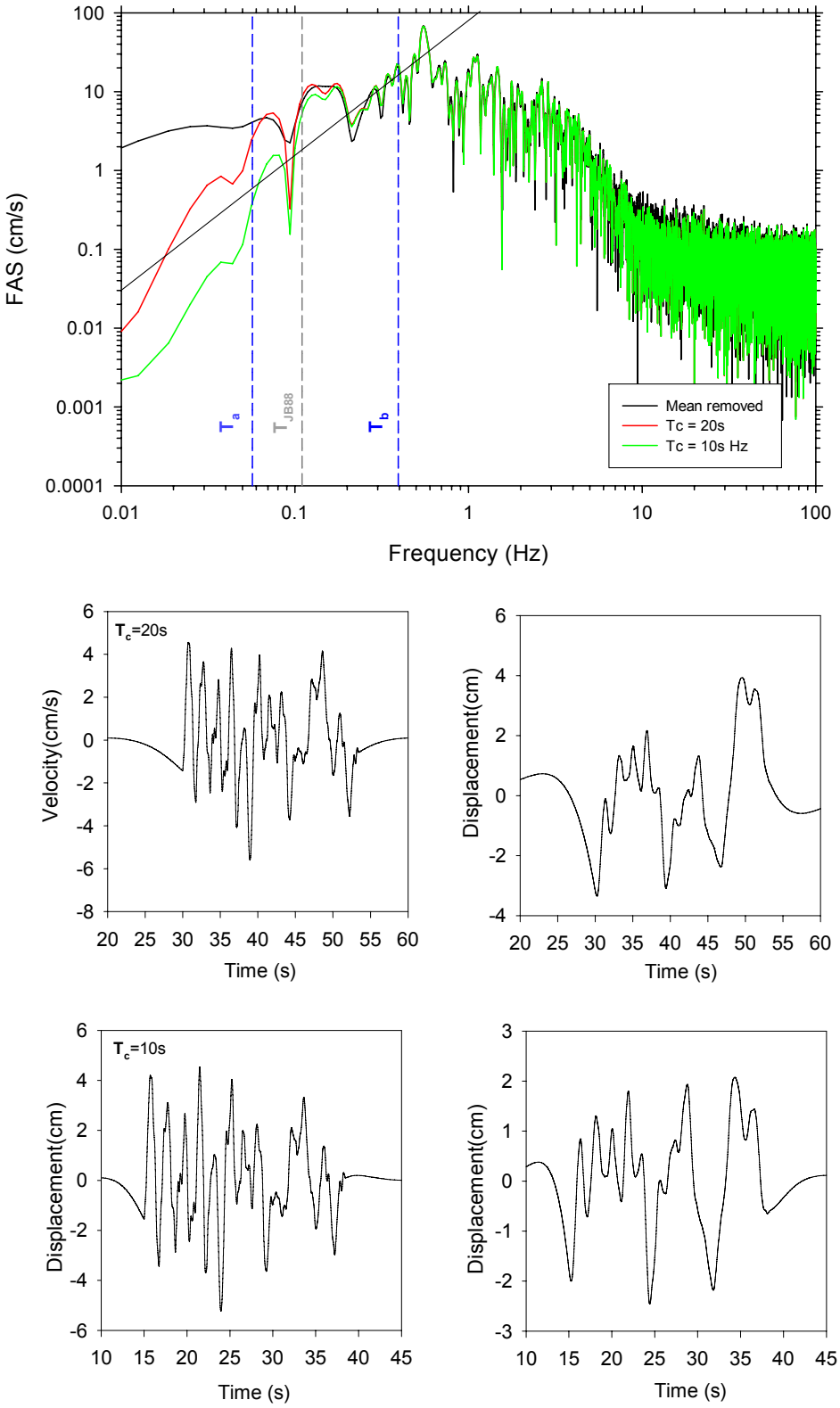

Figure 5.3 Determination of filter-cut off by source-spectrum models (note that the time axis of the velocity and acceleration traces are shifted for a better illustration).

Figure 5.4 shows magnitude vs cut-off period scatter diagrams of the re-processed European ground-motion database for analogue recordings. The classification of the sites are based on the shear-wave velocities that are described in Chapter-4. The theoretical corner periods that are determined by the source spectrum models are also plotted on the same graph. The value of JB88 corner period lies in between the lower and upper corner periods of the AS00 model. In general, a filter cut-off value that is very close to T_b cause the removal of an integral part of the signal while filtering out the long-period noise. When Figure 5.4 is investigated, it can be observed that filtering process has removed a considerable amount of information from some of the large magnitude rock and stiff site recordings. These kind of records should be treated carefully and should not be used for calculating the spectral ordinates at very long spectral periods.

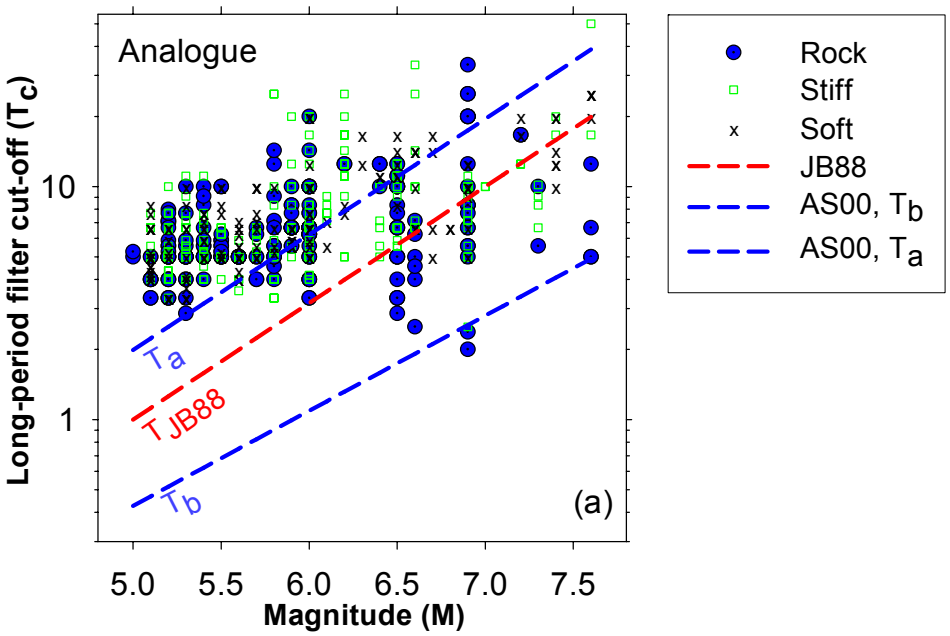

Figure 5.4 Long-period filter cut-off vs moment magnitude for the re-processed European strong ground-motion data set for analogue recordings.

5.3. Effect of Long-Period Filter Cut-off on Elastic Spectral Displacements

The effect of long-period filter cut-off (T_c) on elastic displacement response is investigated in this section using the re-processed database by the procedure presented in the previous section. The effects of T_c on elastic displacements is investigated by presenting basic statistics that describe the behavior of low-cut filtered spectral displacements considering the relationships between the filter cut-off and important oscillator and ground-motion features. The 5% damped displacement spectrum computed from the filtered ground motion was normalized by the spectral displacement of the mean removed data to study the effects of filter cut-off on the processed records and to have a general perspective on the sufficiency of mean removed data in spectral displacement calculations for a certain period interval (the normalized values are designated by $S_{d,proc}/S_{d,unproc}$ on the plots). The value of 1 for $S_{d,proc}/S_{d,unproc}$ indicates that the processed data is not influenced by the filter response at that period of vibration. If this value is less than 1, the conclusion is that filtering has started to influence the spectral displacement by removing some part of the signal in that vibration period. The period axis of the displacement spectrum is normalized by the filter cut-off period to obtain conclusions from the statistics presented about the usable period range of filtered data in terms of T_c.

The earthquake magnitude and site class are the most important factors that influence the long-period information carried by strong ground-motion records. The results presented in Chapter-4 show that different magnitude ranges and site classes play a role for the low-cut filtered spectral displacements and increase or decrease the influence of low-cut filter values in terms of spectral period ranges. The stiff site records are divided

into two magnitude bins in order to bring forward the magnitude influence. The first raw of Figure 5.5 presents the scatters for $5 < M_w < 6$, whereas the second raw shows the scatters for $M_w \geq 6$. Both plots superimpose log-normal probability density functions that display a better representation about the variation in dispersion of $S_{d,proc}/S_{d,unproc}$ in terms of magnitude and filter cut-off influence. The continuous curves are the median $S_{d,proc}/S_{d,unproc}$ values for the given T/T_c interval emphasizing the magnitude contribution to the influence of low-cut filter on elastic spectral displacements. For a better comparison, the median values are superimposed in Figure 5.6 for two different magnitude bins. The standard deviations are shown in Figure 5.7. The results presented in Figures 5.5, 5.6 and 5.7 concern stiff site recordings but the general picture presented in these figures are also valid for other site classes. The plots in Figures 5.5, 5.6 and 5.7 reveal that, on average, an increase in the order of earthquake magnitude results in a longer usable period range. The associated dispersions of larger magnitude earthquakes are smaller when compared to those computed for the smaller magnitude earthquake bin. These results indicate that filter cut-off effects are limited for larger magnitude events, which is the result of rich long-period frequency content of large events. It should be noted that regardless the magnitude ranges concerned, the median $S_{d,proc}/S_{d,unproc}$ values are significantly below 1 for $T/T_c>0.6$. The associated scatter is also significantly large for $T/T_c>0.6$. This observation casts significant doubts about the use of empirical $0.8T_c$ rule to define the usable spectral period ranges for prediction equations used in estimating the spectral quantities.

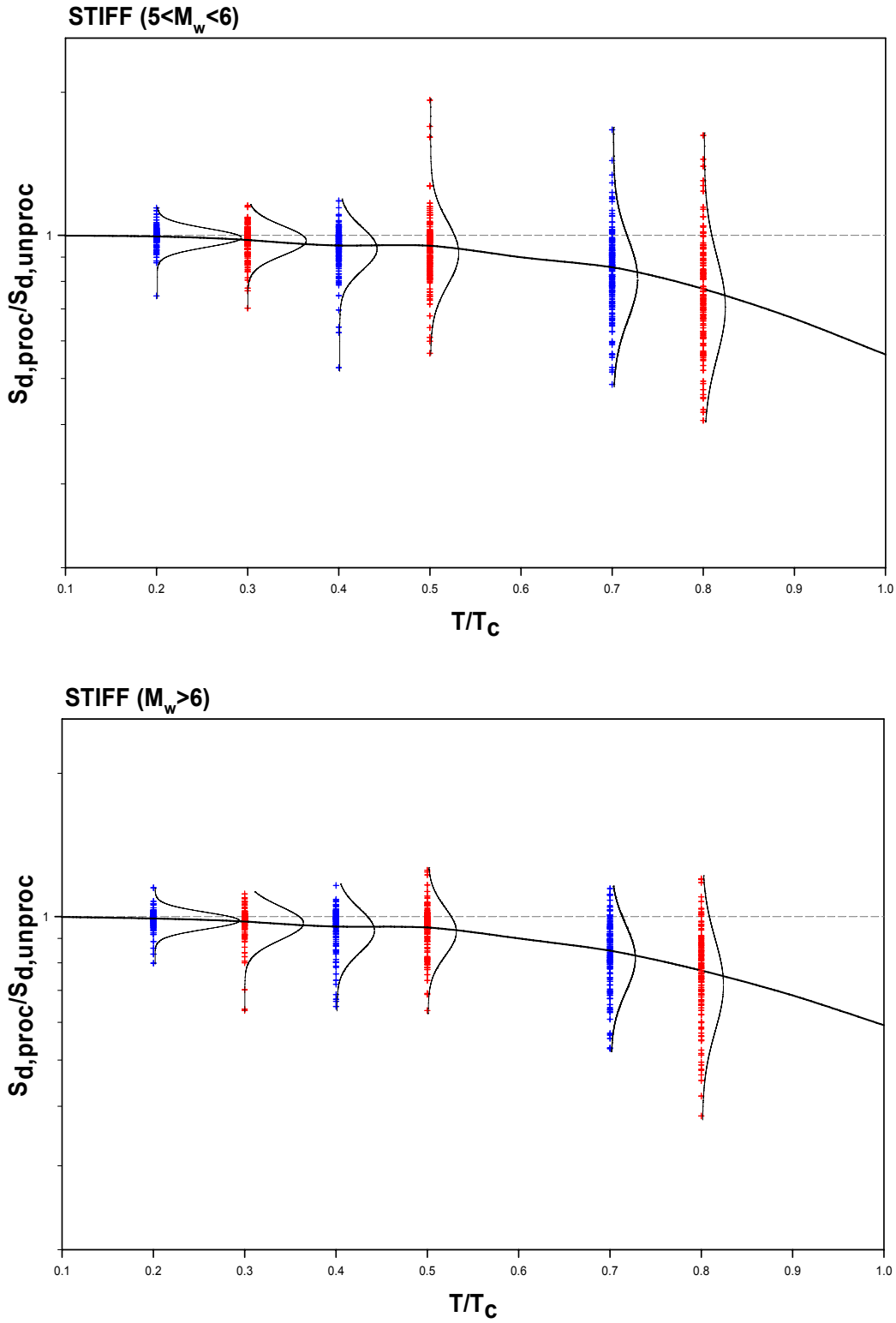

Figure 5.5 The distribution of $S_{d,proc}/S_{d,unproc}$ scatters at distinct T/T_c values for stiff site records for different magnitude bins.

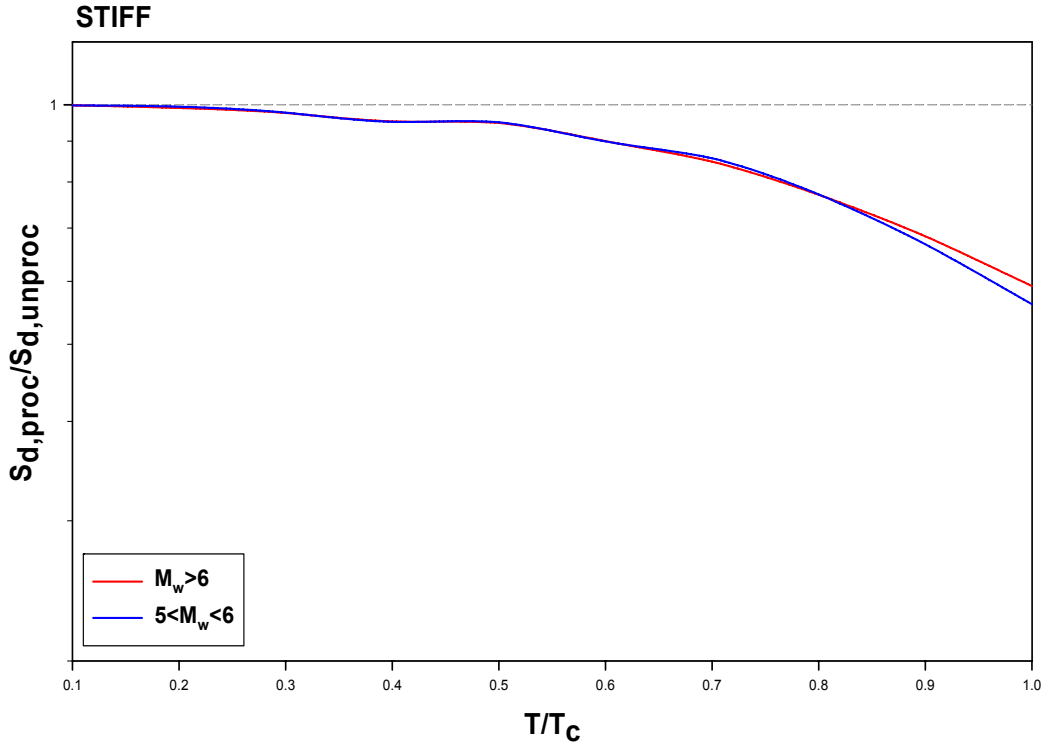

Figure 5.6 Superimposed median values for stiff sites for different magnitude bins.

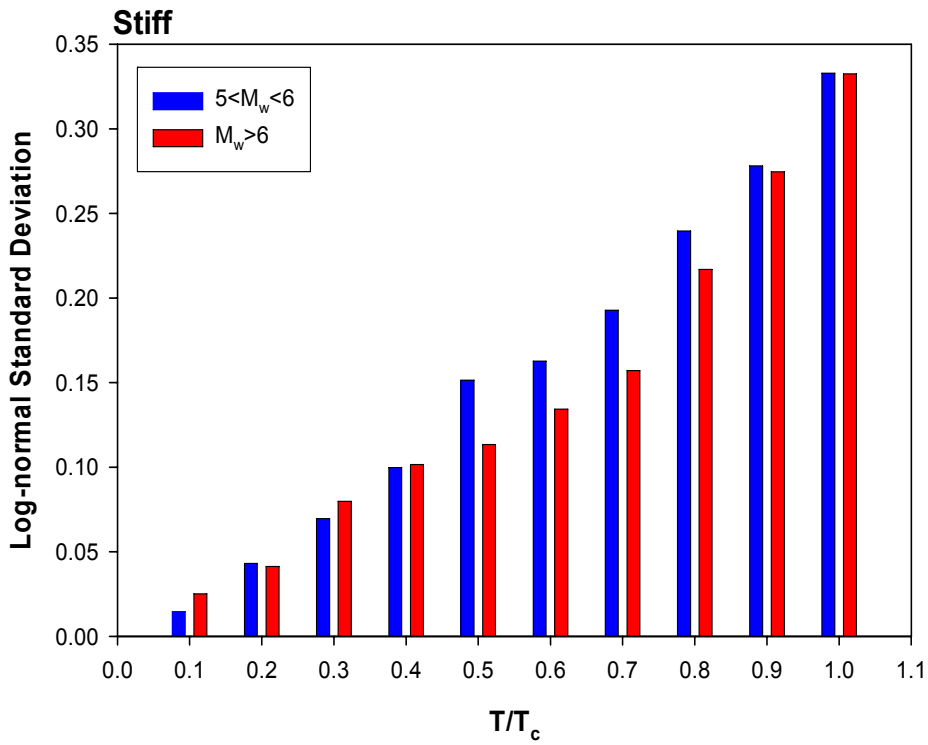

Figure 5.7 Dispersions of stiff site recordings for different magnitude bins.

Figures 5.8,5.9 and 5.10 show similar plots as of Figure 5.5 for rock, stiff and soft sites, respectively. These figures describe the site class effect contribution to the influence of low-cut filter cut off on spectral displacements. Figure 5.11 shows the superimposed median values for different site classes for a better illustration and Figure 5.12 shows the standard deviations for different site classes. The plots indicate that, the ground-motion data recorded on soft soil site class is the least affected group from the filter cut-off value. This observation is the result of rich long-period frequency content of soft site recordings that shift the filter cut-off effect towards longer periods with respect to other site classes. The dispersive behavior increases as the oscillator periods take values closer to the filter cut-off value for all site classes, the stiffer sites being more sensitive.

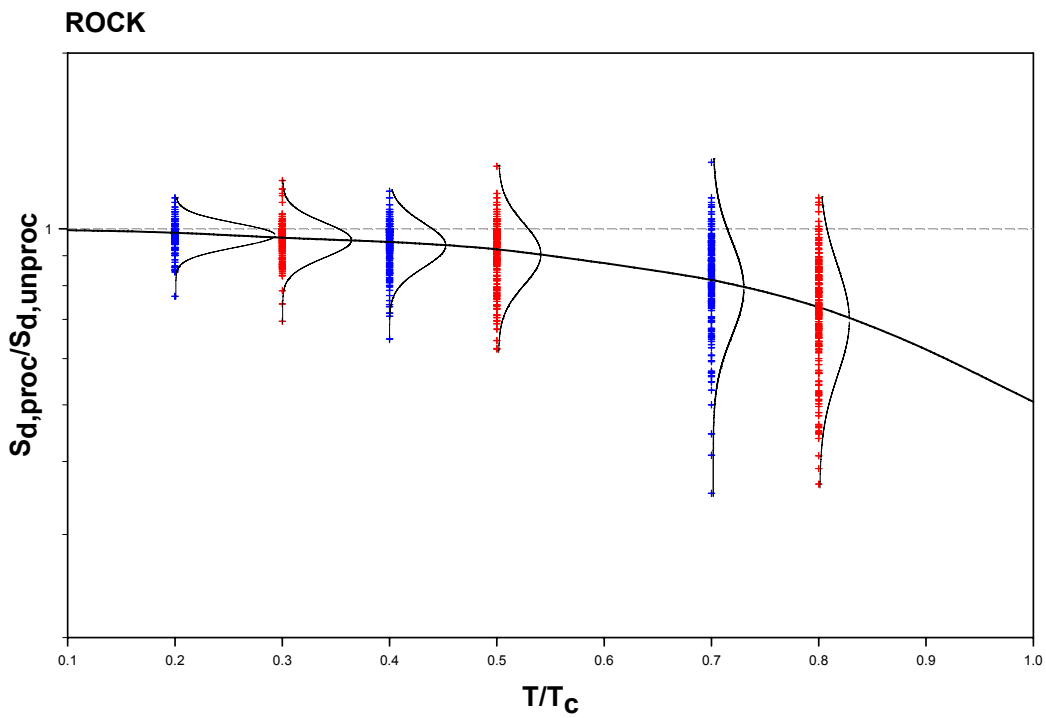

Figure 5.8 The distribution of $S_{d,proc}/S_{d,unproc}$ scatters at distinct T/T_c values for rock site records.

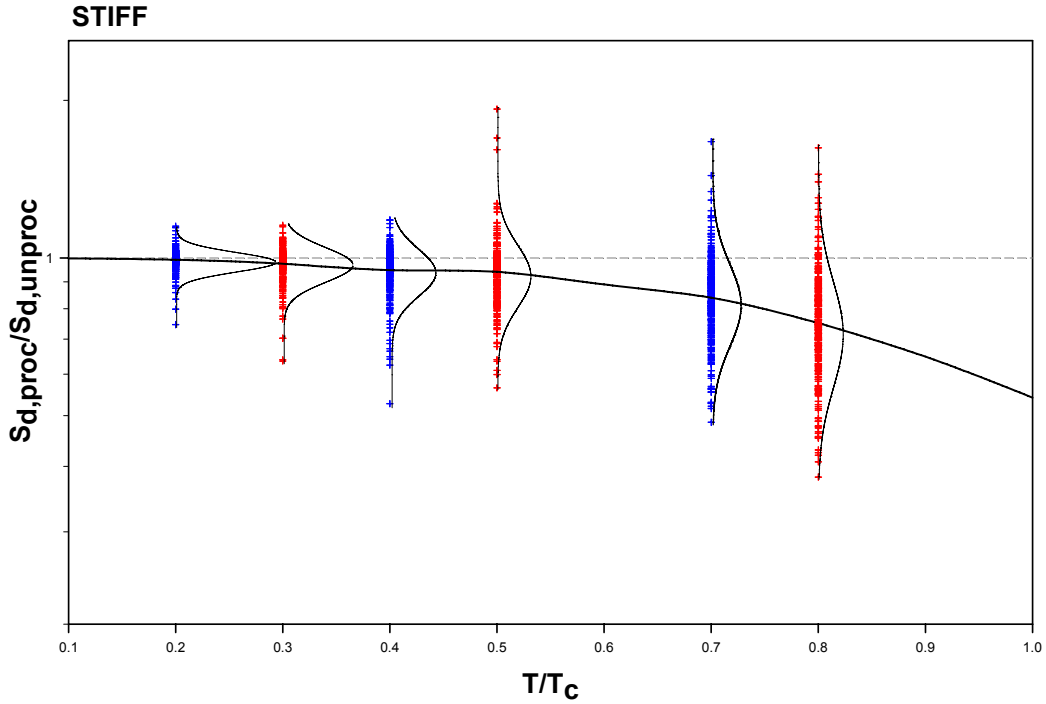

Figure 5.9 The distribution of $S_{d,proc}/S_{d,unproc}$ scatters at distinct T/T_c values for stiff site records.

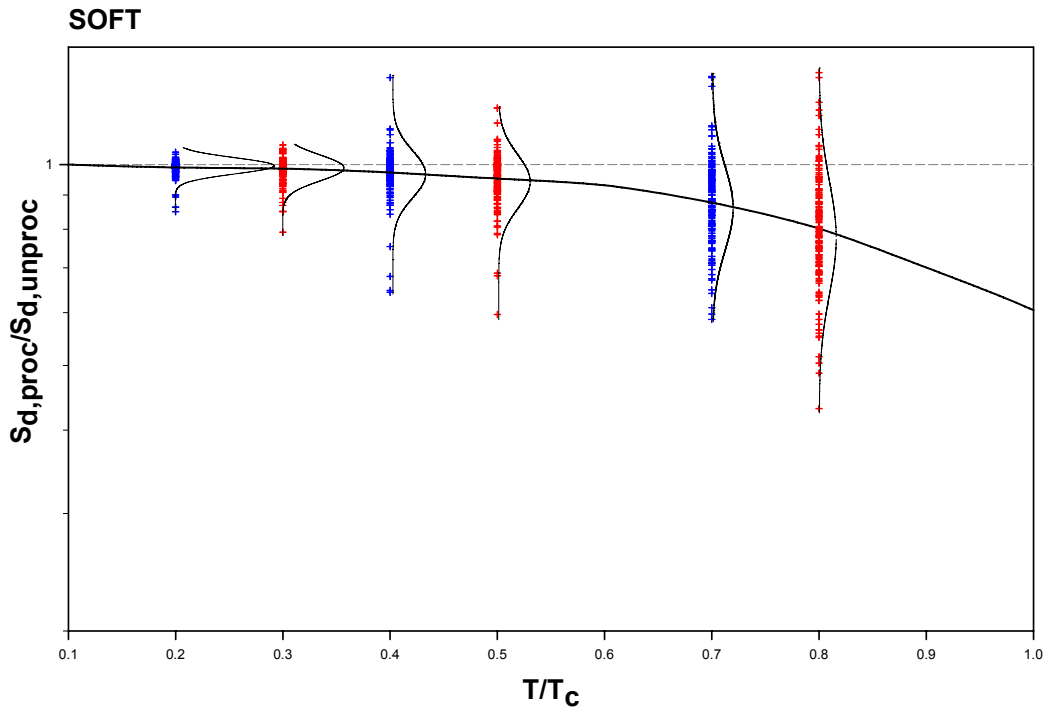

Figure 5.10 The distribution of $S_{d,proc}/S_{d,unproc}$ scatters at distinct T/T_c values for soft site records.

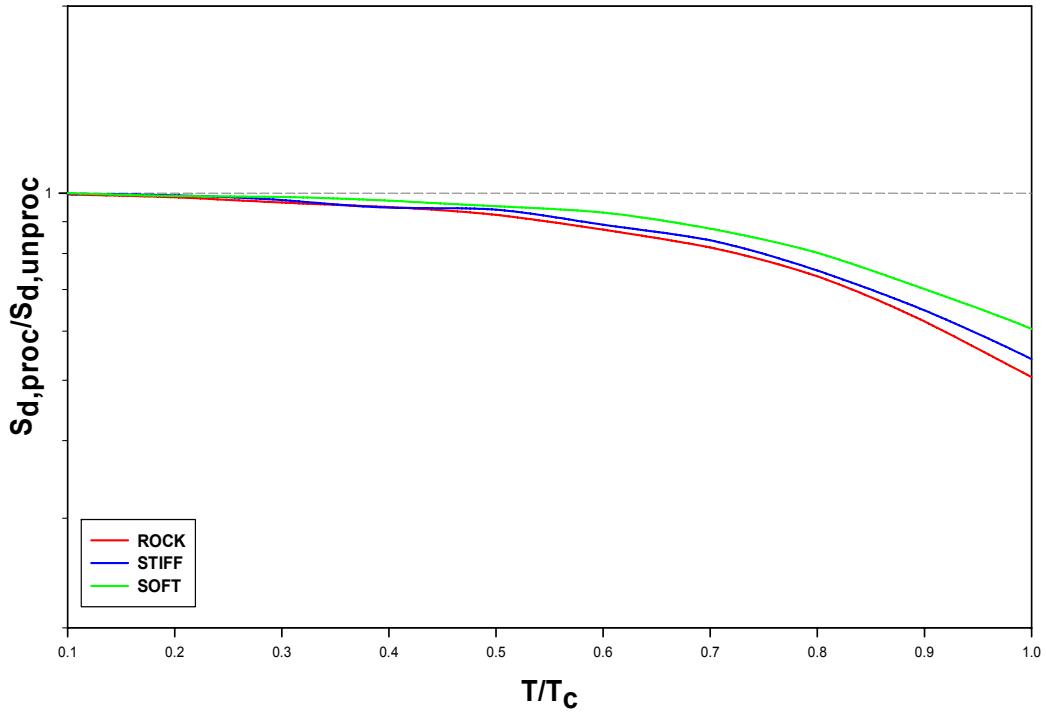

Figure 5.11 Superimposed median values for different site classes.

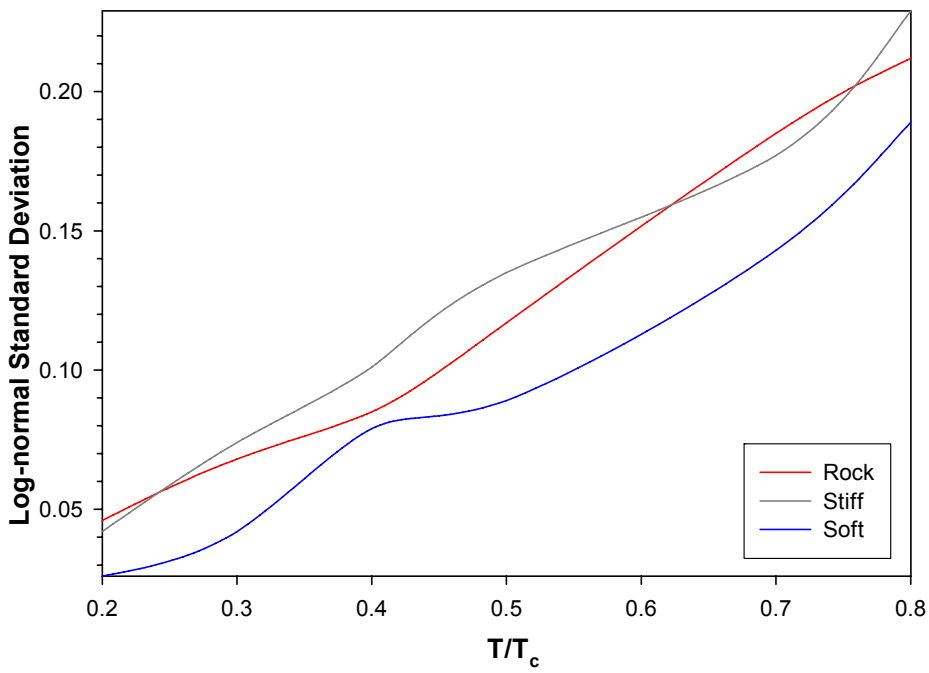

Figure 5.10 Log-normal standard deviations for different site classes.

Table 5.1 presents the probability occurrences of $0.9 < S_{d,proc}/S_{d,unproc} < 1.1$ event for different site classes and different T/T_c values. Similar to the observations presented in the previous plots, the table shows that more long-period information can be retrieved from soft site recordings. The assumed distribution for different site classes and T/T_c values are validated by using Kolmogorov-Smirnov test and the results are presented in Appendix-B. The cumulative probability distributions are shown in Appendix-C.

Table 5.1 Probability of occurrences of $0.9 < S_{d,proc}/S_{d,unproc} < 1.1$ event for different site classes and different T/T_c values.

T/T_c	0.2	0.3	0.4	0.5	0.7	0.8
ROCK	0.959	0.826	0.681	0.501	0.246	0.129
STIFF	0.977	0.797	0.629	0.497	0.289	0.168
SOFT	0.985	0.974	0.767	0.663	0.367	0.227

CHAPTER-6

SUMMARY AND CONCLUSIONS

6.1. Summary and Conclusions

The general objective of the study was to investigate the effects of low-cut filtering period on elastic spectral displacements.

The second and third chapters summarize the strong ground-motion data processing procedures and the theory of digital filters that are the commonly used tools for removing noise contaminated part from the raw accelograms. The emphasis was on the analogue records since they still dominate the strong ground-motion data bases that are used to derive ground-motion prediction equations.

The effect of low-cut filter period on elastic and inelastic displacements were investigated in the fourth chapter by using two different noise spectra that are derived by Trifunac and Todorovska (2001) and Skarlatoudis et al. (2003). The statistics for the peak ground motion values were derived for the data that was filtered by using these alternative noise spectra. In general, it was observed that the peak ground displacement values were very sensitive to the low-cut filter period, whereas the peak ground acceleration and velocity were less sensitive to the low-cut filtering value. The effect of low-cut filter period on peak ground-motion values was

observed to be more prominent for rock and stiff sites. The displacement spectra that were derived for rock, stiff and soft sites for different inelastic levels showed that the displacement spectra are sensitive to the low-cut filtering period at spectral periods significantly shorter than the average low-cut filter values. The level of sensitivity increases as the earthquake magnitude decreases or the level of inelasticity increases.

A consistent data processing scheme was developed with in the context of the study that combines source spectrum models with the fixed trace information of the analogue strong ground motions. This data processing scheme was used to re-process the European strong ground-motion data base to observe the effects of low-cut filtering period on elastic displacement spectra considering site class and earthquake magnitude. The statistics indicated that soft site and large magnitude records are the least affected ground motions from the influence of low-cut filter values due to their rich frequency contents. As the site class becomes stiffer and the magnitude takes smaller values, the records became more vulnerable to low-cut filter values. It was also observed that the use of $0.8T_c$ regardless of the magnitude and site class features may result in biased spectral displacements.

6.2. Future Studies

The data processing scheme proposed in this study should be evaluated for inelastic oscillator response. This way empirical usable period ranges for inelastic displacement spectrum can be determined. These empirical relations can be used further to develop prediction equations for inelastic displacement spectra.

REFERENCES

1. Bazzurro, P., Sjoberg, B., Luco, N., Silwa, W., Darragh, R., 2004, *Effects of Strong Motion Processing Procedures on Time Histories, Elastic and Inelastic Spectra, Invited Workshop on Strong Motion Processing*, Consortium of Organizations for Strong-Motion Observation Systems (COSMOS), Richmond,CA

2. Boore, D.M., Bommer, J.J., 2005, *Processing of Strong-Motion Accelograms: Needs, Options and Consequences*, Soil Dynamics and Earthquake Engineering 2005; 25:93-115

3. Trifunac, M., D., Todorovska, M.,I., 2001, *Evolution of Accelograms, Data Processing, Strong Motion Arrays and Amplitude in Spatial Resolution in Recording Strong Earthquake Motion*, Soil Dynamics and Earthquake Engineering 2001; 21:537-555

4. Trifunac, M.D., Lee, V.W., Todorovska, M.,I., 1999, *Common Problems in Automatic Digitization of Strong Motion Accelograms*, Soil Dynamics and Earthquake Engineering 1999; 18:519-530

5. Trifunac, M.D., Todorovska, M.,I., 2001, *A Note on the Usable Dynamic Range of Accelograms Recording Translation*, Soil Dynamics and Earthquake Engineering 2001; 21- 275-286

6. Douglas, J., 2001, A Critical Reappraisal of Some Problems in Engineering Seismology, PhD. Dissertation, Imperial College of Science, Technology and Medicine, London

7. Skarlatoudis, A., A., Papazachos, C., B., Margaris, B., N., 2003, Determination of Noise Spectra from strong Motion Data Recorded in Greece, Journal of Seismology 2003; 7:533-540, Klawer Academic Publishers, Netherlands

8. Boore, D., M., 2005, On Pads and Filters : Processing Strong Motion Data, Bulletin of the Seismological Society of America, Vol. 95, No.2, pp. 745-750

9. Akkar, S., Bommer, J.,J., 2006, *Influence of long-period filter cut-off on elastic and inelastic spectral displacements*, Earthquake Engineering and Structural Dynamics, 35(9), 1145-1165.

10. Trifunac, M.D., 1971, *Zero Baseline Correction of Strong-Motion Accelograms*, Bulletin of the Seismological Society of America 1971; 61:1201-1211

11. Trifunac, M.D., Udwadio, F.,E, Brady, A.G., 1973, *Analysis of Errors in Digital Strong-Motion Accelograms*, Bulletin of the Seismological Society of America 1973; 63:157-187

12. Lee, V.,W., Trifunac, M.D., 1984, *Current Developments in Data Processing of Strong Motion Accelograms*, Report No. 84-01, Department of Civil Engineering, University of Southern California, Los Angeles

13. Lee, V.,W., Trifunac, M.D., 1990, *Automatic Digitization and Processing of Accelograms Using PC*, Report No. 90-03, Department of Civil Engineering, University of Southern California, Los Angeles

14. Joyner, W.B., Boore, D.M., 1988, *Measurement, Characterization and Prediction of Strong-Motion*, Earthquake Engineering and Soil Dynamics II, Proceedings of American Society of Civil Engineers Geotechnical Engineering Division Specialty Conference, Park City, Utah

15. Atkinson, G.M., Silwa, W., 2000, *Stochastic Modeling of California Ground Motions*, Bulletin of the Seismological Society of America 2000; 90:255-274

16. Kanasewich, E.R., 1975, *Time Sequence Analysis in Geophysics*, The University of Alberta Press, Alberta

17. Smith, S.W., 1999, *The Scientist and Engineer's Guide to Digital Signal Processing*, California Technical Publishing, San Diego

18. Scherbaum, F., 2001, *Of Poles and Zeros*, Kluwer Academic Publishers, Netherlands

19. Converse, A.M., Brady, A.G.,1992, *BAP: Basic Strong-Motion Accelerogram Processing Software; Version 1.0.,* U.S. Geological Survey Open File Report 92-296A

20. Boore, D.M., Akkar, S., 2003, *Effect of Causal and Acausal Filters on Elastic and Inelastic Response Spectra*, Earthquake Engineering and Structural Dynamics, 2003; 32: 1729-1748

21. Ambraseys, N.N., Douglas, J., Sarma, S.K., Smith, P.M., 2005, *Equations for the estimation of strong ground motions from shallow crustal earthqaukes using data from Europe and the Middle East: horizontal peak ground acceleration and the spectral acceleration*, Bulletin of Earthquake Engineering 3(1), 1-53

22. Spudich, P., W.B. Joyner, A.G. Lindh, D.M. Boore, B.M. Margaris, and J.B. Fletcher, 1999, *SEA99: A revised ground motion prediction relation for use in extensional tectonic regimes*, Bulletin of the Seismological Society of America 89 (5), 1156-1170.

23. Abrahamson, N., Silva, W., 1997. *Empirical response spectra relations for shallow crustal earthquakes*, Seismological Research Letters 68 (1), 94-127.

24. Grazier V. M., 1979, *Determination of the true ground displacement by using strong motion records*. Izvestiya Academy of Sciences, USSR, Physics of the Solid Earth, 15(12): 875- 885.

25. Iwan, W.D., Moser, M.A., Peng, C.Y., 1985, *Some observations on strong-motion earthquake measurement using a digital accelerograph*, Bulletin of the Seismological Society of America 1985; 75: 1225–1246.

26. Brune, J.N., *Tectonic stress and the spectra of seismic shear waves from earthquakes,* Journal of Geophysical Research 1970; 75(26): 49975002.

27. HAZUS. 1997, *Earthquake Loss Estimation Methodology*, Technical Manual. National Institute of Building Sciences for Federal Emergency Management Agency: Washington DC, U.S.A., 1997.

28. Bommer J.J., Elnashai A.S., 1999, *Displacement spectra for seismic design*, Journal of Earthquake Engineering 1999; 3:1–32.

29. Ang, A.H-S, Tang, W.H., 1975, *Probability Concepts in Engineering Planning and Design*, vol. 1. Wiley: New York

30. Akkar, S., Bommer, J.J., 2007, *Empirical prediction equations for peak ground velocity derived from strong-motion records from Europe and the Middle East,* Bulletin of the Seismological Society of America, Vol. 97(in press).

31. Iwan, W.D., 1981, *U.S. Strong-Motion Earthquake Instrumentation: Proceedings of the U.S. National Workshop on Strong-Motion Earthquake*

Instrumentation, Technical Report: CaltechEERL:1981.EERL.1981.001, Earthquake Engineering Research Laboratory

32. Gulkan, P., Sozen, M., 1974, *Inelastic response of reinforced concrete structures to earthquakes motions*, ACI Journal, 71:604–610.

APPENDIX-A

Analogue Records from the European Ground-Motion Database Used in the Study

TABLE-1 ROCK SITE STRONG GROUND MOTIONS

Earthquake	Station	Closest Distance	Earthquake Mw
26/04/1997 22:18:34, Strofades (foreshock) (Southern Greece), 5Mw	Kyparrisia-Agriculture Bank (Greece)	26	5
13/11/1998 10:38:34, Oelfus (Iceland region), 5.1Mw	Hveragerdi-Church (Iceland)	9	5.1
26/08/1983 12:52:09, Ierissos (Greece), 5.1Mw	Ouranoupolis-Seismograph Station (Greece)	11	5.1
03/04/1998 07:26:00, Umbria Marche (aftershock) (Central Italy), 5.1Mw	Cassignano (Italy)	17	5.1
13/11/1998 10:38:34, Oelfus (Iceland region), 5.1Mw	Reykjavik-Hus Verslunarinnar (Iceland)	34	5.1
26/08/1983 12:52:09, Ierissos (Greece), 5.1Mw	Poligiros-Prefecture (Greece)	35	5.1
06/10/1991 01:46:47, Turkey-Armenia border (Turkey-Georgia-Armenia border region), 5.1Mw	Toros (Armenia)	40	5.1
16/01/1981 00:37:47, Campano Lucano (aftershock) (Southern Italy), 5.2Mw	Lioni-Macello (Italy)	8	5.2
11/03/1978 19:20:48, Calabria (Southern Italy), 5.2Mw	Ferruzzano (Italy)	10	5.2
07/05/1976 00:23:49, Friuli (aftershock) (Northern Italy), 5.2Mw	Tolmezzo-Diga Ambiesta (Italy)	14	5.2
12/10/1997 11:08:36, Umbria Marche (aftershock) (Central Italy), 5.2Mw	Nocera Umbra-Biscontini (Italy)	24	5.2
12/10/1997 11:08:36, Umbria Marche (aftershock) (Central Italy), 5.2Mw	Nocera Umbra 2 (Italy)	26	5.2
05/03/1993 06:55:06, Near coast of Filiatra (Southern Greece), 5.2Mw	Kyparrisia-Agriculture Bank (Greece)	27	5.2
09/07/1984 18:57:12, Arnissa (Greece), 5.2Mw	Veria-Cultural Center (Greece)	30	5.2
11/09/1976 16:31:11, Friuli (aftershock) (Northern Italy), 5.3Mw	Tarcento (Italy)	8	5.3
10/06/1987 14:50:12, Kalamata (aftershock) (Southern Greece), 5.3Mw	Kyparrisia-Agriculture Bank (Greece)	9	5.3
03/10/1997 08:55:22, Umbria Marche (aftershock) (Central Italy), 5.3Mw	Nocera Umbra (Italy)	10	5.3
03/10/1997 08:55:22, Umbria Marche (aftershock) (Central Italy), 5.3Mw	Assisi-Stallone (Italy)	19	5.3
15/04/1979 06:19:41, Montenegro (Adriatic Sea), 6.9Mw	Makarska-Monastry (Croatia)	22	5.3
18/05/1988 05:17:42, Etolia (Greece), 5.3Mw	Valsamata-Seismograph Station (Greece)	23	5.3
16/09/1977 23:48:08, Friuli (aftershock) (Northern Italy), 5.4Mw	Somplago Centrale-Uscita Galleria (Italy)	9	5.4
16/09/1977 23:48:08, Friuli (aftershock) (Northern Italy), 5.4Mw	Tolmezzo-Base Diga (Italy)	11	5.4
09/04/1979 02:10:21, Montenegro (Albania), 5.4Mw	Ulcinj-Hotel Albatros (Yugoslavia)	15	5.4
16/12/1990 15:45:51, Javakheti Highland (Turkey-Georgia-Armenia border region), 5.4Mw	Akhalkalaki (Georgia)	20	5.4
04/06/1998 21:36:54, Mt. Hengill Area (Iceland), 5.4Mw	Reykjavik-Foldaskoli (Iceland)	27	5.4
11/05/1984 10:41:50, Lazio Abruzzo (aftershock) (Southern Italy), 5.5Mw	Villetta-Barrea (Italy)	2	5.5
06/10/1997 23:24:00, Umbria Marche (aftershock) (Central Italy), 5.5Mw	Nocera Umbra (Italy)	11	5.5
11/05/1984 10:41:50, Lazio Abruzzo (aftershock) (Southern Italy), 5.5Mw	Atina (Italy)	13	5.5
11/05/1984 10:41:50, Lazio Abruzzo (aftershock) (Southern Italy), 5.5Mw	Atina-Pretura Piano Terra (Italy)	13	5.5
11/05/1984 10:41:50, Lazio Abruzzo (aftershock) (Southern Italy), 5.5Mw	Atina-Pretura Terrazza (Italy)	13	5.5
11/05/1984 10:41:50, Lazio Abruzzo (aftershock) (Southern Italy), 5.5Mw	Atina-Pretura Primo Piano (Italy)	13	5.5
06/10/1997 23:24:00, Umbria Marche (aftershock) (Central Italy), 5.5Mw	Gubbio (Italy)	42	5.5
29/04/1984 05:02:59, Umbria (Central Italy), 5.6Mw	Gubbio (Italy)	13	5.6
29/04/1984 05:02:59, Umbria (Central Italy), 5.6Mw	Pietralunga (Italy)	16	5.6
29/04/1984 05:02:59, Umbria (Central Italy), 5.6Mw	Umbertide (Italy)	17	5.6
29/04/1984 05:02:59, Umbria (Central Italy), 5.6Mw	Nocera Umbra (Italy)	19	5.6
13/12/1990 00:24:26, Sicilia-Orientale (Sicily, Italy), 5.6Mw	Sortino (Italy)	29	5.6
26/09/1997 00:33:16, Umbria Marche (Central Italy), 5.7Mw	Nocera Umbra (Italy)	11	5.7

TABLE-1 ROCK SITE STRONG GROUND MOTIONS (continued)

Earthquake	Station	Closest Distance	Earthquake Mw
26/09/1997 00:33:16, Umbria Marche (Central Italy), 5.7Mw	Monte Fiegni (Italy)	22	5.7
26/09/1997 00:33:16, Umbria Marche (Central Italy), 5.7Mw	Cascia (Italy)	31	5.7
19/09/1979 21:35:37, Valnerina (Central Italy), 5.8Mw	Cascia (Italy)	1	5.8
13/09/1999 11:55:30, Izmit (aftershock) (Turkey), 5.8Mw	Izmit-Meteoroloji Istasyonu (Turkey)	15	5.8
19/09/1979 21:35:37, Valnerina (Central Italy), 5.8Mw	Arquata del Tronto (Italy)	19	5.8
15/04/1979 14:43:06, Montenegro (aftershock) (Northwestern Balkan Peninsula), 5.8Mw	Hercegnovi Novi-O.S.D. Pavicic School (Yugoslavia)	22	5.8
06/06/1986 10:39:47, Golbasi (Turkey), 5.8Mw	Golbasi-Devlet Hastanesi (Turkey)	34	5.8
09/01/1988 01:02:47, SE of Tirana (Albania), 5.9Mw	Tirana-Seismological Observatory (Albania)	6	5.9
07/05/1984 17:49:42, Lazio Abruzzo (Southern Italy), 5.9Mw	Atina (Italy)	11	5.9
07/05/1984 17:49:42, Lazio Abruzzo (Southern Italy), 5.9Mw	Ponte Corvo (Italy)	27	5.9
20/06/1994 09:09:03, Firuzabad (Southern Iran), 5.9Mw	Maharlo (Iran)	39	5.9
07/05/1984 17:49:42, Lazio Abruzzo (Southern Italy), 5.9Mw	Roccamonfina (Italy)	44	5.9
07/05/1984 17:49:42, Lazio Abruzzo (Southern Italy), 5.9Mw	Bussi (Italy)	48	5.9
26/09/1997 09:40:30, Umbria Marche (Central Italy), 6Mw	Nocera Umbra (Italy)	1	6
15/09/1976 09:21:19, Friuli (aftershock) (Northern Italy), 6Mw	Tarcento (Italy)	6	6
15/09/1976 09:21:19, Friuli (aftershock) (Northern Italy), 6Mw	Robic (Slovenia)	12	6
07/09/1999 11:56:51, Ano Liosia (Greece), 6Mw	Athens-Ayia Paraskevi (Demokritos) (Greece)	13	6
15/09/1976 03:15:19, Friuli (aftershock) (Northern Italy), 6Mw	Robic (Slovenia)	19	6
26/09/1997 09:40:30, Umbria Marche (Central Italy), 6Mw	Monte Fiegni (Italy)	23	6
25/05/1987 11:31:56, Mt. Vatnafjoll (Iceland), 6Mw	Minni-Nupur (Iceland)	24	6
25/05/1987 11:31:56, Mt. Vatnafjoll (Iceland), 6Mw	Flagbjarnarholt (Iceland)	25	6
15/04/1978 23:33:48, Basso Tirreno (Sicily, Italy), 6Mw	Milazzo (Italy)	26	6
05/05/1986 03:35:38, Golbasi (Turkey), 6Mw	Golbasi-Devlet Hastanesi (Turkey)	27	6
26/09/1997 09:40:30, Umbria Marche (Central Italy), 6Mw	Cascia (Italy)	37	6
26/09/1997 09:40:30, Umbria Marche (Central Italy), 6Mw	Pietralunga (Italy)	44	6
15/04/1978 23:33:48, Basso Tirreno (Sicily, Italy), 6Mw	Messina 1 (Italy)	50	6
24/05/1979 17:23:18, Montenegro (aftershock) (Northwestern Balkan Peninsula), 6.2Mw	Hercegnovi Novi-O.S.D. Pavicic School (Yugoslavia)	28	6.2
06/05/1976 20:00:13, Friuli (Northern Italy), 6.5Mw	Tolmezzo-Diga Ambiesta (Italy)	7	6.5
15/06/1995 00:15:51, Aigion (Greece), 6.5Mw	Mornos Dam-Damfoot (Greece)	19	6.5
23/11/1980 18:34:52, Campano Lucano (Southern Italy), 6.9Mw	Bagnoli-Irpino (Italy)	6	6.9
23/11/1980 18:34:52, Campano Lucano (Southern Italy), 6.9Mw	Auletta (Italy)	10	6.9
15/04/1979 06:19:41, Montenegro (Adriatic Sea), 6.9Mw	Ulcinj-Hotel Albatros (Yugoslavia)	11	6.9
23/11/1980 18:34:52, Campano Lucano (Southern Italy), 6.9Mw	Sturno (Italy)	14	6.9
15/04/1979 06:19:41, Montenegro (Adriatic Sea), 6.9Mw	Hercegnovi Novi-O.S.D. Pavicic School (Yugoslavia)	17	6.9
23/11/1980 18:34:52, Campano Lucano (Southern Italy), 6.9Mw	Bisaccia (Italy)	19	6.9
15/04/1979 06:19:41, Montenegro (Adriatic Sea), 6.9Mw	Titograd-Seismoloska Stanica (Yugoslavia)	41	6.9
12/11/1999 16:57:20, Duzce 1 (Turkey), 7.2Mw	Mudurnu-Kaymakamlik Binasi (Turkey)	34	7.2
16/09/1978 15:35:57, Tabas (Northern and central Iran), 7.3Mw	Dayhook (Iran)	14	7.3
17/08/1999 00:01:40, Izmit (Turkey), 7.6Mw	Izmit-Meteoroloji Istasyonu (Turkey)	5	7.6
17/08/1999 00:01:40, Izmit (Turkey), 7.6Mw	Gebze-Tubitak Marmara Arastirma Merkezi (Turkey)	30	7.6

TABLE-2 STIFF SITE STRONG GROUND MOTIONS

Earthquake	Station	Closest Distance	Earthquake Mw
26/08/1983 12:52:09, Ierissos (Greece), 5.1Mw	Ierissos-Police Station (Greece)	4	5.1
13/11/1998 10:38:34, Oelfus (Iceland region), 5.1Mw	Thorlakshofn (Iceland)	11	5.1
03/04/1998 07:26:00, Umbria Marche (aftershock) (Central Italy), 5.1Mw	Matelica (Italy)	18	5.1
03/04/1998 07:26:00, Umbria Marche (aftershock) (Central Italy), 5.1Mw	Bevagna (Italy)	33	5.1
13/11/1998 10:38:34, Oelfus (Iceland region), 5.1Mw	Kaldarholt (Iceland)	43	5.1
19/08/1999 15:17:45, Izmit (aftershock) (Turkey), 5.1Mw	Yesilkoy-Havaalani (Turkey)	47	5.1
16/01/1981 00:37:47, Campano Lucano (aftershock) (Southern Italy), 5.2Mw	Contrada Fiumicella-Teora (Italy)	4	5.2
16/01/1981 00:37:47, Campano Lucano (aftershock) (Southern Italy), 5.2Mw	Cairano 2 (Italy)	5	5.2
16/01/1981 00:37:47, Campano Lucano (aftershock) (Southern Italy), 5.2Mw	Conza-Vetta (Italy)	5	5.2
16/01/1981 00:37:47, Campano Lucano (aftershock) (Southern Italy), 5.2Mw	Cairano 1 (Italy)	5	5.2
16/01/1981 00:37:47, Campano Lucano (aftershock) (Southern Italy), 5.2Mw	Conza-Base (Italy)	5	5.2
16/01/1981 00:37:47, Campano Lucano (aftershock) (Southern Italy), 5.2Mw	Cairano 3 (Italy)	6	5.2
16/01/1981 00:37:47, Campano Lucano (aftershock) (Southern Italy), 5.2Mw	Cairano 4 (Italy)	7	5.2
16/01/1981 00:37:47, Campano Lucano (aftershock) (Southern Italy), 5.2Mw	Procisa Nuova (Italy)	8	5.2
16/01/1981 00:37:47, Campano Lucano (aftershock) (Southern Italy), 5.2Mw	San Angelo dei Lombardi-Alto (Italy)	12	5.2
11/08/1980 09:15:59, Almiros (aftershock) (Greece), 5.2Mw	Almiros Volos-Town Hall (Greece)	13	5.2
12/10/1997 11:08:36, Umbria Marche (aftershock) (Central Italy), 5.2Mw	Colfiorito (Italy)	14	5.2
17/06/1976 14:28:51, Friuli (aftershock) (Northern Italy), 5.2Mw	Forgaria-Cornio (Italy)	16	5.2
12/10/1997 11:08:36, Umbria Marche (aftershock) (Central Italy), 5.2Mw	Norcia (Italy)	18	5.2
09/11/1985 23:30:43, Drama (Greece), 5.2Mw	Drama-Prefecture (Greece)	19	5.2
09/07/1984 18:57:12, Arnissa (Greece), 5.2Mw	Edessa-Prefecture (Greece)	21	5.2
07/06/1989 19:45:54, Manesion (Southern Greece), 5.2Mw	Patra-National Bank (Greece)	24	5.2
15/03/1992 16:16:16, Pulumur (Turkey), 5.2Mw	Erzincan-Meteorologij Mudurlugu (Turkey)	45	5.2
18/07/1979 13:12:02, Dursunbey (Turkey), 5.3Mw	Dursunbey-Kandilli Gozlem Istasyonu (Turkey)	6	5.3
03/10/1997 08:55:22, Umbria Marche (aftershock) (Central Italy), 5.3Mw	Colfiorito (Italy)	7	5.3
04/11/1993 05:18:37, Gulf of Corinth (Greece), 5.3Mw	Nafpaktos-OTE Building (Greece)	10	5.3
18/05/1988 05:17:42, Etolia (Greece), 5.3Mw	Argostoli-OTE Building (Greece)	12	5.3
11/09/1976 16:31:11, Friuli (aftershock) (Northern Italy), 5.3Mw	Breginj-Fabrika IGLI (Slovenia)	15	5.3
11/09/1976 16:31:11, Friuli (aftershock) (Northern Italy), 5.3Mw	Forgaria-Cornio (Italy)	15	5.3
04/11/1993 05:18:37, Gulf of Corinth (Greece), 5.3Mw	Aigio-OTE Building (Greece)	18	5.3
13/06/1993 23:26:40, Mouzakaiika (Greece-Albania border region), 5.3Mw	Preveza-Town Hall (Greece)	36	5.3
26/06/1991 11:43:32, Kefallinia island (Greece), 5.3Mw	Vasiliki-Town Hall (Greece)	50	5.3
11/09/1976 16:31:11, Friuli (aftershock) (Northern Italy), 5.3Mw	Kobarid-Osn.Skola (Slovenia)	27	5.3
16/09/1977 23:48:08, Friuli (aftershock) (Northern Italy), 5.4Mw	Forgaria-Cornio (Italy)	6	5.4
16/09/1977 23:48:08, Friuli (aftershock) (Northern Italy), 5.4Mw	San Rocco (Italy)	7	5.4
10/03/1981 15:16:20, Preveza (Greece-Albania border region), 5.4Mw	Preveza-OTE Building (Greece)	7	5.4
25/02/1994 02:30:50, Komilion (Greece), 5.4Mw	Vasiliki-Town Hall (Greece)	12	5.4

TABLE-2 STIFF SITE STRONG GROUND MOTIONS (continued)

Earthquake	Station	Closest Distance	Earthquake Mw
09/04/1979 02:10:21, Montenegro (Albania), 5.4Mw	Ulcinj-Hotel Olimpic (Yugoslavia)	18	5.4
26/03/1993 11:58:15, Pyrgos (Southern Greece), 5.4Mw	Amaliada-OTE Building (Greece)	24	5.4
09/04/1979 02:10:21, Montenegro (Albania), 5.4Mw	Petrovac-Hotel Oliva (Yugoslavia)	29	5.4
25/02/1994 02:30:50, Komilion (Greece), 5.4Mw	Preveza-Town Hall (Greece)	29	5.4
25/02/1994 02:30:50, Komilion (Greece), 5.4Mw	Preveza-OTE Building (Greece)	29	5.4
04/06/1998 21:36:54, Mt. Hengill Area (Iceland), 5.4Mw	Kaldarholt (Iceland)	40	5.4
04/07/1991 06:26:29, Racha (aftershock) (Western Caucasus), 5.4Mw	Iri (Georgia)	50	5.4
06/10/1997 23:24:00, Umbria Marche (aftershock) (Central Italy), 5.5Mw	Colfiorito (Italy)	7	5.5
11/09/1976 16:35:03, Friuli (aftershock) (Northern Italy), 5.5Mw	Forgaria-Cornio (Italy)	17	5.5
11/09/1976 16:35:03, Friuli (aftershock) (Northern Italy), 5.5Mw	San Rocco (Italy)	17	5.5
06/10/1997 23:24:00, Umbria Marche (aftershock) (Central Italy), 5.5Mw	Bevagna (Italy)	21	5.5
11/05/1984 10:41:50, Lazio Abruzzo (aftershock) (Southern Italy), 5.5Mw	San Agapito (Italy)	27	5.5
06/10/1997 23:24:00, Umbria Marche (aftershock) (Central Italy), 5.5Mw	Norcia (Italy)	33	5.5
11/09/1976 16:35:03, Friuli (aftershock) (Northern Italy), 5.5Mw	Kobarid-Osn.Skola (Slovenia)	31	5.5
14/07/1993 12:31:50, Patras (Greece), 5.6Mw	Patra-National Bank (Greece)	10	5.6
30/04/1985 18:14:13, Anchialos (Greece), 5.6Mw	Volos-Prefecture (Greece)	15	5.6
14/07/1993 12:31:50, Patras (Greece), 5.6Mw	Nafpaktos-OTE Building (Greece)	27	5.6
05/11/1997 21:10:28, Itea (Greece), 5.6Mw	Aigio-Military Factory (Greece)	28	5.6
14/07/1993 12:31:50, Patras (Greece), 5.6Mw	Aigio-OTE Building (Greece)	30	5.6
23/01/1992 04:24:17, Kefallinia island (Greece), 5.6Mw	Vasiliki-Town Hall (Greece)	42	5.6
26/09/1997 00:33:16, Umbria Marche (Central Italy), 5.7Mw	Colfiorito (Italy)	0	5.7
26/09/1997 00:33:16, Umbria Marche (Central Italy), 5.7Mw	Bevagna (Italy)	23	5.7
26/09/1997 00:33:16, Umbria Marche (Central Italy), 5.7Mw	Matelica (Italy)	24	5.7
27/02/1987 23:34:52, Near NW coast of Kefallinia island (Greece), 5.7Mw	Argostoli-OTE Building (Greece)	35	5.7
26/09/1997 00:33:16, Umbria Marche (Central Italy), 5.7Mw	Norcia-Zona Industriale (Italy)	28	5.7
19/09/1979 21:35:37, Valnerina (Central Italy), 5.8Mw	Spoleto (Italy)	21	5.8
15/04/1979 14:43:06, Montenegro (aftershock) (Northwestern Balkan Peninsula), 5.8Mw	Petrovac-Hotel Oliva (Yugoslavia)	24	5.8
05/05/1990 07:21:17, Potenza (Southern Italy), 5.8Mw	Brienza (Italy)	29	5.8
19/09/1979 21:35:37, Valnerina (Central Italy), 5.8Mw	Mascioni (Italy)	36	5.8
05/05/1990 07:21:17, Potenza (Southern Italy), 5.8Mw	Rionero in Vulture (Italy)	36	5.8
19/09/1979 21:35:37, Valnerina (Central Italy), 5.8Mw	Bevagna (Italy)	37	5.8
15/04/1979 14:43:06, Montenegro (aftershock) (Northwestern Balkan Peninsula), 5.8Mw	Bar-Skupstina Opstine (Yugoslavia)	41	5.8
13/09/1986 17:24:34, Kalamata (Southern Greece), 5.9Mw	Kalamata-Prefecture (Greece)	0	5.9
13/09/1986 17:24:34, Kalamata (Southern Greece), 5.9Mw	Kalamata-OTE Building (Greece)	0	5.9
16/10/1988 12:34:05, Kyllini (Southern Greece), 5.9Mw	Zakynthos-OTE Building (Greece)	11	5.9
18/11/1992 21:10:41, Tithorea (Greece), 5.9Mw	Aigio-OTE Building (Greece)	25	5.9
07/05/1984 17:49:42, Lazio Abruzzo (Southern Italy), 5.9Mw	San Agapito (Italy)	28	5.9
16/10/1988 12:34:05, Kyllini (Southern Greece), 5.9Mw	Amaliada-OTE Building (Greece)	36	5.9
20/06/1994 09:09:03, Firuzabad (Southern Iran), 5.9Mw	Babanar (Iran)	48	5.9
18/11/1992 21:10:41, Tithorea (Greece), 5.9Mw	Amfissa-OTE Building (Greece)	30	5.9

TABLE-2 STIFF SITE STRONG GROUND MOTIONS (continued)

Earthquake	Station	Closest Distance	Earthquake Mw
26/09/1997 09:40:30, Umbria Marche (Central Italy), 6Mw	Colfiorito (Italy)	5	6
15/09/1976 09:21:19, Friuli (aftershock) (Northern Italy), 6Mw	Breginj-Fabrika IGLI (Slovenia)	7	6
07/09/1999 11:56:51, Ano Liosia (Greece), 6Mw	Athens 4 (Kipseli District) (Greece)	8	6
07/09/1999 11:56:51, Ano Liosia (Greece), 6Mw	Athens 3 (Kallithea District) (Greece)	8	6
15/09/1976 09:21:19, Friuli (aftershock) (Northern Italy), 6Mw	Forgaria-Cornio (Italy)	9	6
15/09/1976 09:21:19, Friuli (aftershock) (Northern Italy), 6Mw	San Rocco (Italy)	9	6
07/09/1999 11:56:51, Ano Liosia (Greece), 6Mw	Athens 2 (Chalandri District) (Greece)	9	6
07/09/1999 11:56:51, Ano Liosia (Greece), 6Mw	Athens-Dafni (Greece)	11	6
15/09/1976 03:15:19, Friuli (aftershock) (Northern Italy), 6Mw	Forgaria-Cornio (Italy)	12	6
15/09/1976 03:15:19, Friuli (aftershock) (Northern Italy), 6Mw	San Rocco (Italy)	12	6
15/09/1976 03:15:19, Friuli (aftershock) (Northern Italy), 6Mw	Breginj-Fabrika IGLI (Slovenia)	14	6
15/04/1978 23:33:48, Basso Tirreno (Sicily, Italy), 6Mw	Naso (Italy)	16	6
26/09/1997 09:40:30, Umbria Marche (Central Italy), 6Mw	Matelica (Italy)	21	6
26/09/1997 09:40:30, Umbria Marche (Central Italy), 6Mw	Bevagna (Italy)	22	6
25/05/1987 11:31:56, Mt. Vatnafjoll (Iceland), 6Mw	Hella (Iceland)	31	6
15/09/1976 03:15:19, Friuli (aftershock) (Northern Italy), 6Mw	Codroipo (Italy)	35	6
15/06/1991 00:59:20, Racha (aftershock) (Western Caucasus), 6Mw	Iri (Georgia)	37	6
06/11/1992 19:08:09, Izmir (Aegean Sea), 6Mw	Kusadasi-Meteoroloji Mudurlugu (Turkey)	41	6
15/06/1991 00:59:20, Racha (aftershock) (Western Caucasus), 6Mw	Oni (Georgia)	49	6
15/09/1976 09:21:19, Friuli (aftershock) (Northern Italy), 6Mw	Kobarid-Osn.Skola (Slovenia)	19	6
15/09/1976 03:15:19, Friuli (aftershock) (Northern Italy), 6Mw	Kobarid-Osn.Skola (Slovenia)	25	6
26/09/1997 09:40:30, Umbria Marche (Central Italy), 6Mw	Norcia-Altavilla (Italy)	32	6
26/09/1997 09:40:30, Umbria Marche (Central Italy), 6Mw	Norcia-Zona Industriale (Italy)	34	6
21/12/1990 06:57:43, Griva (Greece), 6.1Mw	Edessa-Prefecture (Greece)	31	6.1
21/12/1990 06:57:43, Griva (Greece), 6.1Mw	Kilkis-Hospital (Greece)	31	6.1
05/07/1983 12:01:27, Biga (Turkey), 6.1Mw	Gonen-Meteoroloji Mudurlugu (Turkey)	45	6.1
24/05/1979 17:23:18, Montenegro (aftershock) (Northwestern Balkan Peninsula), 6.2Mw	Budva-PTT (Yugoslavia)	10	6.2
24/05/1979 17:23:18, Montenegro (aftershock) (Northwestern Balkan Peninsula), 6.2Mw	Petrovac-Hotel Rivijera (Yugoslavia)	12	6.2
24/05/1979 17:23:18, Montenegro (aftershock) (Northwestern Balkan Peninsula), 6.2Mw	Bar-Skupstina Opstine (Yugoslavia)	15	6.2
24/05/1979 17:23:18, Montenegro (aftershock) (Northwestern Balkan Peninsula), 6.2Mw	Kotor-Naselje Rakite (Yugoslavia)	19	6.2
24/05/1979 17:23:18, Montenegro (aftershock) (Northwestern Balkan Peninsula), 6.2Mw	Tivat-Aerodrom (Yugoslavia)	19	6.2
24/05/1979 17:23:18, Montenegro (aftershock) (Northwestern Balkan Peninsula), 6.2Mw	Kotor-Zovod za Biologiju Mora (Yugoslavia)	21	6.2
24/05/1979 17:23:18, Montenegro (aftershock) (Northwestern Balkan Peninsula), 6.2Mw	Ulcinj-Hotel Olimpic (Yugoslavia)	35	6.2
01/10/1995 15:57:13, Dinar (Turkey), 6.4Mw	Cardak-Saglik Ocagi (Turkey)	39	6.4
01/10/1995 15:57:13, Dinar (Turkey), 6.4Mw	Burdur-Meteoroloji Mudurgulu (Turkey)	39	6.4
15/06/1995 00:15:51, Aigion (Greece), 6.5Mw	Aigio-OTE Building (Greece)	7	6.5
06/05/1976 20:00:13, Friuli (Northern Italy), 6.5Mw	Codroipo (Italy)	34	6.5
15/06/1995 00:15:51, Aigion (Greece), 6.5Mw	Amfissa-OTE Building (Greece)	22	6.5
13/03/1992 17:18:40, Erzincan (Turkey), 6.6Mw	Erzincan-Meteorologij Mudurlugu (Turkey)	1	6.6
30/10/1983 04:12:28, Panisler (Turkey), 6.6Mw	Horasan-Meteoroloji Mudurlugu (Turkey)	17	6.6

TABLE-2 STIFF SITE STRONG GROUND MOTIONS (continued)

Earthquake	Station	Closest Distance	Earthquake Mw
18/11/1997 13:07:41, Strofades (Ionian Sea), 6.6Mw	Zakynthos-OTE Building (Greece)	39	6.6
15/04/1979 06:19:41, Montenegro (Adriatic Sea), 6.9Mw	Bar-Skupstina Opstine (Yugoslavia)	3	6.9
15/04/1979 06:19:41, Montenegro (Adriatic Sea), 6.9Mw	Petrovac-Hotel Oliva (Yugoslavia)	3	6.9
15/04/1979 06:19:41, Montenegro (Adriatic Sea), 6.9Mw	Ulcinj-Hotel Olimpic (Yugoslavia)	13	6.9
23/11/1980 18:34:52, Campano Lucano (Southern Italy), 6.9Mw	Calitri (Italy)	13	6.9
23/11/1980 18:34:52, Campano Lucano (Southern Italy), 6.9Mw	Brienza (Italy)	23	6.9
23/11/1980 18:34:52, Campano Lucano (Southern Italy), 6.9Mw	Rionero in Vulture (Italy)	29	6.9
23/11/1980 18:34:52, Campano Lucano (Southern Italy), 6.9Mw	Mercato San Severino (Italy)	33	6.9
23/11/1980 18:34:52, Campano Lucano (Southern Italy), 6.9Mw	Benevento (Italy)	41	6.9
15/04/1979 06:19:41, Montenegro (Adriatic Sea), 6.9Mw	Titograd-Geoloski Zavod (Yugoslavia)	42	6.9
12/11/1999 16:57:20, Duzce 1 (Turkey), 7.2Mw	Goynuk-Devlet Hastanesi (Turkey)	47	7.2
16/09/1978 15:35:57, Tabas (Northern and central Iran), 7.3Mw	Tabas (Iran)	8	7.3
16/09/1978 15:35:57, Tabas (Northern and central Iran), 7.3Mw	Boshroyeh (Iran)	39	7.3
20/06/1990 21:00:08, Manjil (Western Iran), 7.4Mw	Qazvin (Iran)	49	7.4
17/08/1999 00:01:40, Izmit (Turkey), 7.6Mw	Goynuk-Devlet Hastanesi (Turkey)	31	7.6

TABLE-3 SOFT SITE STRONG GROUND MOTIONS

Earthquake	Station	Closest Distance	Earthquake Mw
03/04/1998 07:26:00, Umbria Marche (aftershock) (Central Italy), 5.1Mw	Nocera Umbra-Salmata (Italy)	6	5.1
29/11/1994 14:30:30, Off coast of Levkas island (Greece), 5.1Mw	Lefkada-Hospital (Greece)	17	5.1
29/11/1994 14:30:30, Off coast of Levkas island (Greece), 5.1Mw	Lefkada-OTE Building (Greece)	18	5.1
03/04/1998 07:26:00, Umbria Marche (aftershock) (Central Italy), 5.1Mw	Castelnuovo-Assisi (Italy)	27	5.1
31/08/1999 08:10:49, Izmit (aftershock) (Turkey), 5.1Mw	Adapazari A.Babalioglu Evi (Turkey)	39	5.1
31/08/1999 08:10:49, Izmit (aftershock) (Turkey), 5.1Mw	Adapazari Toyotasa (Turkey)	39	5.1
31/08/1999 08:10:49, Izmit (aftershock) (Turkey), 5.1Mw	Adapazari Kadin D. Cocuk B. Evi (Turkey)	39	5.1
19/08/1999 15:17:45, Izmit (aftershock) (Turkey), 5.1Mw	Istanbul-K.M.Pasa (Turkey)	45	5.1
07/06/1989 19:45:54, Manesion (Southern Greece), 5.2Mw	Patra-OTE Building (Greece)	24	5.2
11/03/1978 19:20:48, Calabria (Southern Italy), 5.2Mw	Pellaro (Italy)	33	5.2
14/02/2000 06:56:35, Duzce 1 (aftershock) (Turkey), 5.2Mw	Gon (Turkey)	45	5.2
14/02/2000 06:56:35, Duzce 1 (aftershock) (Turkey), 5.2Mw	Met (Turkey)	49	5.2
11/09/1976 16:31:11, Friuli (aftershock) (Northern Italy), 5.3Mw	Buia (Italy)	9	5.3
03/10/1997 08:55:22, Umbria Marche (aftershock) (Central Italy), 5.3Mw	Nocera Umbra-Salmata (Italy)	13	5.3
01/04/1978 14:25:25, Gacko (Northwestern Balkan Peninsula), 4.5ML	Gacko-Zemlj. Zadruga (Bosnia and Herzegovina)	18	5.3
04/11/1993 05:18:37, Gulf of Corinth (Greece), 5.3Mw	Patra-OTE Building (Greece)	19	5.3
13/06/1993 23:26:40, Mouzakaiika (Greece-Albania border region), 5.3Mw	Lefkada-OTE Building (Greece)	33	5.3
26/03/1993 11:58:15, Pyrgos (Southern Greece), 5.4Mw	Pyrgos-Agriculture Bank (Greece)	10	5.4
25/02/1994 02:30:50, Komilion (Greece), 5.4Mw	Lefkada-Hospital (Greece)	15	5.4
25/02/1994 02:30:50, Komilion (Greece), 5.4Mw	Lefkada-OTE Building (Greece)	16	5.4
10/03/1981 15:16:20, Preveza (Greece-Albania border region), 5.4Mw	Lefkada-OTE Building (Greece)	21	5.4
16/12/1990 15:45:51, Javakheti Highland (Turkey-Georgia-Armenia border region), 5.4Mw	Bakuriani (Georgia)	44	5.4
11/09/1976 16:35:03, Friuli (aftershock) (Northern Italy), 5.5Mw	Buia (Italy)	7	5.5
06/10/1997 23:24:00, Umbria Marche (aftershock) (Central Italy), 5.5Mw	Nocera Umbra-Salmata (Italy)	15	5.5
11/05/1984 10:41:50, Lazio Abruzzo (aftershock) (Southern Italy), 5.5Mw	Cassino-Sant' Elia (Italy)	20	5.5
06/10/1997 23:24:00, Umbria Marche (aftershock) (Central Italy), 5.5Mw	Castelnuovo-Assisi (Italy)	20	5.5
14/07/1993 12:31:50, Patras (Greece), 5.6Mw	Patra-OTE Building (Greece)	10	5.6
14/08/1996 02:59:41, Cerkes (aftershock) (Turkey), 5.6Mw	Merzifon-Meteoroloji Mudurlugu (Turkey)	13	5.6
13/12/1990 00:24:26, Sicilia-Orientale (Sicily, Italy), 5.6Mw	Catania-Piana (Italy)	24	5.6
29/04/1984 05:02:59, Umbria (Central Italy), 5.6Mw	Citta di Castello-Regnano (Italy)	30	5.6
13/12/1990 00:24:26, Sicilia-Orientale (Sicily, Italy), 5.6Mw	Giarre (Italy)	45	5.6
26/09/1997 00:33:16, Umbria Marche (Central Italy), 5.7Mw	Castelnuovo-Assisi (Italy)	21	5.7
04/11/1973 15:52:12, Ionian (Greece), 5.8Mw	Lefkada-OTE Building (Greece)	11	5.8
13/09/1999 11:55:30, Izmit (aftershock) (Turkey), 5.8Mw	Iznik-Karayollari Sefligi Muracaati (Turkey)	49	5.8
07/05/1984 17:49:42, Lazio Abruzzo (Southern Italy), 5.9Mw	Cassino-Sant' Elia (Italy)	18	5.9
16/10/1988 12:34:05, Kyllini (Southern Greece), 5.9Mw	Pyrgos-Agriculture Bank (Greece)	49	5.9
15/09/1976 09:21:19, Friuli (aftershock) (Northern Italy), 6Mw	Buia (Italy)	8	6
15/09/1976 03:15:19, Friuli (aftershock) (Northern Italy), 6Mw	Buia (Italy)	9	6

TABLE-3 SOFT SITE STRONG GROUND MOTIONS (continued)

Earthquake	Station	Closest Distance	Earthquake Mw
15/04/1978 23:33:48, Basso Tirreno (Sicily, Italy), 6Mw	Patti-Cabina Prima (Italy)	13	6
26/09/1997 09:40:30, Umbria Marche (Central Italy), 6Mw	Castelnuovo-Assisi (Italy)	17	6
15/06/1991 00:59:20, Racha (aftershock) (Western Caucasus), 6Mw	Oni-Base Camp (Georgia)	48	6
09/07/1998 05:19:07, Faial (Azores Islands, Portugal), 6.1Mw	Horta (Portugal)	11	6.1
20/06/1978 20:03:22, Volvi (Greece), 6.2Mw	Thessaloniki-City Hotel (Greece)	13	6.2
25/02/1981 02:35:53, Alkion (Greece), 6.3Mw	Korinthos-OTE Building (Greece)	19	6.3
01/10/1995 15:57:13, Dinar (Turkey), 6.4Mw	Dinar-Meteoroloji Mudurlugu (Turkey)	0	6.4
15/06/1995 00:15:51, Aigion (Greece), 6.5Mw	Patra-OTE Building (Greece)	36	6.5
06/05/1976 20:00:13, Friuli (Northern Italy), 6.5Mw	Barcis (Italy)	37	6.5
24/02/1981 20:53:39, Alkion (Greece), 6.6Mw	Xilokastro-OTE Building (Greece)	8	6.6
24/02/1981 20:53:39, Alkion (Greece), 6.6Mw	Korinthos-OTE Building (Greece)	10	6.6
07/12/1988 07:41:24, Spitak (Turkey-Georgia-Armenia border region), 6.7Mw	Gukasian (Armenia)	20	6.7
23/11/1980 18:34:52, Campano Lucano (Southern Italy), 6.9Mw	Bovino (Italy)	39	6.9
12/11/1999 16:57:20, Duzce 1 (Turkey), 7.2Mw	Duzce-Meteoroloji Mudurlugu (Turkey)	0	7.2
17/08/1999 00:01:40, Izmit (Turkey), 7.6Mw	Duzce-Meteoroloji Mudurlugu (Turkey)	12	7.6
17/08/1999 00:01:40, Izmit (Turkey), 7.6Mw	Iznik-Karayollari Sefligi Muracaati (Turkey)	29	7.6

APPENDIX-B

Kolmogorov-Smirnov Tests for Different Site Classes and Different T/T_c Values

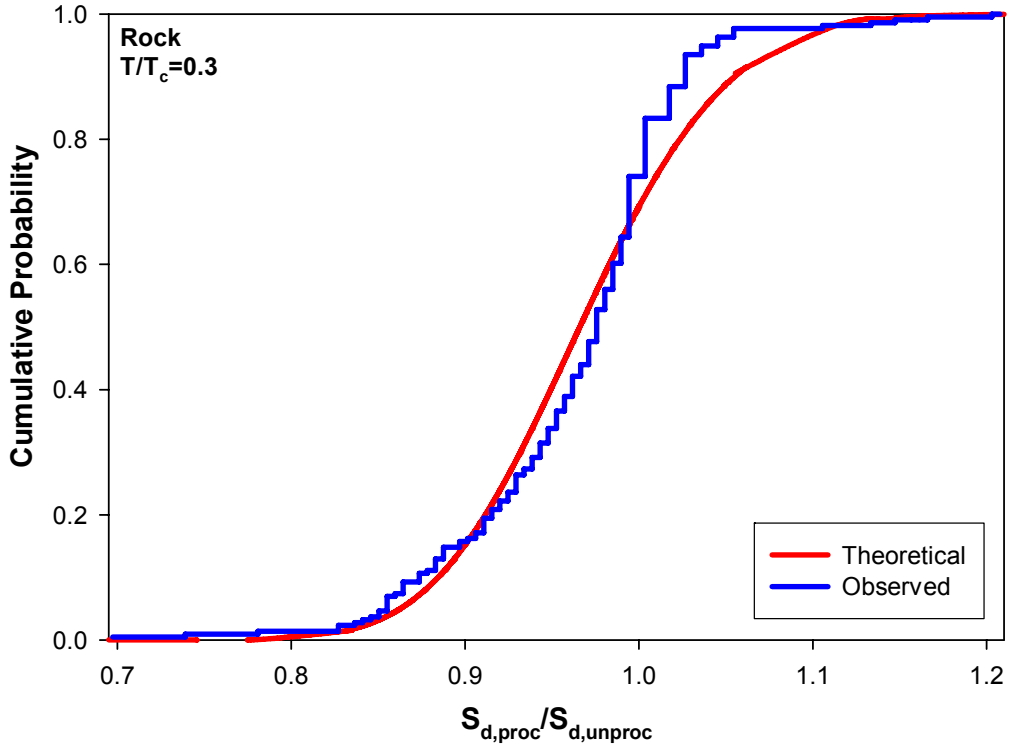

Figure B.1 Kolmogorov-Smirnov Test for Rock Sites for T/T$_c$=0.3

$$D_n = \max\left|F(x) - S_n(x)\right| = 0.102$$

$$D_n^{0.01} = 0.111$$

$D_n < D_n^{0.01} \rightarrow$The data can be assumed to have a log-normal distribution due to Kolmogorov-Smirnov test.

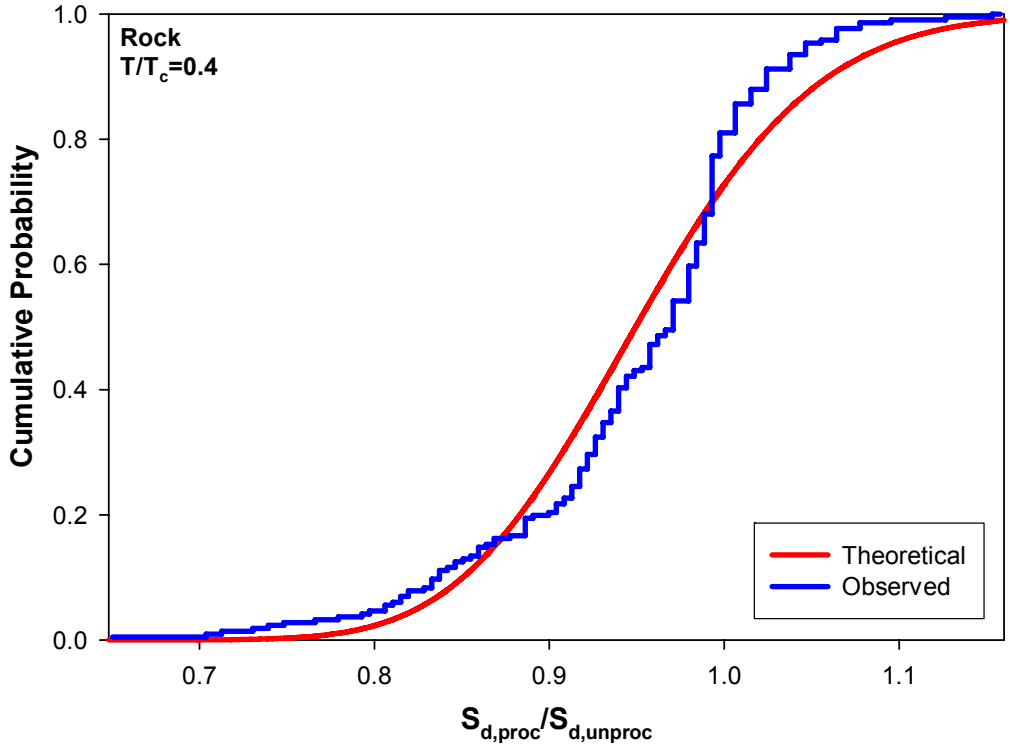

Figure B.2 Kolmogorov-Smirnov Test for Rock Sites for T/T_c=0.4

$$D_n = \max\left|F(x) - S_n(x)\right| = 0.079$$

$$D_n^{0.01} = 0.111$$

$D_n < D_n^{0.01} \rightarrow$The data can be assumed to have a log-normal distribution due to Kolmogorov-Smirnov test.

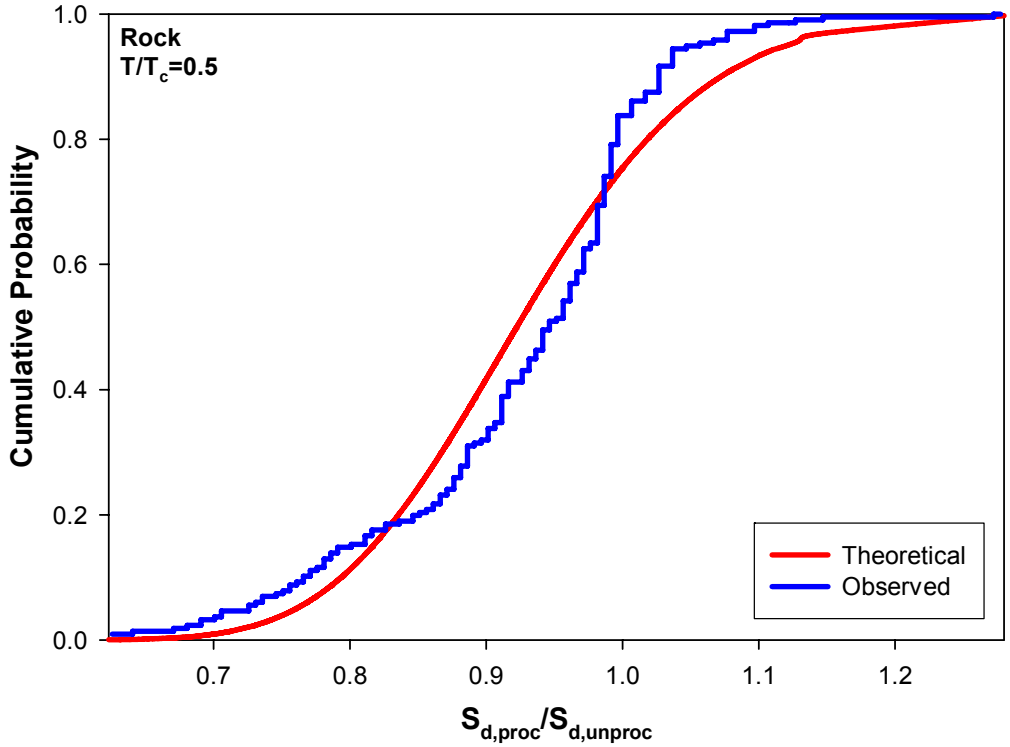

Figure B.3 Kolmogorov-Smirnov Test for Rock Sites for T/T$_c$=0.5

$$D_n = \max\left|F(x) - S_n(x)\right| = 0.106$$

$$D_n^{0.01} = 0.111$$

$D_n < D_n^{0.01} \rightarrow$The data can be assumed to have a log-normal distribution due to Kolmogorov-Smirnov test.

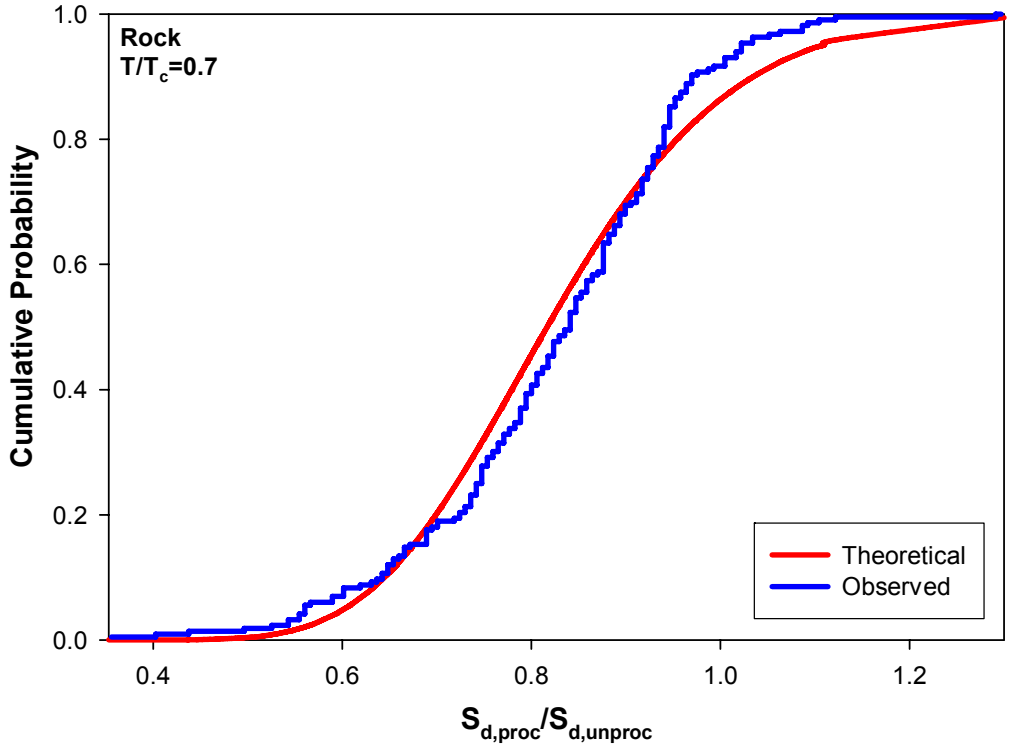

Figure B.4 Kolmogorov-Smirnov Test for Rock Sites for T/T$_c$=0.7

$$D_n = \max\left|F(x) - S_n(x)\right| = 0.074$$

$$D_n^{0.01} = 0.111$$

$D_n < D_n^{0.01} \rightarrow$The data can be assumed to have a log-normal distribution due to Kolmogorov-Smirnov test.

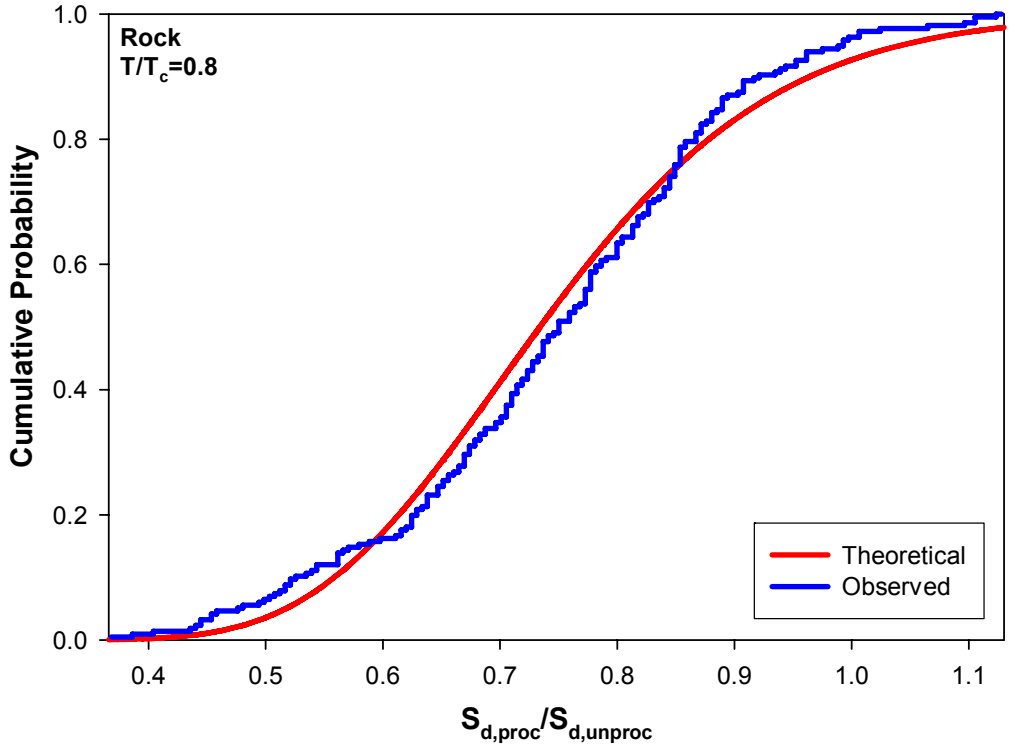

Figure B.5 Kolmogorov-Smirnov Test for Rock Sites for T/T$_c$=0.8

$$D_n = \max\left|F(x) - S_n(x)\right| = 0.045$$

$$D_n^{0.01} = 0.111$$

$D_n < D_n^{0.01} \rightarrow$The data can be assumed to have a log-normal distribution due to Kolmogorov-Smirnov test.

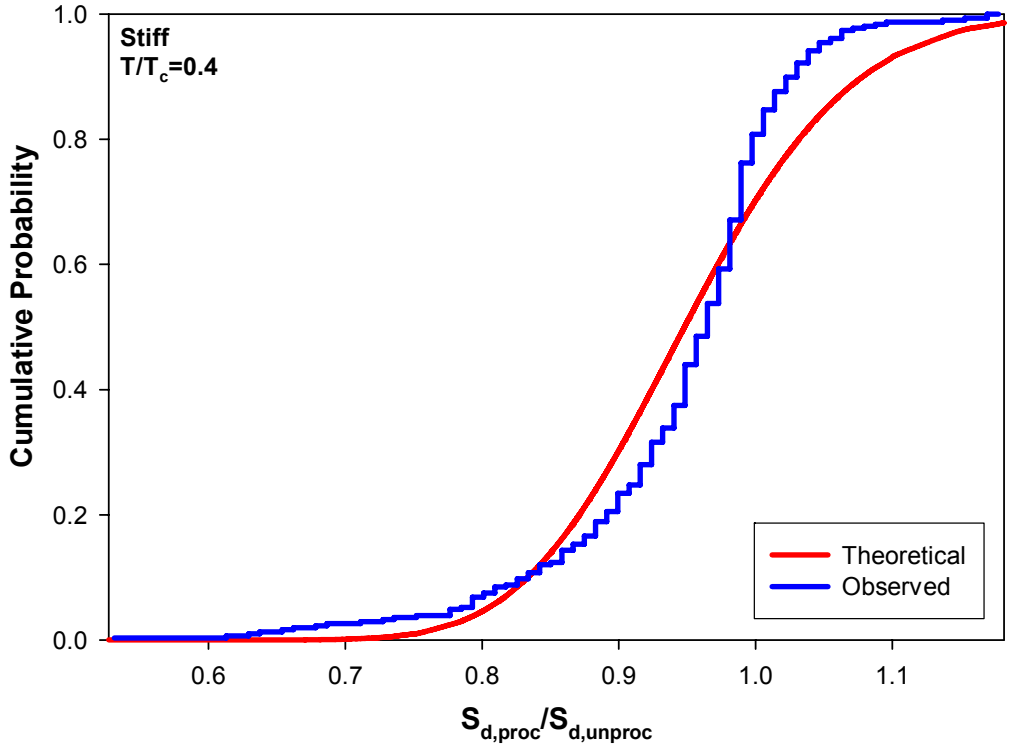

Figure B.6 Kolmogorov-Smirnov Test for Stiff Sites for T/T$_c$=0.4

$$D_n = \max\left|F(x) - S_n(x)\right| = 0.091$$

$$D_n^{0.01} = 0.093$$

$D_n < D_n^{0.01} \rightarrow$The data can be assumed to have a log-normal distribution due to Kolmogorov-Smirnov test.

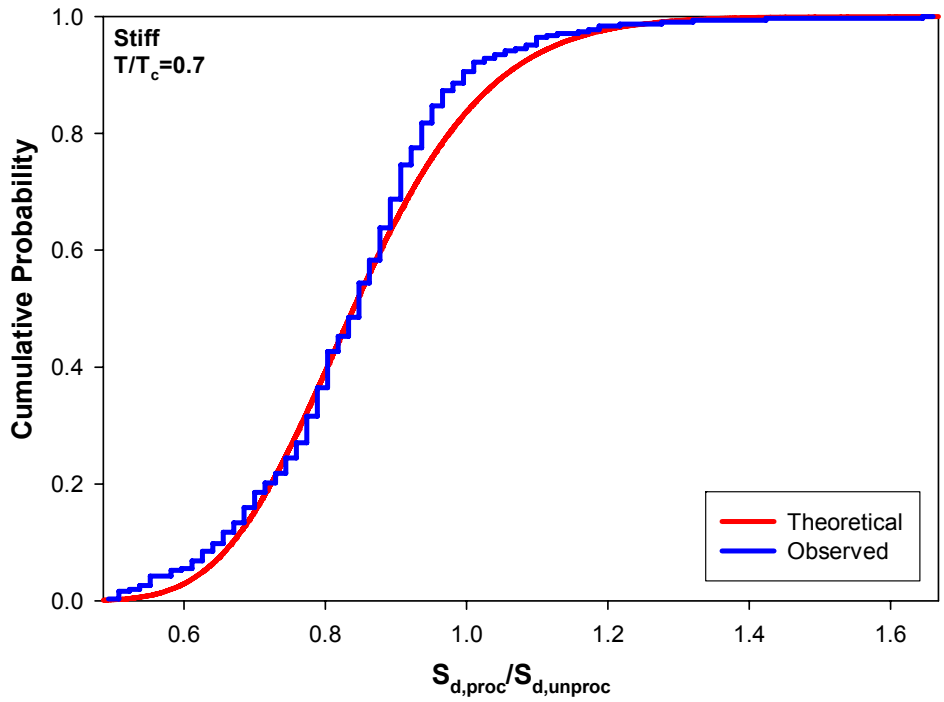

Figure B.7 Kolmogorov-Smirnov Test for Stiff Sites for T/T$_c$=0.7

$$D_n = \max\left|F(x) - S_n(x)\right| = 0.079$$

$$D_n^{0.01} = 0.093$$

$D_n < D_n^{0.01} \rightarrow$The data can be assumed to have a log-normal distribution due to Kolmogorov-Smirnov test.

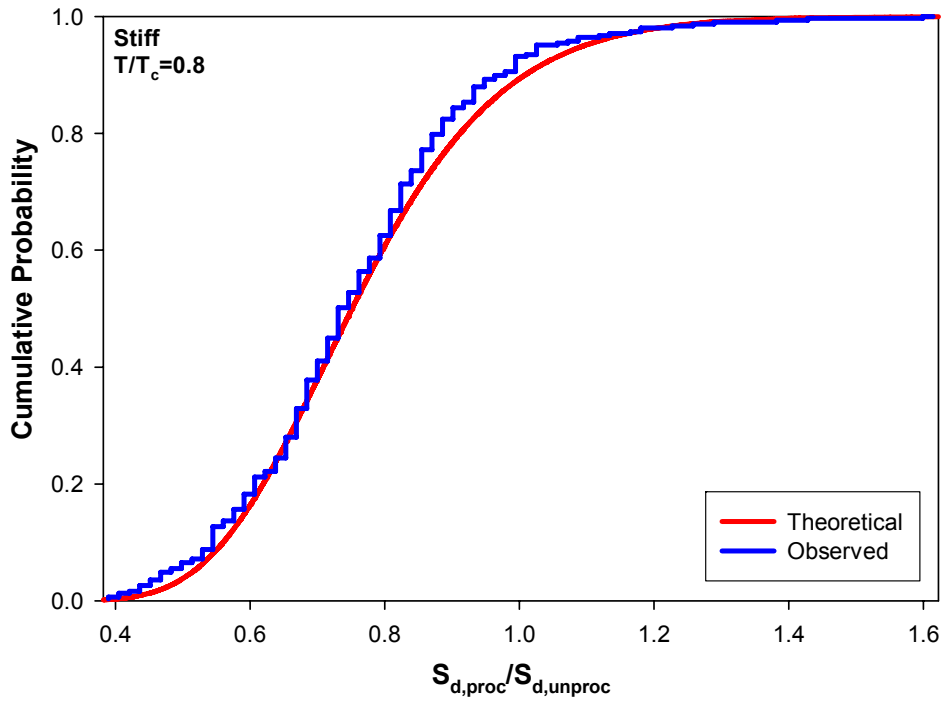

Figure B.8 Kolmogorov-Smirnov Test for Stiff Sites for T/T$_c$=0.8

$$D_n = \max\left|F(x) - S_n(x)\right| = 0.057$$

$$D_n^{0.01} = 0.093$$

$D_n < D_n^{0.01} \rightarrow$The data can be assumed to have a log-normal distribution due to Kolmogorov-Smirnov test.

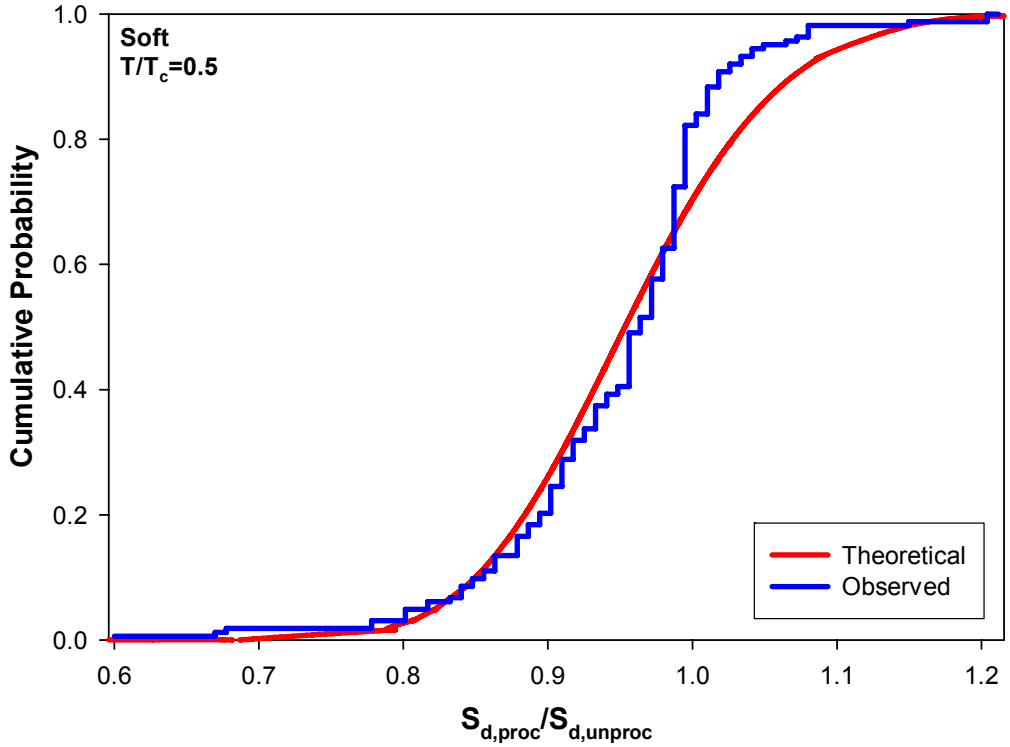

Figure B.9 Kolmogorov-Smirnov Test for Soft Sites for T/T$_c$=0.5

$$D_n = \max\left|F(x) - S_n(x)\right| = 0.125$$

$$D_n^{0.01} = 0.128$$

$D_n < D_n^{0.01} \rightarrow$The data can be assumed to have a log-normal distribution due to Kolmogorov-Smirnov test.

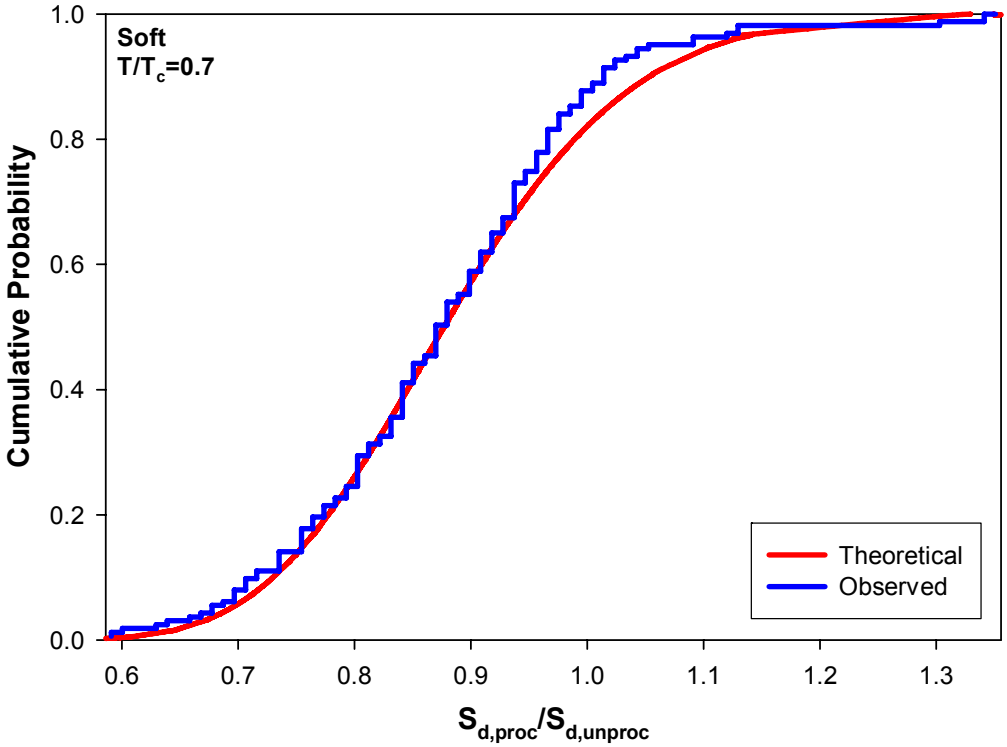

Figure B.10 Kolmogorov-Smirnov Test for Soft Sites for T/T$_c$=0.7

$$D_n = \max\left|F(x) - S_n(x)\right| = 0.068$$

$$D_n^{0.01} = 0.128$$

$D_n < D_n^{0.01} \rightarrow$The data can be assumed to have a log-normal distribution due to Kolmogorov-Smirnov test.

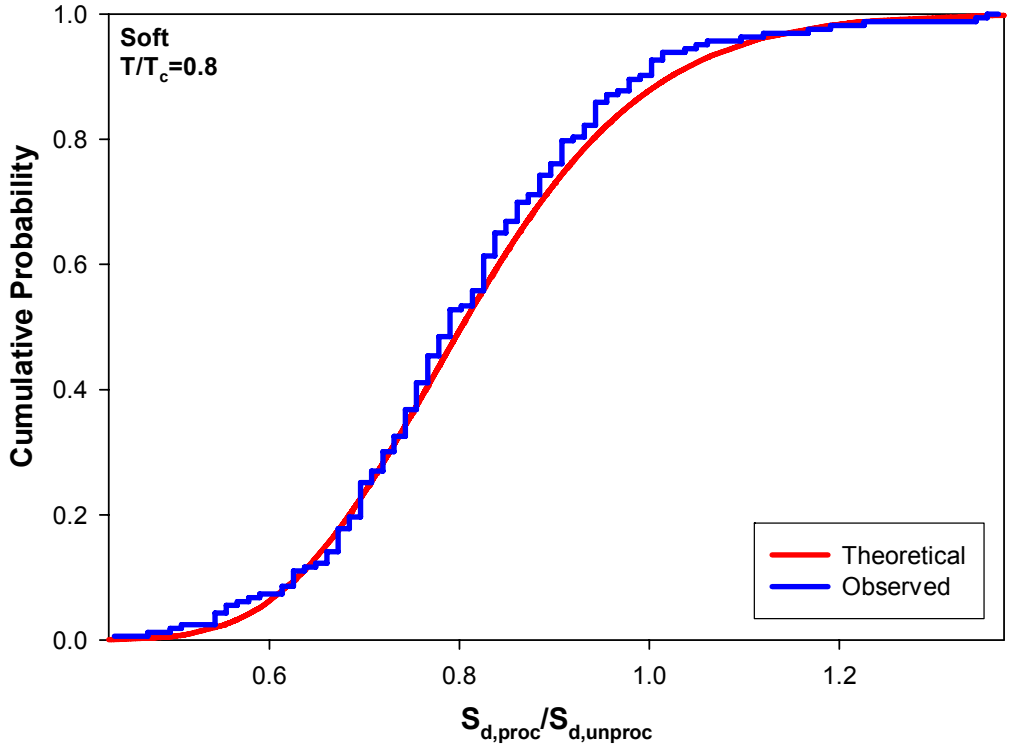

Figure B.11 Kolmogorov-Smirnov Test for Soft Sites for T/T$_c$=0.8

$$D_n = \max\left|F(x) - S_n(x)\right| = 0.045$$

$$D_n^{0.01} = 0.128$$

$D_n < D_n^{0.01} \rightarrow$The data can be assumed to have a log-normal distribution due to Kolmogorov-Smirnov test.

APPENDIX-C

Cumulative Probability Functions for Different Site Classes and Different T/T_c Values

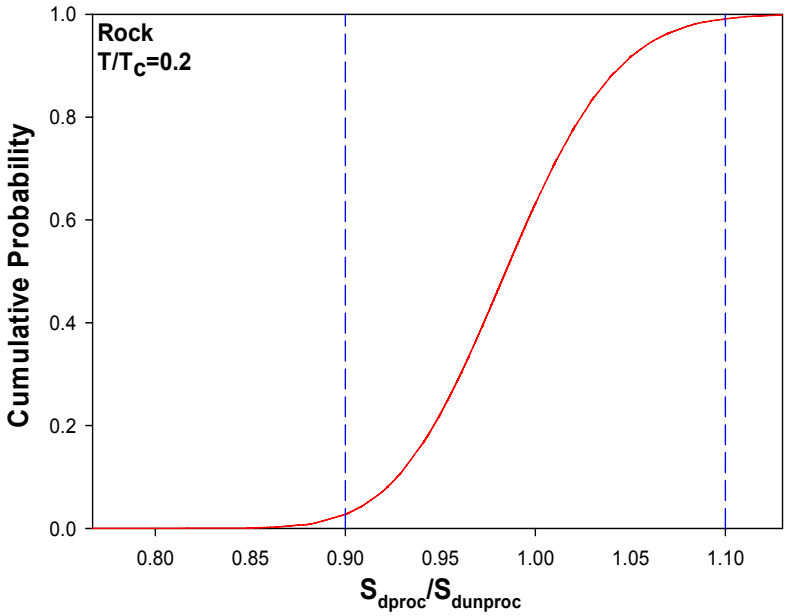

Figure C.1 Cumulative probability function for rock sites for T/T_c=0.2

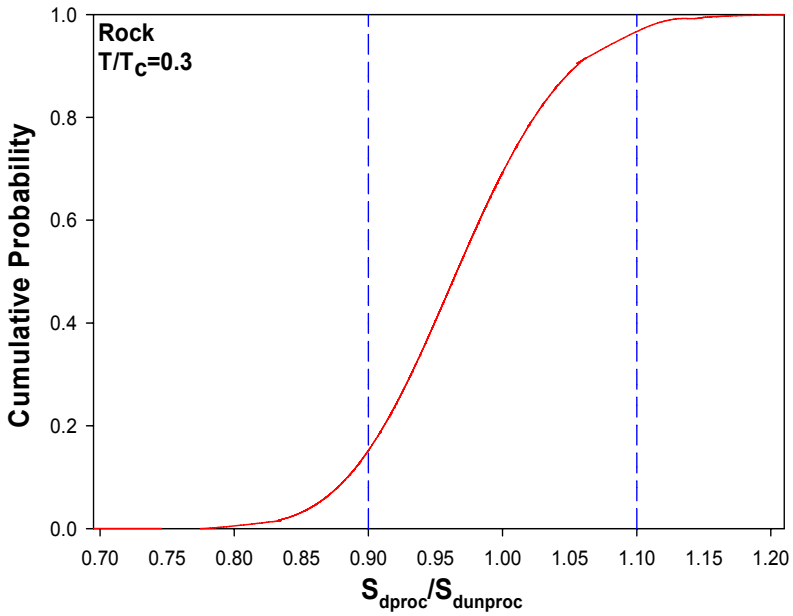

Figure C.2 Cumulative probability function for rock sites for T/T_c=0.3

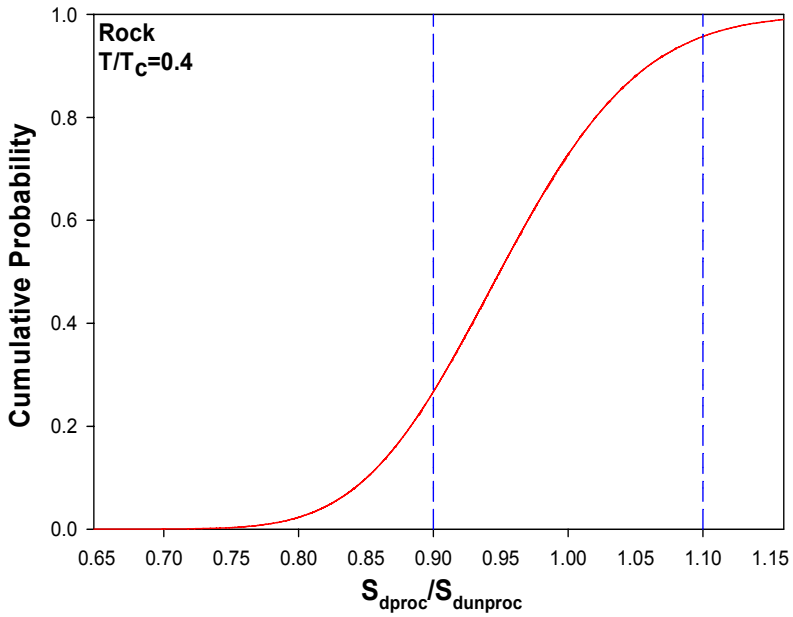

Figure C.3 Cumulative probability function for rock sites for T/T_c=0.4

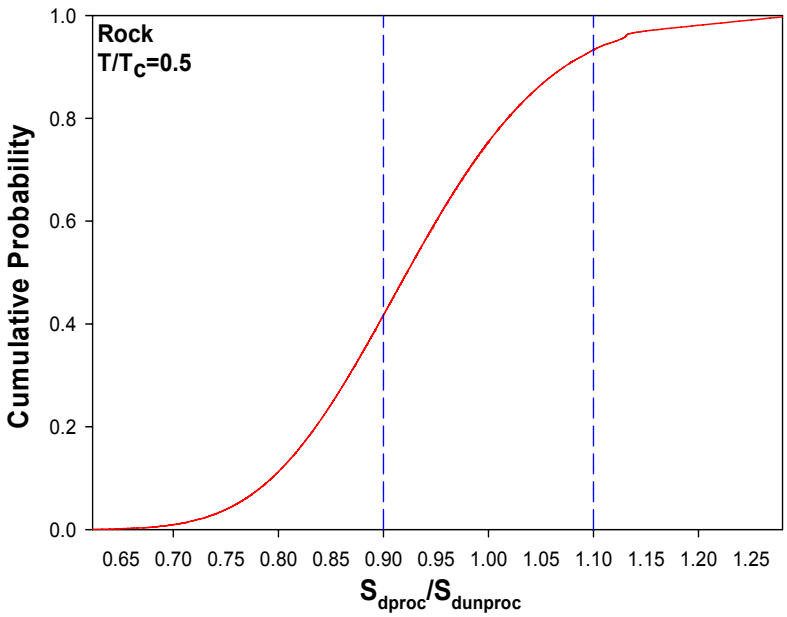

Figure C.4 Cumulative probability function for rock sites for T/T_c=0.5

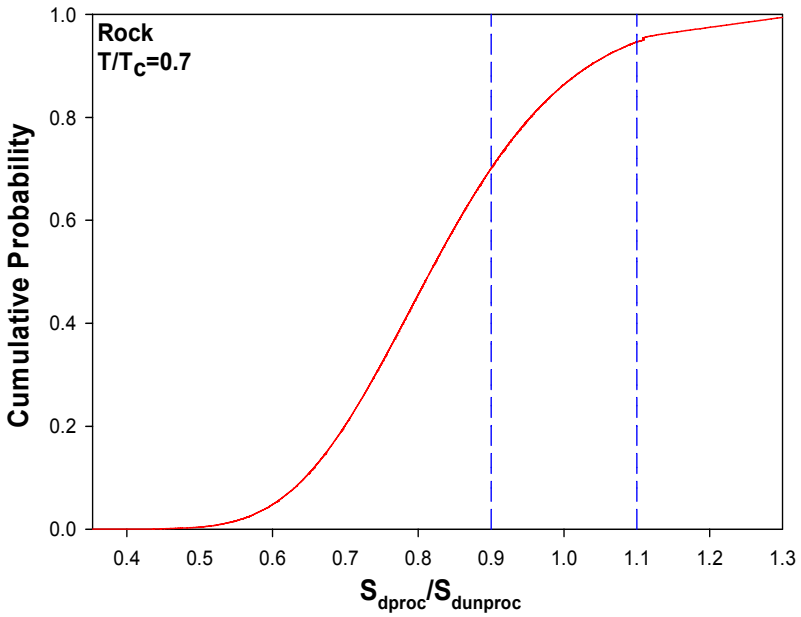

Figure C.5 Cumulative probability function for rock sites for T/T_c=0.7

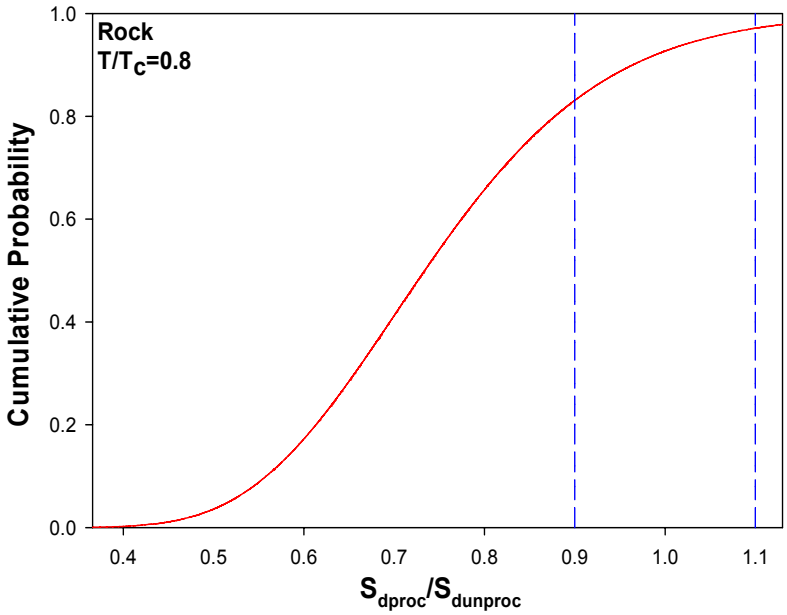

Figure C.6 Cumulative probability function for rock sites for T/T_c=0.8

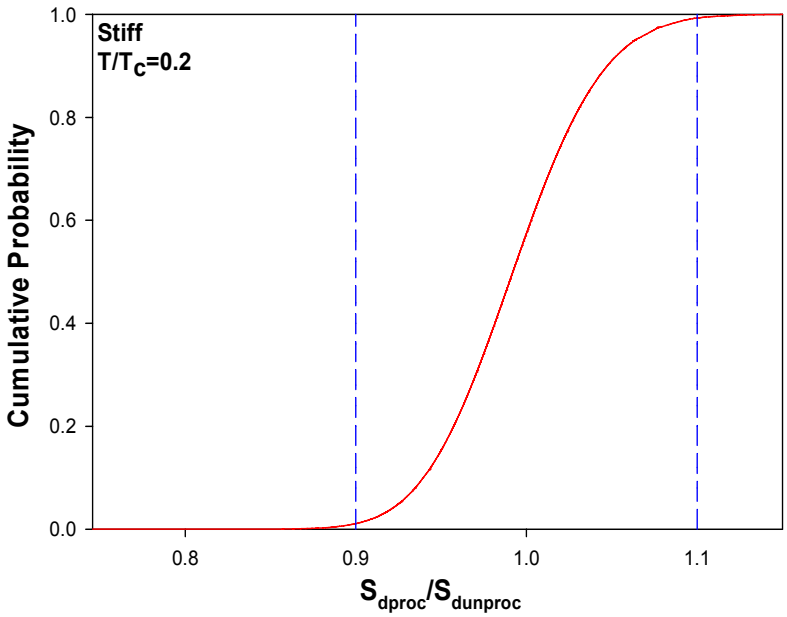

Figure C.7 Cumulative probability function for stiff sites for T/T_c=0.2

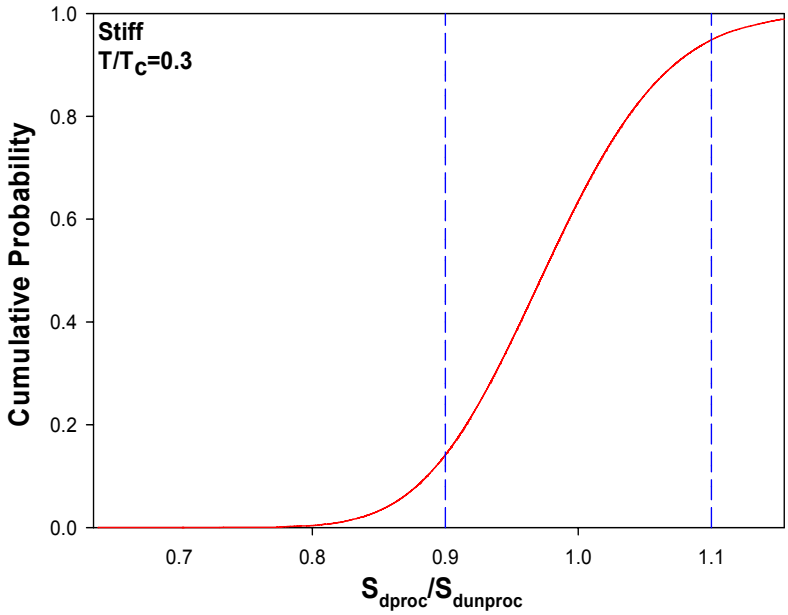

Figure C.8 Cumulative probability function for stiff sites for T/T_c=0.3

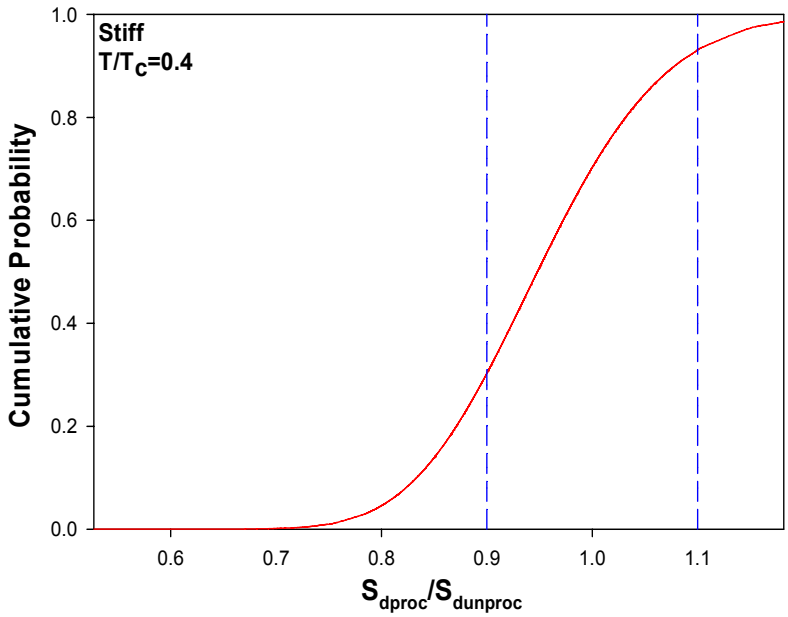

Figure C.9 Cumulative probability function for stiff sites for T/T_c=0.4

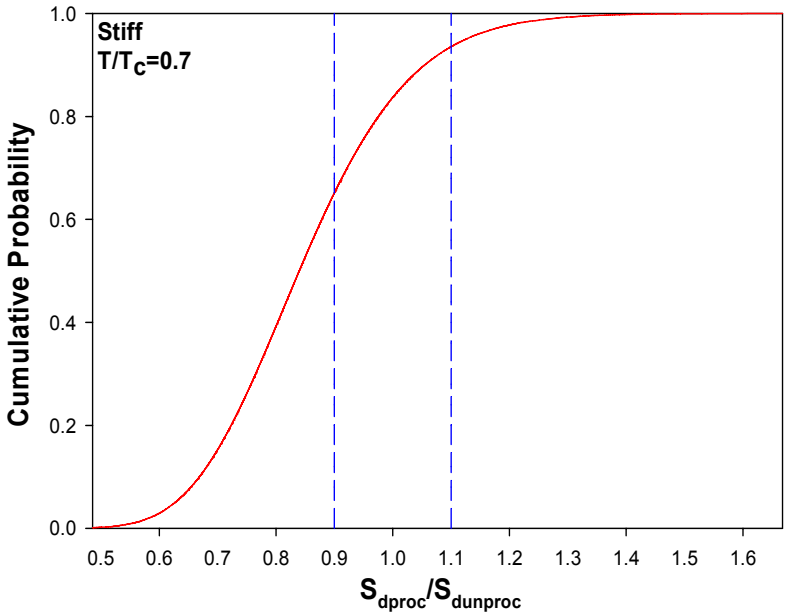

Figure C.10 Cumulative probability function for stiff sites for T/T_c=0.7

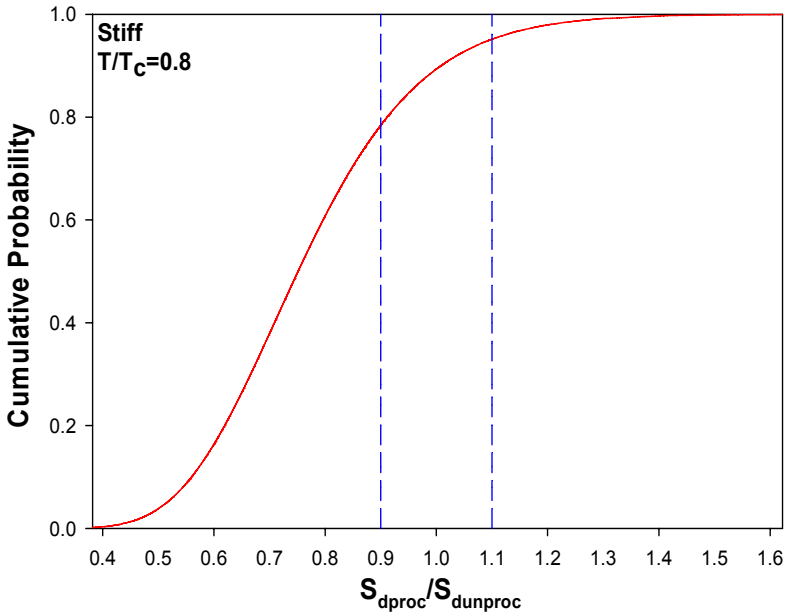

Figure C.11 Cumulative probability function for stiff sites for T/T_c=0.8

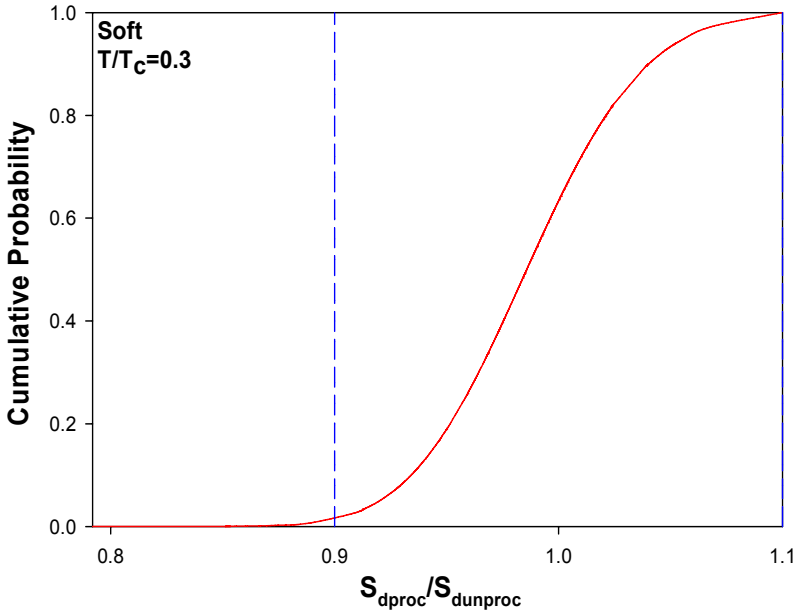

Figure C.12 Cumulative probability function for soft sites for T/T_c=0.3

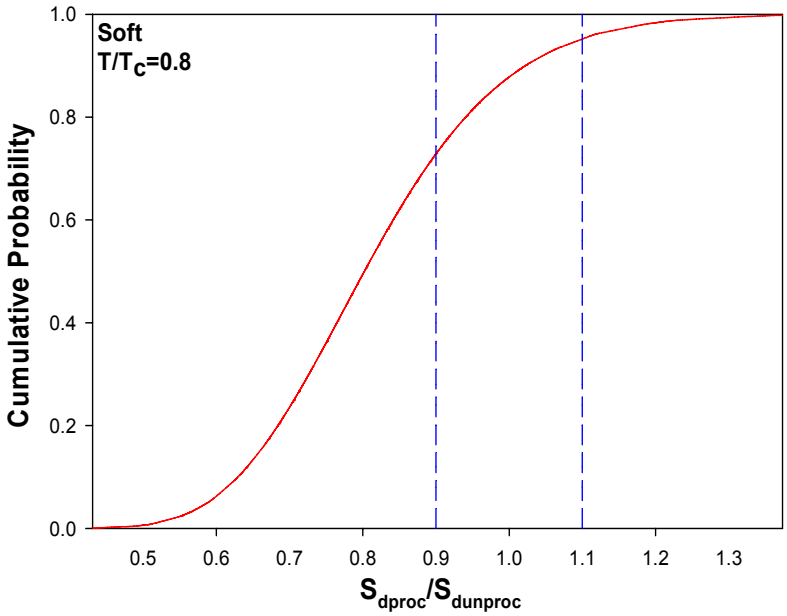

Figure C.13 Cumulative probability function for stiff sites for T/T_c=0.8